3D SCANNING OF TRANSPARENT OBJECTS

by

Gönen EREN

Submitted to Ecole Doctorale Environment - Sante/STIC (E2S)
in partial fulfillment of the requirements for the degree of
Docteur en Instrumentation et Informatique de l'Image

Université de Bourgogne

Submitted to the Graduate School of Engineering and Natural Sciences
in partial fulfillment of the requirements for the degree of
Doctor of Philosophy

Sabancı University

October 2010

3D SCANNING OF TRANSPARENT OBJECTS

APPROVED BY:

Prof.Dr. Frederic TRUCHETET, (Dissertation Supervisor)

. . . . . .

Prof.Dr. Aytül ERÇIL , (Dissertation Supervisor)

. . . . . .

Dr. Olivier AUBRETON , (Dissertation Co-supervisor)

. . . . . .

Prof. Dr. Christophe ODET

. . . . . .

Dr. Ceyhun Burak AKGÜL

. . . . . .

DATE OF APPROVAL: . . . . . .

Abstract

Many practical tasks in industry, such as automatic inspection or robot vision, often require scanning of three-dimensional shapes with non-contact techniques. However, transparent objects, such as those made of glass, still pose difficulties for classical scanning techniques. The reconstruction of surface geometry for transparent objects is complicated by the fact that light is transmitted through, refracted and in some cases reflected by the surface. Current approaches can only deal relatively well with sub-classes of objects. The algorithms are still very specific and not generally applicable. Furthermore, many techniques require considerable acquisition effort and careful calibration.

This thesis proposes a new method of determining the surface shape of transparent objects. The method is based on local surface heating and thermal imaging. First, the surface of the object is heated with a laser source. A thermal image is acquired, and pixel coordinates of the heated point are calculated. Then, the 3D coordinates of the surface are computed using triangulation and the initial calibration of the system. The process is repeated by moving the transparent object to recover its surface shape. This method is called Scanning From Heating. Considering the laser beam as a point heating source and the surface of the object locally flat at the impact zone, the Scanning From Heating method is extended to obtain the surface normals of the object, in addition to the 3D world coordinates. A scanner prototype based on Scanning From Heating method has been developed during the thesis.

Acknowledgements

I offer my sincere gratitudes to my advisors, Aytul Ercil and Frederic Truchetet, and to my co-advisor Olivier Aubreton, for trusting me from the beginning and for giving their support and guidance all along this thesis.

I thank Fabrice Meriaudeau, David Fofi, L.A. Sanchez Secades, A. Teoman Naskali, E. Deniz Kunt for helping me out on my research.

I thank to all LE2I and VPA laboratory members for the help and pleasant environment they provided and especially to Gulbin Akgun and to O. Rahmi Ficici for their technical support.

This thesis was partially supported by:

- Government of France
- SAN-TEZ(00335.STZ.2008-2)
- SPICE(FP6-2004-ACCSSA-2)
- Galatasaray University

TABLE OF CONTENTS

List of Tables

List of Figures

1 INTRODUCTION

Many practical tasks in industry, such as automatic inspection or robot vision, often require the scanning of three-dimensional shapes by use of non-contact techniques. There is also an increasing demand for three-dimensional(3D) applications such as object modeling, preservation of historic artifacts, reverse engineering, quality assurance, etc., both in research and in the industry. Despite tremendous interest in object digitization, the acquisition of transparent objects has not received much attention. While the 3D acquisition of opaque surfaces with lambertian reflectance is a well-studied problem, transparency still pose challenges for acquisition systems.

1.1 Motivation

Transparent objects violate most of the fundamental assumptions made by vision algorithms. For instance, they cause the projection of a background scene to the image plane to be deformed. Furthermore, this projection can vary from one viewpoint to the next. Additionally the reflection of light by the surface complicates the reconstruction process. Figure 1.1 illustrates these facts and presents a transparent glass object and its reconstruction by an industrial laser scanner: Minolta VI-910 Non Contact 3D Digitizer. The 3D reconstruction of the object is affected by refractions and specular reflections and can not be properly obtained.

Different techniques have been developed to deal with these problems. Re-

(a)

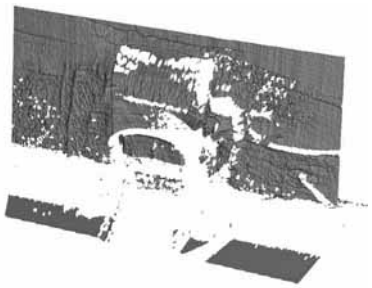

(b)

Figure 1.1: (a) Transparent glass object, (b) 3D reconstruction by Minolta VI-910 Non Contact 3D Digitizer.

searchers studied the deformations of a known background to estimate the surface of transparent objects. Some analyzed the reflection of light by a transparent surface, while others used polarization, photometry and many other methods to obtain the 3D geometry of an given transparent object. However, the proposed approaches are still specialized and targeted at very specific object classes.

On the other hand, the industry is in high demand for in-line 3D quality control of transparent products. There exist scanners capable of realizing the 3D quality control of flat panels [3]. For other geometric forms haptic devices are often used. However, these devices are far too slow to meet the speed requirements for an in-line inspection. As a consequence, the quality control process is achieved by statistical sampling. For example, for transparent automotive glasses, one piece in five hundred is sampled and is scanned using a haptic device. If an error is detected, all the products between two scanned samples are discarded. This is time and resource consuming. Additionally, if erroneous products are produced between two faultless samples and sent to the client, a discontinuity in the car production line can be caused. A non-contact scanner which has the ability to scan different types of transparent surfaces at high

speeds is needed.

1.2 Contribution

This thesis proposes a new solution to 3D scanning of transparent objects. The developed method, using local surface heating and thermal imaging, achieves scanning of different transparent materials and type of surfaces.

The working principle of the method is as follows: First, the surface of the object is heated with a laser source. A thermal image is acquired, and pixel coordinates of the heated point are calculated. Then, the 3D coordinates of the surface are computed using triangulation and the initial calibration of the system. The process is repeated by moving the transparent object to recover its surface shape. This method is called *Scanning From Heating*.

Considering the laser beam as a point heating source and the surface of the object locally flat at the impact zone, the Scanning From Heating method is extended to obtain the surface normals of the object, in addition to the 3D world coordinates.

The thesis also discusses, a shape from silhouette method and a laser line projection system based on Scanning From Heating.

A scanner prototype has been designed and realized to demonstrate the efficiency of the method. Results on several transparent objects are presented.

1.3 Thesis Structure

The thesis is organized as follows: Chapter 2 gives a literature survey on the subject. First some key 3D acquisition methods are presented and their application to

transparent objects is discussed. Then the state of the art on transparent object reconstruction is given.

Chapter 3 presents the theoretical background of the proposed method, and discusses the absorption of light and the emissivity of materials.

Chapter 4 describes the Scanning from Heating method, discusses the application of the method on transparent glass objects. It presents the scanner prototype and the experimental results. Additionally a line projection application is shown.

Chapter 5 demonstrates the extension of the method to recover surface normals.

Finally, Chapter 6 concludes the thesis.

2 LITERATURE SURVEY

Three-dimensional acquisition techniques differ in many aspects, including precision, scanning time and amount of required human interaction. Another central aspect is the categories of objects that can be scanned by complexity and surface properties. Table 2.1 presents a taxonomy of object classes based on increasing complexity in light transport. The light transport models are illustrated in Fig.2.1. While the 3D acquisition of opaque surfaces with lambertian reflectance (class 1 and class 2 in Table 2.1) is a well-studied problem, transparent, refractive, specular and potentially dynamic scenes (class 3 to 9 in Table 2.1) pose challenges for acquisition systems.

In the case of transparent objects, the reconstruction of surface geometry is complicated by the fact that light is transmitted through, reflected (Fig.2.1.c), refracted (Fig.2.1.d), scattered underneath the surface (Fig.2.1.e) and absorbed (Fig.2.1.f), complicating the 3D reconstruction (These phenomenons are further detailed in the Appendix B section of the thesis). Tracking refracted scene features might be difficult due to severe magnification or minimization of the background pattern. Additionally, if the object is not completely transparent, absorption might change the intensity of the observed features, complicating feature tracking. In the case of reflections, when changing the view point, features appear to move on the surface; no surface feature can be observed directly, and the law of reflection has to be taken into account [1].

This chapter presents a literature survey on methods that have been proposed

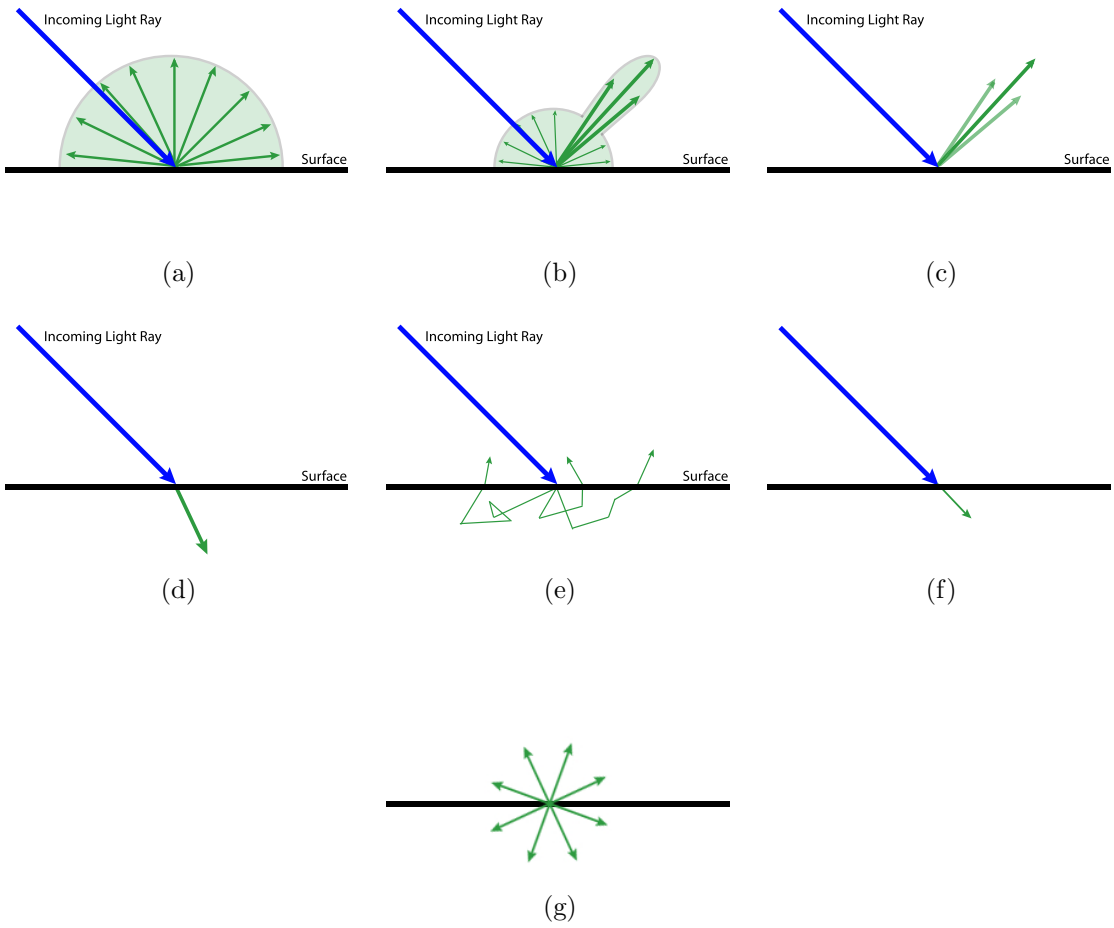

Figure 2.1: Light transport models: (a) Diffuse or near diffuse reflectance , (b) mixed diffuse and specular reflectance , (c) ideal or near ideal specular reflectance, (d) ideal or near ideal specular refraction, (e) multiple scattering underneath the surface, (f) absorption, (g) emission.

Table 2.1: A taxonomy of object classes based on increasing complexity in light transport. [1]

Object Type		Surface / Volume Type	Image Formation
Opaque	1	surface, rough	diffuse or near diffuse reflectance
	2	surface, glossy	mixed diffuse and specular reflectance
Translucent, Transparent	3	surface, smooth	ideal or near ideal specular reflectance
	4	surface, sub-surface scattering	multiple scattering underneath the surface
	5	surface, smooth	ideal or near ideal specular refraction
	6	volume, emission / absorption	integration along viewing ray
	7	volume, single scattering	integration along viewing ray
	8	volume, multiple scattering	full global light transport with occluders
Inhomogeneous	9	mixed scenes, containing many / all above	full global light transport

to deal with transparent objects. In the following paragraphs, we first briefly recall some key non-contact 3D object acquisition techniques such as, time of flight, laser triangulation, pattern projection, stereo vision and shape from focus. These techniques are grouped into two sections: active and passive range scanning. We discuss for each section, the application of the methods to transparent objects. Then the state of the art in transparent object reconstruction, giving illustrations of the employed techniques, is presented. Finally, a conclusion on the presented methods is given.

2.1 Overview of traditional 3D object acquisition techniques

Most of the three-dimensional acquisition techniques that have been developed over the past two decades have focused on opaque objects with lambertian reflectance properties. A wide range of methods has been proposed, which can be coarsely divided into active and passive range sensing (Fig.2.2).

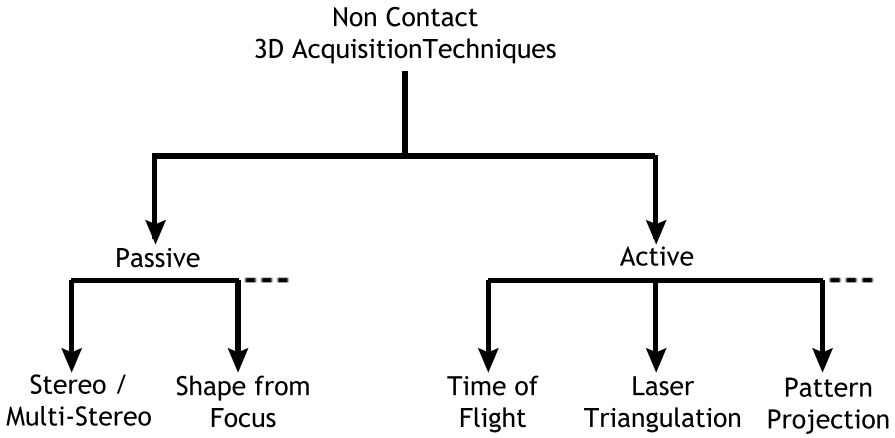

Figure 2.2: General regrouping of common non contact 3d acquisition techniques. [2]

Active range scanning techniques control the lighting in the scene, e.g., by projecting patterns of light. Time of Flight, laser projection and structured light projection systems are some examples of active range scanning. On the other hand, passive range scanning techniques do not influence the scene lighting. Examples of passive range sensing include stereo, multi-view stereo and shape from focus.

2.1.1 Active Range Scanning Techniques

Time of Flight Scanner

Time of Flight Scanner analyzes the distance to a surface by timing the round-trip time of a pulse of laser light. Figure 2.3 illustrates the working principle of the method. The speed of light, c, is a known and the round-trip time, $2t$, determines the travel distance of the light, which is twice the distance between the scanner and the surface. The distance to the scanner, D, is then given by $D = ct$. The accuracy of a time of flight scanner is dependent on how precisely it can measure the time. The laser beam is then swept across the scene to acquire a point cloud. An actual Time of Flight Scanner can scan up to 50000 points in a second and can have an extensive range up to 200 meters.

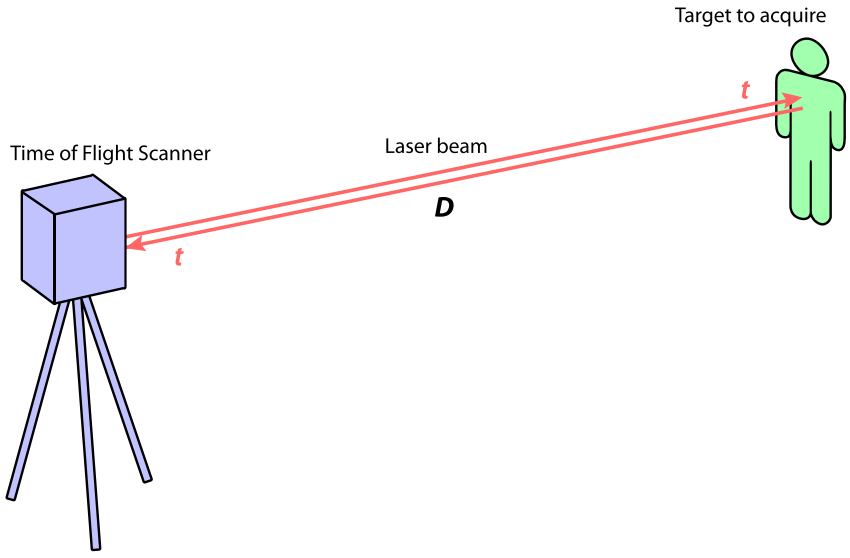

Figure 2.3: Working principle of a Time of Flight Scanner.

Laser Scanner

Laser scanners are also active scanners that use triangulation to acquire the 3D data. The method is illustrated in Fig.2.4. The laser dot, the camera and the laser emitter form a triangle. As the distance between the camera and the laser emitter, d, and the angle of the laser emitter corner, θ, is known, the angle of the camera corner, β, can be determined by looking at the location of the laser dot in the cameras field of view. This allows to fully determine the shape and size of the triangle and respectively the 3D position of the laser dot. In most cases a laser stripe, instead of a single laser dot, is swept across the object to speed up the acquisition process. Laser scanners based on triangulation technique have shown to be accurate and cost effective and there exist many commercially available scanner models.

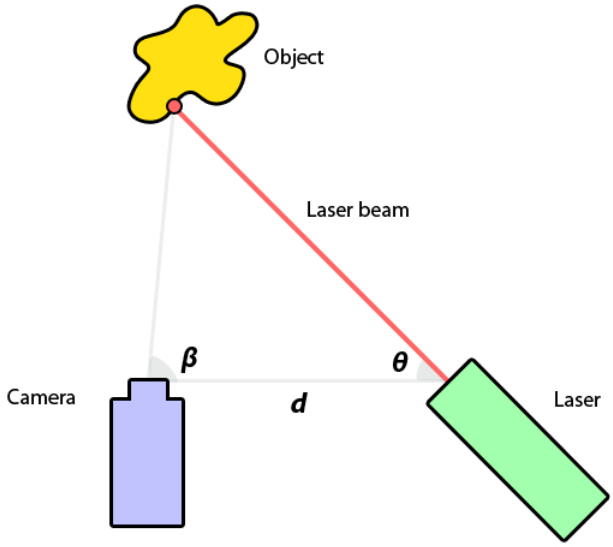

Figure 2.4: Laser triangulation.

Pattern Projection

Pattern projection techniques use multiple stripes or patterns projected simultaneously on the object, rather than scanning a single laser line or point on the scene and processing independent range profiles. Figure 2.5 illustrates the technique. The most popular method is the application of moire principle which uses two precisely matched pairs of gratings, the projected light is spatially amplitude modulated by the grating, and the camera grating demodulates the viewed pattern and creates interference fringes whose phases are proportional to range [4]. Other methods propose the use of a projective pattern and the detection of the same pattern from multiple views using stereoscopic systems [5]. The sequential projection of encoded patterns [6] is another commonly used method.

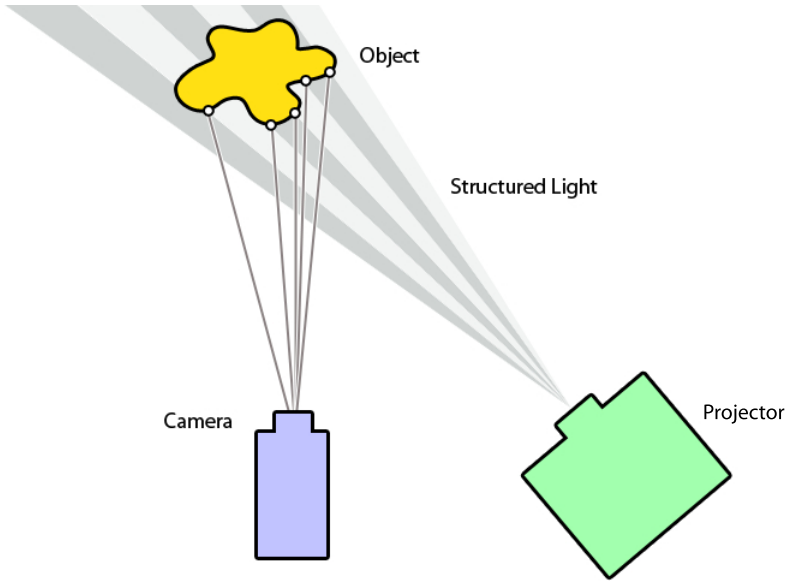

Figure 2.5: Working principle of pattern projection technique.

Application to Transparent Objects:

We have presented some key active scanning techniques. A detailed review of the methods and comparison of commercial available scanners can be found in [7]. Active range scanning techniques belong to the most accurate object acquisition approaches known today. However, most of them rely on a clearly detectable pattern of light being reflected by the objects surface. Consequently, these methods do not yield good results on transparent, refractive and specular surfaces. Researchers tried different approaches to improve the efficiency of the methods on these type of surfaces. For instance, Curless and Levoy [8] analyzed spacetime properties of the acquired 3D data to correct the artifacts caused by partial reflections. The proposed space-time analysis improves range scanning results for glossy surfaces (Table 2.1, class 2). Unfortunately, the efforts did not led to a generally applicable method to recover the surface of transparent and/or specular objects.

2.1.2 Passive Range Scanning Techniques

Stereo Vision:

Stereo vision is a technique that uses two cameras to measure distances from the cameras, similar to human depth perception with human eyes. The process uses two parallel cameras aligned at a known distance of separation. Each camera captures an image and these images are analyzed for common features. Triangulation is used with the relative position of these matched pixels in the images as illustrated in Figure 2.6. Triangulation requires knowledge of the focal length of the camera f, the distance between the camera bases b, and the center of the images on the image plane c_1 and

c_2. Disparity d is the difference between the lateral distances to the feature pixel v_2 and v_1 on the image plane from their respective centers. Using the concept of similar triangles, the distance from the cameras D is calculated as $D = \frac{b.f}{d}$. Correspondences between pixels are established by searching through the image and using methods like correlation or sum of square differences measures to compare local neighborhood. The raw output of a stereo system is an image of the disparity or, equivalently inverse range, between images at each pixel. It is also possible to use multiple cameras, also called multi-view stereo, and to compute image to image correspondences between image pairs, and to obtain independent depth estimates for each camera viewpoint. A common 3D model is then obtained fusing all the estimates.

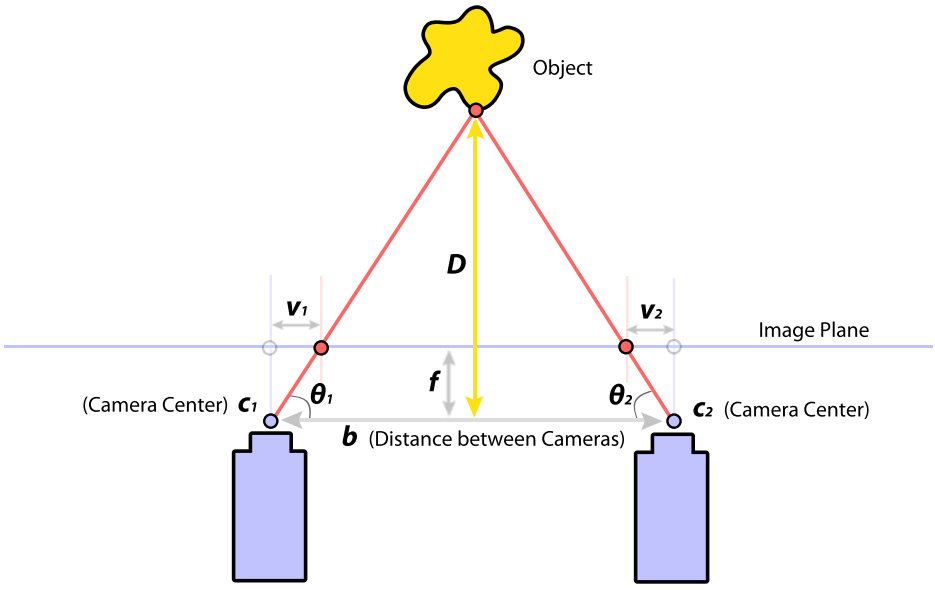

Figure 2.6: Stereo vision triangulation.

Stereo vision is a popular method and there exist many commercially available stereo vision scanners. However, the accuracy of the method depends on the feature

detection and matching of the features on both images. Surfaces which do not contain detectable features can not be properly reconstructed using this method.

Shape from Focus:

The shape from focus method moves the object with respect to the imaging system and obtains a sequence of images that correspond to different levels of object focus. Figure 2.7 illustrates the method. The sum-modified-Laplacian (SML) focus operator is used to measure the relative degree of focus between images. The operator is applied to the image sequence to obtain a set of focus measures at each image point. The focus measure values at each point are modeled and interpolated to obtain accurate depth estimates [9].

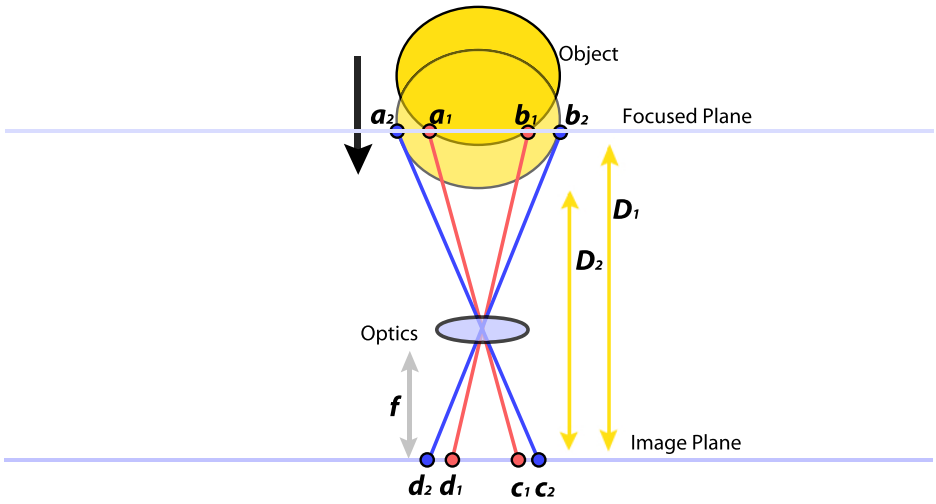

Figure 2.7: Shape from Focus.

Application to Transparent Objects

We have presented some key passive scanning techniques. A detailed review of the methods can be found in [10]. Passive range scanning techniques usually make assumptions about the material properties of the scene, the most common being Lambertian surface reflectance and detectable features on the surface. As a consequence they can not be directly applied to transparent materials. Researches proposed methods to extend passive range scanning techniques to non-Lambertan surfaces. For instance, Bhat et al. [11] proposed a multi-view stereo system, using three cameras, to recover the surface shape of specular objects. As specularity is viewpoint dependent, they have determined trinocular configurations, independent of surface roughness, such that each scene point is visible to all sensors and at least one stereo pair produces the correct depth. Nayar et al. [12] also proposed an algorithm for separating the specular and diffuse components of reflection from images. The method uses color and polarization, simultaneously, to obtain constraints on the reflection components at each image point. There exist many other extensions to passive range scanning techniques but still, none of them proposes a generally applicable method to specular, transparent or refractive objects.

2.2 State of the Art in Transparent Object Reconstruction

The previous discussions provide a quick overview of the active and passive 3D range scanning techniques. However, these techniques are designed to obtain the shape of opaque surfaces and are based on analysis of the diffuse (body) reflection component

of an object's surface. Transparent objects, such as those made of glass, still pose difficulties for these techniques. Researchers have proposed different approaches to deal with transparent objects:

2.2.1 Structured Light

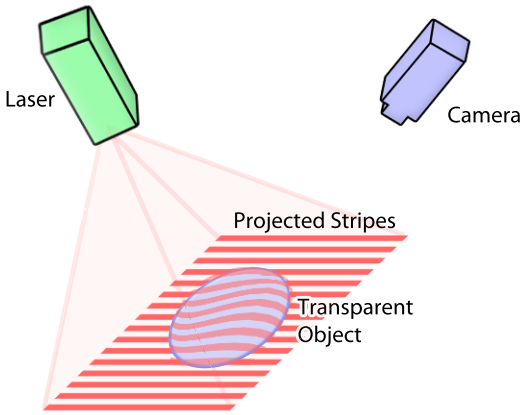

Figure 2.8: Illustration of structured light setup of Hata et al..

There has been intensive study of the refracted light in transparent objects for 3D surface recovery. Hata et al. [13] used a structured light setup to project stripe patterns into the object. Considering that the object has one flat side, they placed it on a plate and observed the distorted patterns by an imaging sensor. Figure 2.8 illustrates their experimental setup. Hata et al. first extracted from the image a 2D contour of the transparent object. They have generated 3D models from the stripes inside this contour. They have selected points on the 3D models and considered them as genes. They employed a genetic algorithm to cross-over and mutate these genes and to obtain new 3D models. At each step of the genetic algorithm, they have

compared the new generated models using an error function. They have repeated the process until they obtain a 3D model under a given error threshold. However, this method can only be applied to homogenous objects with smooth surfaces and with one flat side, which limits the application areas.

2.2.2 Scatter Trace

Morris and Kutulakos [14] proposed a method for reconstructing the exterior surface of a complex transparent scene with inhomogeneous interior. Their approach involves capturing images of the scene from one or more viewpoints while moving a proximal light source to a 2D or 3D set of positions. This gives a 2D (or 3D) dataset per pixel, called the scatter trace. The key idea of their approach is that even though light transport within a transparent scenes interior can be exceedingly complex, the scatter trace of each pixel has a highly constrained geometry that reveals the contribution of direct surface reflection, and leads to a simple "scatter-trace stereo" algorithm for computing the local geometry of the exterior surface. Figure 2.9 illustrates a transparent object with complex inhomogeneous interior and the reconstruction obtained by the method.

2.2.3 Shape from Motion

Ben-Ezra and Nayar [15] proposed a model-based approach to recover the shapes and the poses of transparent objects from known motion. They showed that it is possible to estimate the shapes of transparent objects immersed in an environment of unknown structure from a sequence of images taken during a known motion. The objects should be homogenous and the refractive index of the material should be

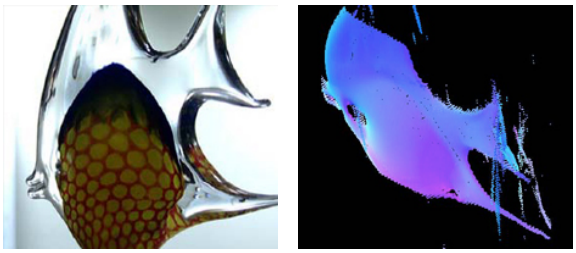

(a) (b)

Figure 2.9: (a) A transparent object with complex inhomogeneous interior, (b) 3D Surfel view of the reconstruction obtained by Morris and Kutulakos method

known. The algorithm assumes a parametric form for the shapes of the transparent objects, and estimates the shape parameters from the motion of features within the image of the object. Since the parametric model is used, the algorithm is not restricted to any particular form and can be used for a wide class of shapes. However, even for very simple shapes, the underlying problem is complicated as it involves highly non-linear interactions between light rays and the object surfaces.

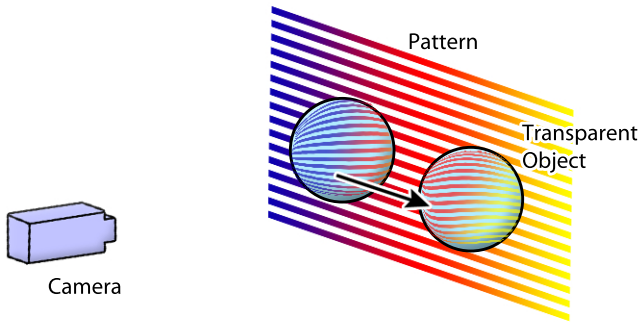

Figure 2.10: Illustration of Shape from Motion experimental setup of Ben-Ezra and Nayar.

2.2.4 Optical Flow

Agarwal et al. [16] generalized the optical flow equation to the case of refraction, and developed a method for recovering the refractive structure of an object (a representation of how the object warps and attenuates or amplifies the light passing through it) from a video sequence, acquired as the background behind the refracting object moves. Figure 2.11 illustrates the method. A transparent object is placed in front of a camera and the background scene is controlled using a projector. The method provides satisfactory results for simple homogenous transparent objects like spheres and cylinders where the refractive index is also known.

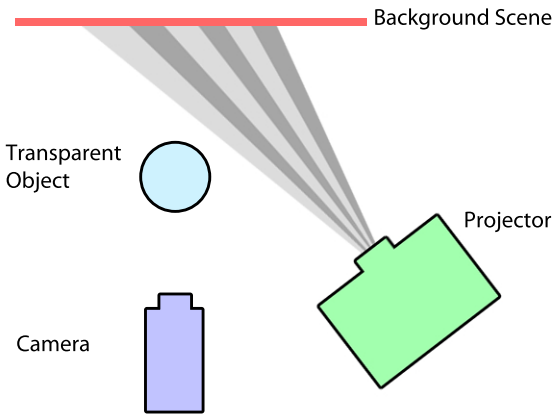

Figure 2.11: Illustration of experimental setup of Agarwal et al..

2.2.5 Fluorescence

Hullin et al. [17] embeds the object into a fluorescent liquid. By analyzing the light rays that become visible due to fluorescence, they detect the intersection points between the projected laser sheet and the object surface. Figure 2.12 illustrates the

method. For transparent objects, they directly depict a slice through the object image by matching its refractive index to the one of the embedding liquid. This enables a direct sampling of the object geometry without the need for computational reconstruction. A 3D volume can be obtained by sweeping a laser plane through the object. It is possible using this method to obtain accurate 3D surface profiles but the object should be homogenous and the refractive index should be known. The application of the method is complicated by the fact that, for each type of object, a different solution matching the refractive index should be prepared. Additionally embedding objects into a liquid for scanning makes it difficult to apply the method to an industrial application.

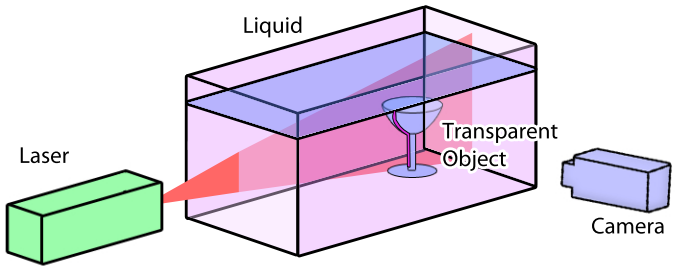

Figure 2.12: Illustration of experimental setup of Hullin et al.

Rantoson et al. [18] use an UV laser to create fluorescence on the surface of a transparent object. They observe the spot by an UV camera and are using triangulation to determine the 3D position of the spot. However, the method is affected by internal reflections of the laser beam, making it difficult to determine the fluorescence

surface spot.

2.2.6 Direct Ray Measurements

A practical algorithm for specular surface reconstruction based on direct ray measurements is developed by Kutulakos and Steger [19]. They assume that exactly one reflection event occurs along the ray. Using the reflected ray and the viewing ray, a surface position and an associated normal direction are recovered independently for every pixel. It is possible, using this method, to obtain precise measurements for planar objects.

2.2.7 Shape From Distortion

Researchers also investigated methods based on reflection of the light off the surface. Tarini et al. [20] proposed a shape-from-distortion method which, in order to obtain the 3D geometry, observes images of a nearby monitor that are reflected on the surface of the object. The method is illustrated in Fig.2.13. The projected stripe pattern consists of linear ramps in the RGB color channels. Given the captured matte, the internal camera parameters, and the position of the monitor relative to the camera, normal directions are converted into depth values and vice versa. A ray trough each pixel on the image plane can be traced and these rays can be reflected by the surface so that they hit the corresponding pixel on the monitor (according to the matte). This constraint allows to directly calculate a depth value from a given normal and the other way around. Furthermore, given the normal and a depth value at a pixel and under the assumption of surface continuity, depth values can be calculated for neighboring pixels by following the slope determined by the normal. A

theoretical analysis of shape-from-distortion for specular surfaces has been presented by Savarese et al. [21, 22].

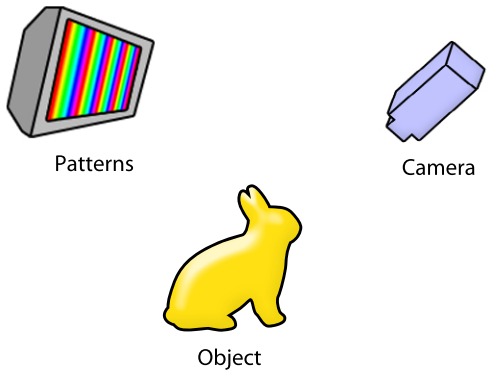

Figure 2.13: Illustration of experimental setup of Tarini et al.

2.2.8 Photometry

Ikeuchi [23] proposed determination of the reflectance of a shiny surface by using photometry based on different illumination distributions over the surface of the object. Figure 2.14 illustrates the method. A planer surface is illuminated by linear lamps. The camera is placed in the middle of the planer surface and observes the object through a hole. The reflectance map of the planar surface, which is assumed to have the Lambertian characteristics, is calculated. Image irradiance at a particular point is then proportional to the source radiance in a direction which depends on the orientation of the corresponding surface patch. The brightness of a particular surface patch is simply equal to the brightness of the part of the extended source. The method works good only on smooth surfaces but allows on the other hand de-

termination of normals at a given patch.

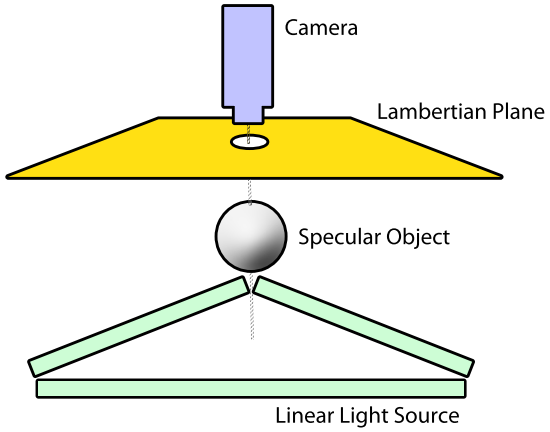

Figure 2.14: Illustration of experimental setup of Ikeuchi.

2.2.9 Specular Motion

Zheng et al.[24] proposed a method to estimate the shape of a specular object by analyzing specular motion using circular lights illumination. Figure 2.15 illustrates the method. The object is rotated and for each rotation step an image is taken. Circular lights that generate cones of rays are used to illuminate the rotating object. When the lights are properly set, each point on the object can be highlighted during the rotation. The reflection of the circular lights on the image are detected and the 3D profiles are calculated. A 3D graphics model is subsequently reconstructed by combining the profiles at different rotational planes.

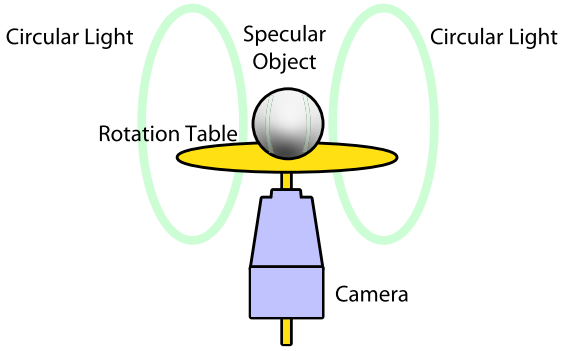

Figure 2.15: Illustration of experimental setup of Zheng et al.

2.2.10 Polarization

Recently, techniques based on the use of polarization to estimate the shape of transparent and specular objects have been investigated in-depth. Miyazaki et al. [25, 26] proposed a method for obtaining surface orientations of transparent surfaces through analysis of the degree of polarization in surface reflection and emission in visible and far-infrared wavelengths, respectively. Figure 2.16 illustrates the experimental setup.

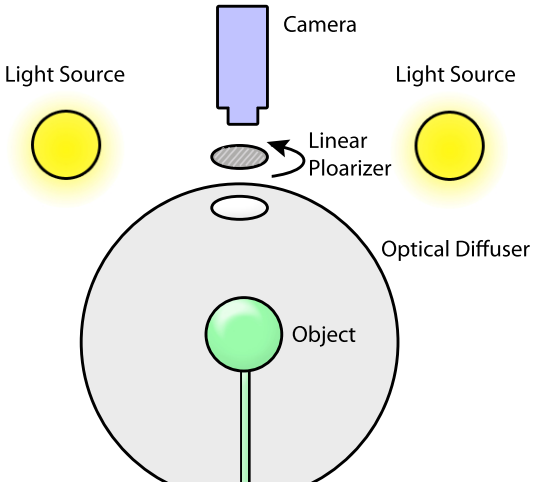

Figure 2.16: Illustration of experimental setup of Miyazaki et al.

The measurement setup consists of a single camera equipped with a linear polarizer. The refractive object is mounted inside a geodesic dome of light sources that are diffused by a plastic sphere surrounding the object. The shape of the objects back surface as well as its refractive index and the illumination distribution are assumed to be known. The measurement process consists of acquiring four differently polarized images by rotating the linear polarizer in front of the camera. The reconstruction is then performed using an iterative scheme that minimizes the difference between the measured polarization state and the polarization ray-traced image assuming a specific surface configuration. The polarization degree at visible wavelengths provides two possible solutions. The proposed method uses the polarization degree at far-infrared wavelengths to resolve this ambiguity.

Ferraton et al. [27] proposed a multispectral imaging technique for 3D reconstruction of transparent objects based on shape from polarization technique. They used a multispectral active lighting system which enables to cope with the two ambiguities on the zenith angle and azimuth angle.

2.2.11 X-Ray Imaging and Haptic Devices

It is also possible to use X-Ray imaging to detect transparent objects like glass [28], but unfortunately the devices do not provide sufficient accuracy for 3D surface reconstruction.

Haptic devices are currently used in industry to achieve quality control of transparent objects, like automotive glass. But these devices do not meet the speed requirements for an in-line inspection. In the field of robotics, researchers are investigating the use of robot arms for measuring non-flat objects by touch sensors [29, 30].

The research is concentrated on not breaking the target object and decreasing the number of touching points at the object surface in order to reduce the measuring time.

2.3 Conclusion

We have presented in this section key methods to obtain 3D surface reconstruction of transparent objects. There exist many extensions to these methods and further details and a review of the state of the art methods on transparent and specular object reconstruction can be found in [31]. The aforementioned methods for the recovery of surface geometry of transparent objects deal relatively well only with subclasses of objects. The algorithms are still very specific and not generally applicable. Furthermore, many techniques require considerable acquisition effort and careful calibration.

In this thesis, we propose a novel method to obtain three dimensional surface profiles of transparent objects. The method is capable of scanning complex objects and works on different types of materials making. The following chapter presents the basis of the method. Then the method is introduced in chapter IV

3 BACKGROUND

3.1 Introduction

Transparency is generally defined as the physical property allowing visible light to pass through a material. Visible light is only a small fraction of the entire spectrum of electromagnetic radiation, which is classified according to the wavelength of the light. The electromagnetic radiation outside the visible spectrum also interacts with matter in a behavior that could be described as a combination of transmission, reflection and absorption of energy. This includes (in order of increasing frequency): radio waves, microwaves, terahertz radiation, infrared radiation, visible light, ultraviolet (UV) radiation, X-rays and gamma rays (Fig.3.1). Absorption occurs during the propagation, if the frequency of the light is resonant with the transition frequencies of the atoms in the medium. In this case, the beam will be attenuated as it progresses. The transmission of the medium is clearly related to the absorption, because only unabsorbed light will be transmitted. Many materials are selective in their absorption of light frequencies. They absorb certain portions of the visible spectrum, while reflecting others. Selective absorption is responsible for the coloration of optical materials. Rubies, for example, are red because they absorb blue and green light, but not red [32, 33]. Making use of the selective light absorption can help us resolve different problems. For example human flesh is transparent to X-rays, while bone is not, making X-ray imaging useful for medical applications.

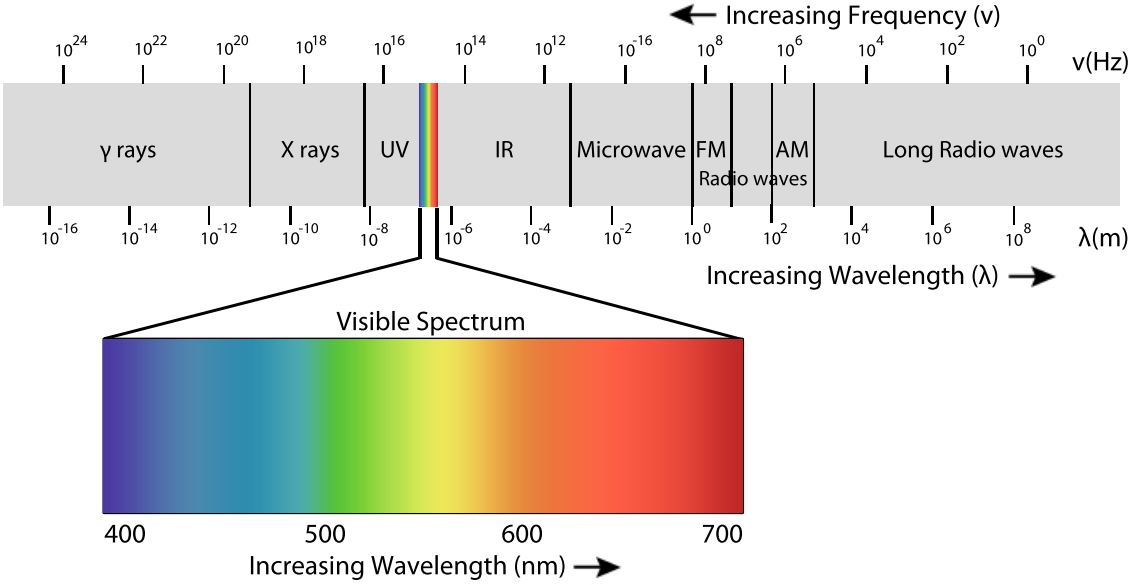

Figure 3.1: Complete spectrum of electromagnetic radiation with the visible portion highlighted.

Before describing, in the next chapter, our approach to recover the 3D shapes of transparent objects, we first look at how absorption of light works, detailing its fundamental properties. We give examples on glass, as it is the most commonly used transparent material. Furthermore we introduce a shape from silhouette and a stereo vision method based on the selective light absorption of materials. Next, we present the emissivity of materials, as it plays a key role in our reconstruction method, with again examples on transparent glass objects. Finally, we conclude the chapter introducing the basis of our method.

3.2 Absorption of Light

Objects have a tendency to selectively absorb, reflect or transmit light of certain frequencies. The manner in which light interacts with an object is dependent upon the frequency of the light, the nature of the atoms in the object, and often the nature of the electrons in the atoms of the object. Mechanisms of selective light wave absorption include:

- Electronic: Transitions in electron energy levels within the atom . These transitions are typically found in the ultraviolet (UV) and/or visible portions of the spectrum.
- Vibrational: Resonance in atomic/molecular vibrational modes. These transitions are typically found in the infrared portion of the spectrum.

3.2.1 Electronic Absorption

Absorption of light in the ultraviolet and visible regions of the spectrum is due to electronic transitions. The phenomena can be described as the process by which the energy of a photon is taken up by another entity, for example, by an atom whose valence electrons make a transition between two electronic energy levels. The photon is destroyed in the process. The absorbed energy can be lost by heat and radiation.

The absorbance of an object quantifies how much light is absorbed by it. This may be related to other properties of the object through the Beer-Lambert law:

$$\frac{I}{I_0} = \exp(-\alpha x) \tag{3.1}$$

where, I_0 is the intensity of the entering beam into a volume with a depth x, I is the intensity of the emergent beam, and α is the absorption coefficient, which is defined by:

$$\alpha = \frac{4\pi}{\lambda} K(\lambda) \tag{3.2}$$

with $K(\lambda)$ being the absorption index and λ being the wavelength [34]. The amount of absorption can vary with the wavelength of the light, leading to the appearance of color in pigments that absorb some wavelengths but not others.

3.2.2 Vibrational Absorption

While there are some lower energy electronic transitions in the infrared region of the spectrum, most optical absorptions in this region are due to vibrational transitions. The frequency, v, of a vibrational absorption in a diatomic molecule is given by:

$$v = \left(\frac{1}{2\pi}\right) \sqrt{\frac{F}{\mu}} \tag{3.3}$$

where F is the force constant for the bond and, u is the reduced mass of the molecule, as given by the expression:

$$\mu = \frac{m_1 m_2}{m_1 + m_2} \tag{3.4}$$

where m_1, and m_2, are the masses of the two atoms forming the molecule. The force constant is proportional to the bond strength, while the reduced mass is determined by the atomic weights of the atoms present. This model predicts that a

vibrational absorption will shift toward the infrared if the bond is weak or if the masses of the atoms are large. It follows that replacement of a small, highly charged, low atomic number atom by a large, low field strength, high atomic number atom will result in a significant shift toward the infrared. Replacement of hydrogen by deuterium, termed the isotope effect, which does not significantly alter the force constant, will shift the band toward the infrared due to the change in mass. [35]

3.2.3 Example Case of Glass

Glass is the most commonly used transparent material, and it has many applications in different industries, such as automotive, construction, optics and packaging. In the following paragraphs we will discuss the selective light absorption of glass.

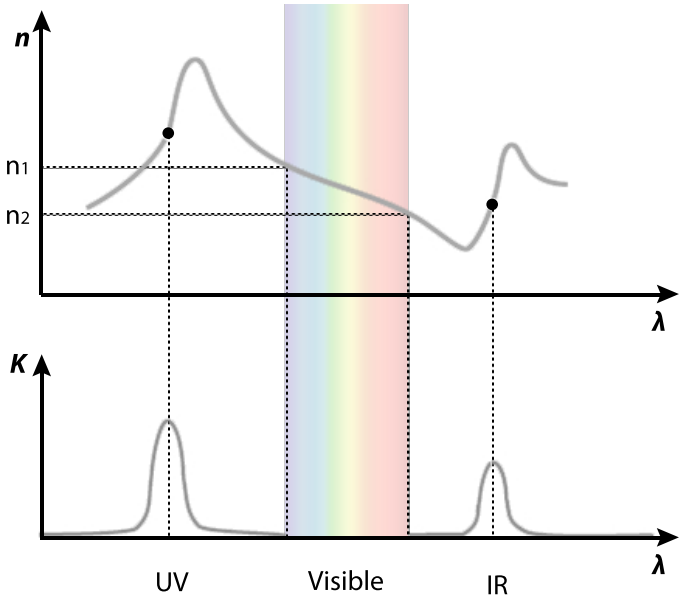

Figure 3.2: Evolution of the refraction and absorption index of glass depending on the wavelength.

Figure 3.2 presents the evolution of the refraction and absorption index of glass depending on the wavelength [34]. Absorptions are located in the UV domain and infrared domain of the spectrum. In these domains of the electromagnetic spectrum, glass loses its transparency and becomes semi-transparent or opaque. Figure 3.3 illustrates this fact and shows an image of a glass bottle, placed in front of an infrared illumination and observed with a long wave infrared camera sensitive to $8 - 14\ \mu m$. The object does not transmit the light coming from the source and appears to be opaque.

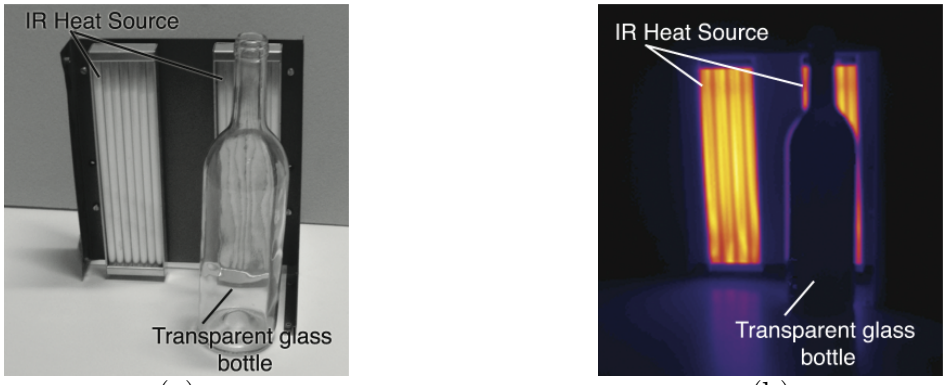

(a) (b)

Figure 3.3: (a) Transparent glass bottle in front of an infrared heat source. (b) Image taken with a long wave infrared camera sensitive to $8 - 13\mu m$.

Making use of this property, we have developped several methods to obtain 3D surface reconstruction of transparent objects:

Shape from Silhouette Approach: As glass can be considered as an opaque material in some regions of the electromagnetic spectrum, we propose to use this property to develop an approach based on Shape from Silhouette (SFS) method. SFS is a shape reconstruction method which constructs a 3D shape estimate of an

object using silhouette images [36]. We have developed, with the collaboration of two students of the IUT of Le Creusot, an experimental setup for the application of SFS on transparent glass using thermal images. The schematic of the experimental setup is presented in Figure 3.4. The glass object is positioned on a rotating platform. An infrared camera is used to observe the silhouette of the object. The objet is rotated and for each position a silhouette is acquired. Figure 3.5 presents a transparent glass object and its reconstruction by SFS method applied in the infrared domain. The result obtained is quite good but the reconstruction time is prohibitive. Additionally, holes and pits on the surface of the object can not be acquired using SFS method, making it ineffective for quality control applications.

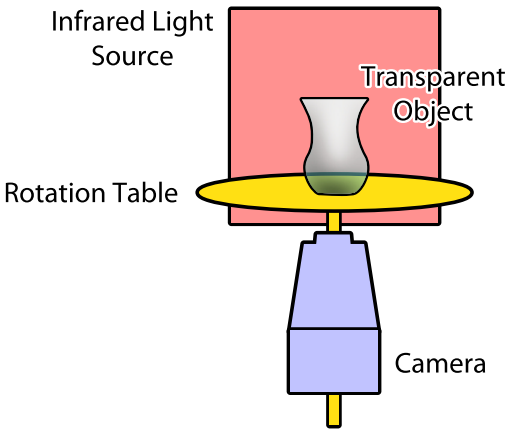

Figure 3.4: Experimental setup for the application of SFS on transparent glass using thermal images

Stereo Vision Approach: Researchers have previously used stereo vision in thermal images for human detection and tried to estimate the distance of objects in dark

(a) (b)

Figure 3.5: (a) Transparent glass object. (b) Reconstruction by SFS method.

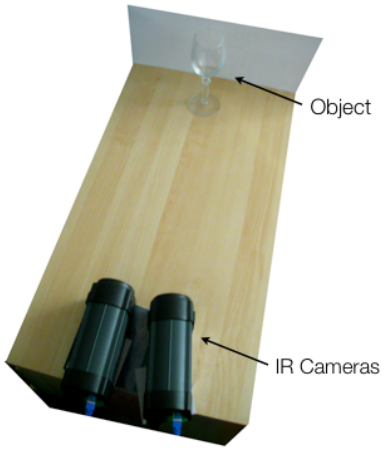

Figure 3.6: Experimental setup for the application of stereo vision on transparent glass using thermal images

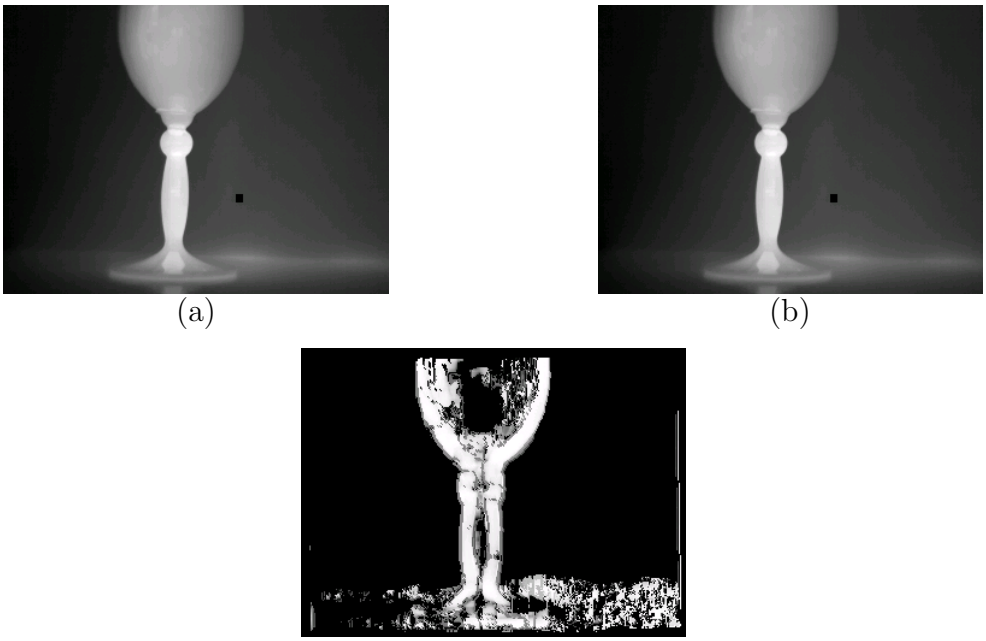

Figure 3.7: Stereo vision using thermal images (a) Thermal image of the left camera, (b) Thermal image of the right camera, (c) Disparity map.

environments [37]. We have developed a stereo vision approach to obtain 3D surface profiles of transparent materials. The technique makes use of the selective light absorption properties of the material. Figure 3.6 illustrates the experimental setup. Two thermal cameras observe a transparent glass object. Figure 3.7 presents the results obtained on a wine glass. The object appears opaque to the thermal cameras. However the thermal stereo method only works if there exist temperature gradients on the objects surface. Otherwise there are no distinctive features to detect. The borders of the object can be recovered due to a temperature difference with the background, but the surface reconstruction can not be properly achieved.

Laser Triangulation Approach: With the increase of the absorption index in the UV and infrared domain of the spectrum, the refraction index of glass also increases (Fig.3.2). This results in reflection of the incident light on smooth surfaces. It is then difficult to apply active range scanning methods, such as laser triangulation. Scanning of specular surfaces, such as shiny metal objects and mirrors, is a very difficult task in computer vision and still an active research topic. Specular objects do not have an appearance of their own, they simply distort the appearance of other objects nearby, creating an indirect view of the original objects. Unlike perspective images, where 3D points project along straight lines, indirect views are created by light that travels along a piecewise-linear light path. Therefore, there are no surface features that can be observed directly. When changing the view point, features appear to move on the surface and the law of reflection has to be taken into account [19, 1]. There are techniques [20, 21, 22, 38, 23, 39, 24, 40, 41, 19, 42], to recover the 3D surface of specular objects, but they only deal with sub-classes of surfaces and are not generally applicable [1].

In conclusion, although glass is opaque in certain domains of the electromagnetic spectrum, working in these wavelengths does not provide a direct solution for 3D digitalization. We propose to investigate and to make use of the radiative properties of materials in combination with the selective light absorption to propose a new approach.

3.3 Thermal Radiation

All substances continuously emit electromagnetic radiation because of the molecular and atomic agitation associated with their internal energy, which is proportional to the material temperature. We call a blackbody an idealized object that absorbs and emits electromagnetic radiation, in each direction at every wavelength. From the Planck radiation law, radiation energy, w, from the blackbody at the temperature T and the wavelength λ is:

$$w = \frac{2hc^2}{\lambda^5} \frac{1}{\exp(hc/\lambda kT) - 1} \tag{3.5}$$

where $h = 6.6262x10^{-34}[J.s]$ is the Plank constant, $c + 2.997925x10^{8}[m/s]$ is the speed of light, and $k = 1.38066x10^{-23[J/K]}$ is the Boltzmann constant. The energy distribution of the blackbody expressed as in Equation (3.5) is shown in Figure 3.8. From the figure, it is apparent that the radiation energy increases with the temperature of the object, and most of the emission is in the infrared region.

By integrating w in Equation (3.5) through all wavelengths, the Stephan-Boltzman law is derived:

$$W = \sigma T^4 \tag{3.6}$$

where $\sigma = 5.6705x10^{-8}[W/m^2.K^4]$ is the Stephan-Boltzmann constant. Given that any object has a positive temperature, this equation proves that any object radiates energy.

Unlike the intensity from a blackbody, the intensity emitted from a real body depends on direction. The following paragraph discusses the emissivity of a real

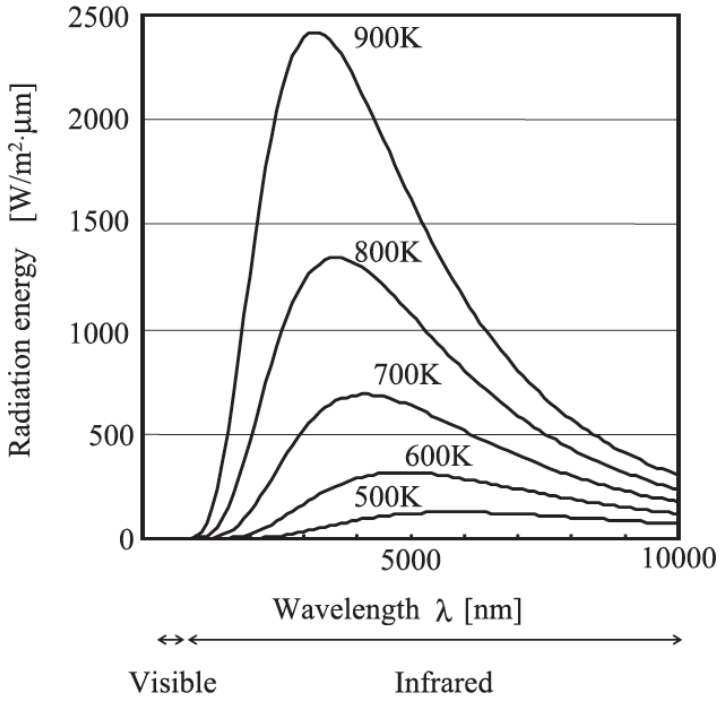

Figure 3.8: Energy distribution of a blackbody.

body.

3.3.1 Emissivity

Emissivity specifies how well a real body radiates energy compared to an ideal body, called a blackbody. Emissivity can depend on factors such as body temperature, wavelength of the emitted energy, and angle of emission. Emissivity is often measured experimentally in a direction normal to the surface and as a function of wavelength. For calculating the entire energy loss by a body, an emissivity that includes all directions and wavelengths is needed.

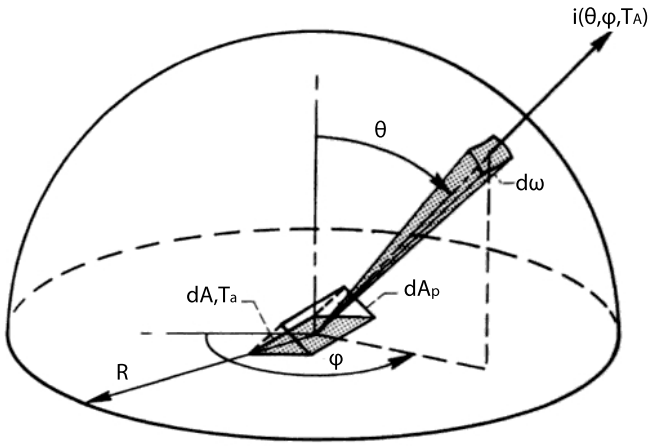

Figure 3.9: Angular emissivity.

Considering the geometry for emitted radiation in Fig.3.9 [43], the radiation intensity is defined by the energy per unit time emitted in direction (θ, φ) per unit of projected area dA_p normal to this direction, per unit solid angle and per unit of

wavelength interval. For a blackbody, the surface intensity has the same value in all directions. Unlike the intensity from a blackbody, the intensity emitted from a real body does depend on direction. The energy leaving a real surface dA of temperature T_A per unit time in the wavelength interval $d\lambda$ and within the solid angle $d\omega$ is then given by:

$$d^2Q_\lambda(\lambda, \theta, \varphi, T_A)d\lambda = i_\lambda(\lambda, \theta, \varphi, T_A)dA\cos\theta d\lambda d\omega \tag{3.7}$$

For a black body the intensity $i_{\lambda b}(\lambda)$ is independent of direction. The T_A notation is introduced to clarify that the quantities are temperature dependent. So the blackbody intensity is noted $i_{\lambda b}(\lambda, T_A)$. The energy leaving a blackbody area per unit time within $d\lambda$ and $d\omega$ is given by:

$$d^2Q_{\lambda b}(\lambda, \theta, T_A)d\lambda = i_{\lambda b}(\lambda, T_A)dA\cos\theta d\lambda d\omega \tag{3.8}$$

The emissivity is then defined as the ratio of the emissive ability of the real surface to that of a black body. The directional spectral emissivity is given by [43]:

$$\varepsilon_\lambda(\lambda, \theta, \varphi, T_A) = \frac{d^2Q_A(\lambda, \theta, \varphi, T_A)d\lambda}{d^2Q_{\lambda b}(\lambda, \theta, T)d\lambda} \tag{3.9}$$

$$= \frac{i_\lambda(\lambda, \theta, \varphi, T_A)}{i_{\lambda b}(\lambda, T_A)} \tag{3.10}$$

3.3.2 The Use of Thermal Radiation

The use of thermal radiation has enjoyed a variety of applications in computer vision. Bertozzi et al. used thermal images and a stereo vision-based algorithm for 3D pedestrian detection [44]. Maldague proposed a method for defect detection by

heating the surface and recording a time sequence of thermal images (called thermograms) to observe the temperature decay of the inspected surface [45]. Pelletier et al. also used thermal images to estimate a shape and proposed a 2D approach for shape extraction using a distant uniform heat source [46].

We propose, in this thesis, the use of thermal radiation for 3D surface recovery. The main idea is to bring a spot on the surface at a given temperature and observe it with a thermal camera. However, once the surface is heated, the emission should be omnidirectional so that the thermal camera can capture accurately the heated spot on different curvatures of the surface.

3.3.3 Example Case of Glass

Figure 3.10 illustrates the angular emissivity of a dielectric sphere like glass [47]. The radiation approaches the one of a blackbody emitting almost in every direction. It is then possible to consider a heated spot on the surface of a glass object as a lambertian source, i.e. if we can create a heat spot on the surface of a glass object, it can be observed from different angles by a thermal camera.

Figure 3.11 illustrates thermal images taken with an infrared camera from a glass plate placed on a rotation table. It is possible to observe a heat spot created on the surface of the glass plate for different angles of the rotation table.

To create a heat spot on the surface of a transparent glass object, we can benefit from its selective absorption properties and use a laser heating source working in a wavelength in which glass does not transmit the light.

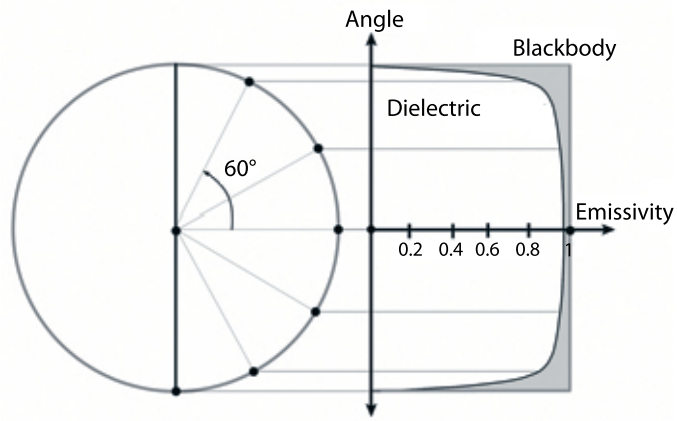

Figure 3.10: Emissivity of a dielectric sphere.

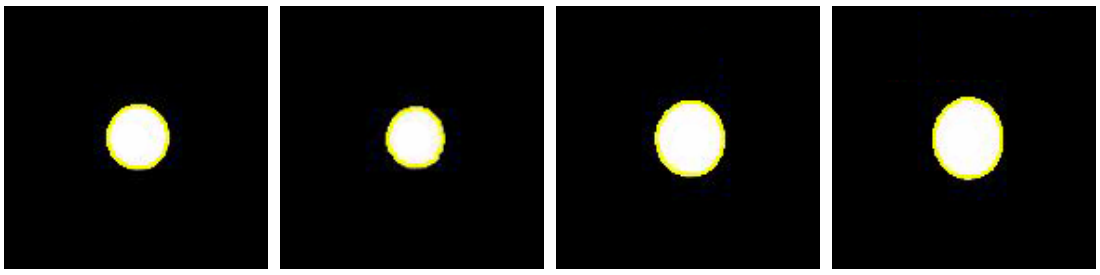

(a) (b) (c) (d)

Figure 3.11: Thermal images acquired from a glass plate placed on a rotation table: (a) 12 degrees, (b) 18 degrees, (c) 21 degrees,(d) 24 degrees. It is possible to observe the heat spot created on the surface of the glass plate for different angles of the rotation table.

3.4 Conclusion

Materials have often a selective light absorption and they are transparent to some frequencies of light while opaque to others. We have seen with the glass examples that techniques, such as shape from silhouette, can be applied in these frequencies to recover the shape of objects which are transparent in the visible domain. However shape from silhouette technique does not allow recovery of holes on the surface and does not properly work on protruding surfaces. We have seen that, for transparent glass objects, passive range scanning techniques, such as stereo vision, does not yield good results due to lack of features on the surfaces. Moreover, reflections on the surface are making active range scanning techniques, such as laser triangulation, ineffective. Consequently, we have proposed to use radiative properties of the materials. We have seen that, for transparent glass, if we locally heat the surface, we can observe the heated zone with a thermal camera. This information can be exploited to reconstruct the surface geometry. Additionally we have introduced the idea to use a laser, which is working in the selective absorption bands, to heat the surface. The next chapter introduces our new approach to scan transparent objects.

4 SCANNING FROM HEATING

4.1 Introduction

Current reconstruction methods for transparent objects are mainly working in the visible domain of the spectrum and are trying to resolve difficulties caused by transparency using algorithms and systems based on visible light. But materials often have a selective light absorption. They absorb certain frequencies while reflecting or transmitting others. For example, glass objects which are transparent in the visible domain appear to be opaque in UV and infrared domain of the electromagnetic spectrum. However, due to reflections in these selective light absorption bands, the reconstruction problem becomes similar to scanning of specular surfaces, such as metals and mirrors in the visible domain, which is also an active research topic. Consequently, working in these wavelengths does not provide a direct solution for 3D digitalization of transparent objects.

We propose to make use of the radiative properties of materials in combination with the selective light absorption. All materials continuously emit electromagnetic radiation, which is proportional to their temperature. The idea is to bring a spot on the surface of the transparent object to a given temperature. Once the heat spot is created, it will emit thermal radiation, whose intensity is higher then the rest of the surface. This spot is easily perceivable by a thermal camera. Nevertheless, the emission should be omnidirectional so that the thermal camera could observe the

heated spot on different curvatures of the surface. Finally the problem of heating the surface can be solved by using a laser heating source working in the selective absorption band of the material. The object surface is then opaque to the laser source, and the laser cannot penetrate into the object, causing only local surface heating.

In the following paragraphs we introduce the *Scanning from Heating* method and show its application on transparent glass. We present the 3D Scanner prototype and the results obtained on different types of surfaces. Furthermore we show an application of the method, a 3D scanner based on laser line projection.

4.2 Assumptions

For *Scanning from Heating* method to work, the following assumptions are made:

1. The transparent object is supposed to be homogenous, i.e. uniform in structure and composition, and isotropic, i.e. the physical properties of the material are independent of direction.

2. To be able to create a heat spot on the surface of the object, a laser heating source working in the absorption band of the material should be used. The object surface is then opaque to the laser heating source, and laser energy is absorbed without penetrating in. This assumes that there exist an absorption band for the material in question and a laser heating source working in these wavelengths.

3. Once the surface is heated, the emission of thermal radiation should be omnidirectional, so that it can be observed by the thermal camera on different curvatures of the surface. If not, the heated spot may not be detected by the camera in some regions of a protruding surface. This assumes that the angular emission of the material in question approaches the one of an ideal body (also called blackbody), emitting thermal radiation in every direction.

4.3 Method

Scanning from Heating employs triangulation for the recovery of the surface shape. Triangulation is one of the most commonly used 3D reconstruction methods and there are many commercial 3D scanners based on this technique.

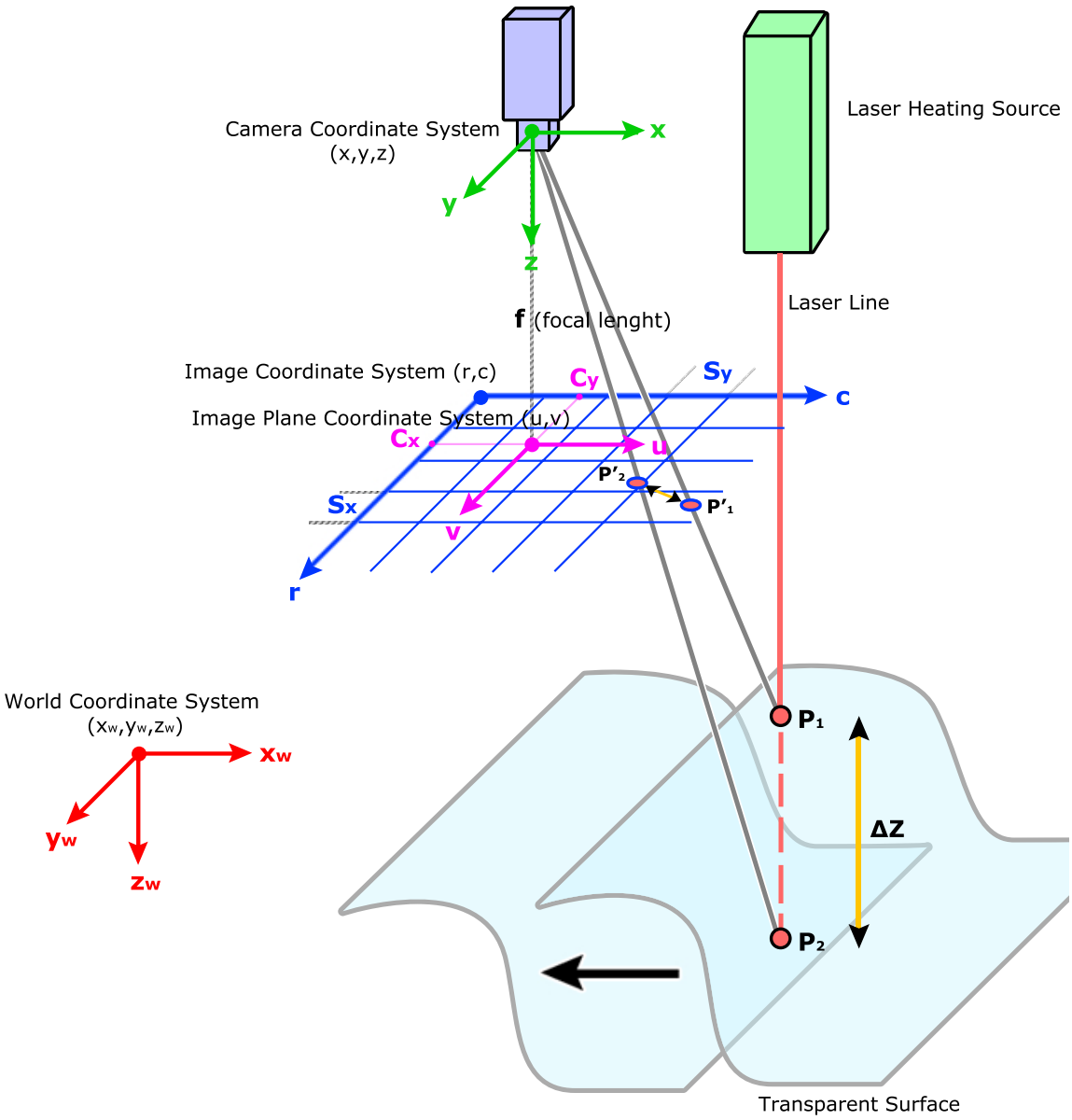

Figure 4.1: Scanning from Heating method.

Figure 4.1 illustrates the method. The transparent object is placed on a X-Y moving platform. The laser heating source and the thermal camera are fixed. When the laser fires, the surface of the object is heated at a point. We call P_1 the heated point on the surface of the object, and (x_1, y_1, z_1) its coordinates in the world coordinate system (x_w, y_w, z_w). The heated spot is observed by the thermal camera and a thermal image is acquired. The projection of the heated spot on the thermal image corresponds to the pixel which has a higher gray value intensity then the rest of the image. The coordinates of this pixel is determined on the image. The projection of P_1 on the image is called P_1', and its coordinates (r_1, c_1) in the image coordinate system (r, c). Using the pinhole camera model [48] and intrinsic camera parameters, the coordinates of P_1' on the image plane (u_1, v_1) are determined. The calibration process to obtain the camera parameters and the determination of the coordinates on the image plane are described in the next section. In the next step the object is moved to a new position. The laser is fired again and a second heated spot, P_2, is obtained on the surface of the object. The coordinates of P_2 in the world coordinate system are called (x_2, y_2, z_2). The projection of P_2 on the image is called P_2', and its coordinates (r_2, c_2). Using the same procedure, the coordinates of P_2' on the image plane (u_2, v_2) are determined. The variation of height between P_1 and P_2, ΔZ, can then be obtained by triangulation and is given by:

$$\Delta Z = |z_1 - z_2| = k.\sqrt{(u_1 - u_2)^2 + (v_1 - v_2)^2} \tag{4.1}$$

where k is a constant. The value of k can be determined by an initial calibration, which consists of determining the camera coordinates of at least two points of a known object. The surface heating process is repeated for several positions of the

moving platform and for each position the 3D coordinates are calculated.

4.3.1 Calibration

Camera calibration is defined as the determination of the parameters that model the optical projection of a 3D world point $P_w = (x_w, y_w, z_w)$ into pixel coordinates (r, c) in the image. This projection consists of multiple steps: First, the point P_w is transformed from world coordinates into camera coordinates $P_c = (x, y, z)$. This is expressed in terms of homogeneous coordinates by:

$$\begin{pmatrix} P_c \\ 1 \end{pmatrix} = \begin{pmatrix} x \\ y \\ z \\ 1 \end{pmatrix} = \begin{pmatrix} R & t \\ 0 & 1 \end{pmatrix} \begin{pmatrix} P_w \\ 1 \end{pmatrix} \tag{4.2}$$

where R is a 3x3 rotation matrix corresponding to the camera's orientation and t is the camera's position in the world coordinate system:

$$R = \begin{pmatrix} r_{11} & r_{12} & r_{13} \\ r_{21} & r_{22} & r_{23} \\ r_{31} & r_{32} & r_{33} \end{pmatrix}, t = \begin{pmatrix} t_x \\ t_y \\ t_z \end{pmatrix} \tag{4.3}$$

In the pinhole camera model [48], the projection of the point $P_c = (x, y, z)$ in camera coordinates into image plane coordinates (u, v) is given by:

$$\begin{aligned} u &= f\frac{x}{z} \\ v &= f\frac{y}{z} \end{aligned} \tag{4.4}$$

where f denotes the focal length of the camera.

The radial distortions caused by the camera lens can be modeled by the division model [49] which uses one parameter, κ, to model the distortions. The corrected coordinates (u', v') can be expressed, according to the model, by:

$$u' = \frac{2u}{1 + \sqrt{1 - 4\kappa(u^2 + v^2)}}$$
$$v' = \frac{2v}{1 + \sqrt{1 - 4\kappa(u^2 + v^2)}} \tag{4.5}$$

Finally, the point is transformed from the image plane coordinate system into the image coordinate system:

$$c = \frac{u'}{S_x} + C_x, r = \frac{v'}{S_y} + C_y \tag{4.6}$$

where, S_x, is the horizontal distance between two neighboring cells on the sensor, S_y, the vertical distance between two neighboring cells on the sensor, C_x, column coordinate of the image center point and, C_y, row coordinate of the image center point.

The calibration process determines, from a set of 3D points and their corresponding pixel coordinates, R and t, called the external parameters, and $f, \kappa, S_x, S_y, C_x, C_y$ called internal parameters of the acquisition system. The image width and height are also considered as internal parameters but are defined by the frame-grabber. To recover the internal and external parameters, the known 3D points are projected in the image and the sum of the squared distance between these projections and the corresponding image points is minimized. If the minimization converges, the

interior and exterior camera parameters are determined. The minimization process of the calibration depends on the initial values of the interior and exterior camera parameters. These initial parameters are usually provided by the manufacturer.

4.4 Application to Glass

Glass is one of the most commonly used transparent material. It has many use in automotive, construction, optics and packaging industries. In the following paragraphs we discuss the application of *Scanning from Heating* method to transparent glass. We first examine the selection of the laser heating source which will allow us create a heat spot on the surface of a glass object. We then look at to the selection of the thermal camera, examining different infrared sensor technologies. Once we have determined the proper camera and the laser to use, we discuss the pre-determination of the laser power to bring the surface of an object to a given temperature without damaging the surface. Finally, we discuss the detection of the laser irradiation on the thermal image acquired by the camera.

4.4.1 Selection of the Laser Heating Source

To be able to heat the surface of the glass by a laser source, we should first find out the light absorption frequencies of glass. Figure 4.2 presents the transmission of light as a percentage in the infrared domain of most commonly used glasses. For each type, there is a wavelength such that the transmission is close to 0%. This wavelength is called the infrared cut-off, and it depends on the composition of the glass [35]. At a wavelength higher than $10\mu m$, the glasses presented in Fig. 4.2 can

be considered as opaque objects. Therefore we propose to use a CO_2 laser source at $10.6\mu m$ to heat the surface of the glass.

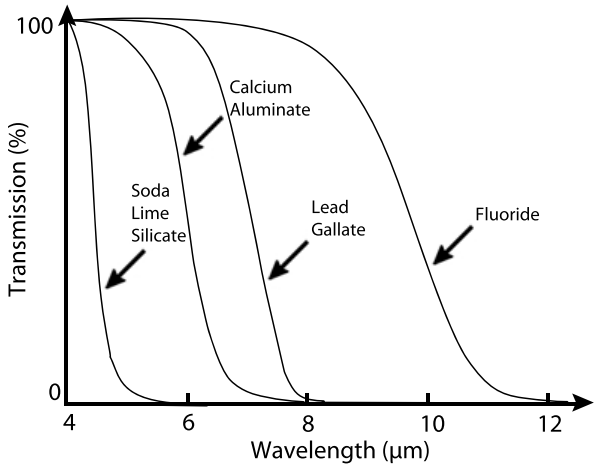

Figure 4.2: Transmission of light as a percentage in the infrared domain of commonly used glasses.

4.4.2 Selection of the Camera

Figure 4.3 shows the infrared part of the electromagnetic spectrum, illustrating the atmospheric transmittance of light in percentage. The infrared spectrum can be subdivided into five regions, based on a combination of the atmospheric transmittance windows, i.e. the wavelengths regions in which infrared radiation is better transmitted through the atmosphere and the detector materials used to build the infrared sensors [50]. The Near Infrared (NIR) band, from 0.7 to 1.0 μm (from the approximate end of the response of the human eye to that of silicon), is mostly used in fiber optic telecommunication systems since silica (SiO_2) provides a low attenuation

losses medium for the infrared. The Short Wave Infrared (SWIR) band, from 1.0 to 3 μm (from the cut off of silicon to that of the MWIR atmospheric window), allows to work on long-distance telecommunications (remote sensing) using a combinations of detector materials. In this band, $InGaAs$ based sensors covers up to about 1.8 micrometers. The Medium Wavelength Infrared (MWIR) band, 3 to 5 μm (defined by the atmospheric window and covered by Indium antimonide, $InSb$, and $HgCdTe$ and partially by lead selenide $PbSe$), and the Long Wavelength Infrared (LWIR) band, 8 to 14 μm (Covered by $HgCdTe$ and microbolometers), find applications in infrared thermography. The Very Long Wavelength Infrared (VLIR) band, 12 to 30 μm (Covered by doped silicon), is used in spectroscopy and astronomy.

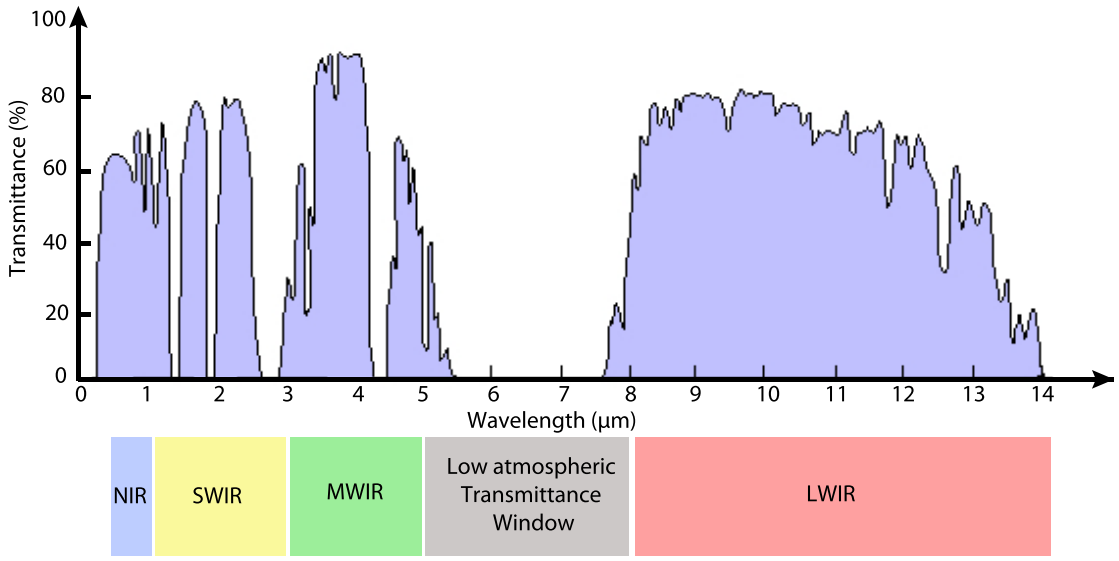

Figure 4.3: Transmission of light as a percentage in the infrared domain.

Table 4.1 provides a summary of the regions in the infrared part of the electromagnetic spectrum and the corresponding detector materials or technology. If Fig.4.2,

the transmission of light as a percentage in the infrared domain of commonly used glasses, and table 4.1 are analyzed together, it is possible to observe that commonly used glasses are opaque for LWIR sensors. Consequently a microbolometer camera sensible to 8 to 14 μm can be used to observe the surface of the glass, once it is heated. The camera then captures the electromagnetic radiation coming only from the surface of the object and is not affected by the internal heat propagation by conduction. We propose to use a FLIR A320G LWIR microbolometer camera for the experiments. LWIR microbolometer cameras are smaller then other types and are less costly. However, their resolution and image quality tend to be lower than cooled detectors in MWIR band. Nevertheless MWIR cameras can be used for Soda Lime Silicate type of glasses which have a 4-4.5μm cut-off frequency. (In Chapter IV, for the recovery of surface normals based on scanning from heating method, MWIR cameras are used for their superior image quality.)

Table 4.1: Regions in the infrared part of the electromagnetic spectrum and the corresponding detector materials

Spectral Band	Range (μm)	Detector Materials or Technology
NIR	0.74 - 1	SiO_2
SWIR	1 - 3	$InGaAs$,PbS
MWIR	3 - 5	$InSb$, $PbSe$, $PtSi$, $HgCdTe$
LWIR	8 - 14	$HgCdTe$, microbolometer
VLIR	12 - 30	dopped slicon
Si:Silicon, SiO_2:Silica, In:Indium, Ga:Gallium, As:Arsenic, Pb:Lead, S:Sulfur, Sb:Antimony, Se:Selenium, Pt:Platinium, Hg:Mercury, Cd:Cadmium, Te:Tellurium		

4.4.3 Calibration of the Camera

For the calibration of the system a custom calibration plate has been designed. A known pattern has been imprinted on an electrical circuit board. When the circuit board is uniformly heated, it is possible, due to the emissivity difference, to visualize the pattern using the thermal camera. Fig.4.4 illustrates the heated calibration plate and its thermal image.

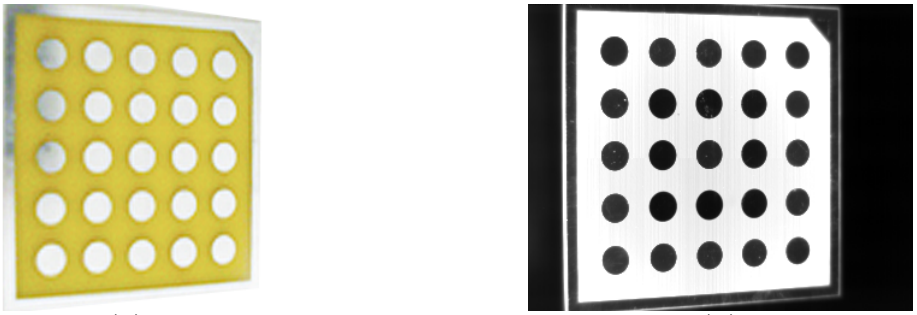

(a) (b)

Figure 4.4: (a) Custom calibration plate (b) Custom calibration plate, as seen by the thermal camera.

Given some initial values for the camera parameters, which are provided by the manufacturer, the known 3D locations of the circular calibration marks can be projected into the camera plane. Then, the camera parameters are determined such that the distance of the projections of the calibration marks and the mark locations extracted from the imagery is minimized. This minimization process returns fairly accurate values for the camera parameters. However, to obtain the camera parameters with the highest accuracy, it is essential that more than one image of the calibration plate is taken, where the plate is placed and rotated differently in each image to use all degrees of freedom of the exterior orientation (Fig.4.5).

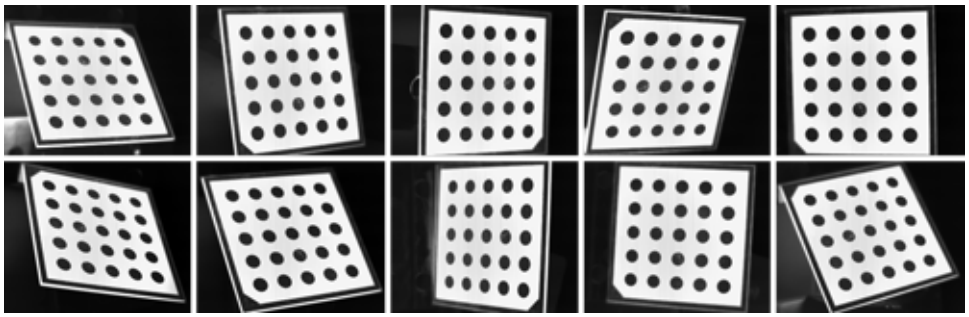

Figure 4.5: Calibration plate is placed and rotated differently in each image.

As a result of the calibration process, f, the focal length of the camera, κ, the radial distortion coefficient, S_x, the horizontal distance between two neighboring cells on the sensor, S_y, the vertical distance between two neighboring cells on the sensor, C_x, column coordinate of the image center point and, C_y, row coordinate of the image center point are determined.

4.4.4 Pre-determination of the Laser Power

The prediction of the laser power, to bring the surface of the object to a given temperature, is crucial to obtain a detectable heat zone without damaging the surface. Additionally the laser beam, in reality, has a given radius ($1.5mm$ for the experimental setup), and detection of the spot by the camera is complicated by the fact that the laser irradiation is observed as a surface heating zone and not a point. To predict the laser power and the heat distribution of the laser irradiation zone, we apply a mathematical model proposed by Jiao et al. for a glass plate heated by a CO_2 laser (Fig. 4.6) [51].

For a laser beam traveling in direction x at a constant velocity v, we consider the laser power to have a Gaussian distribution as in Eq. (4.7). We treat the CO_2

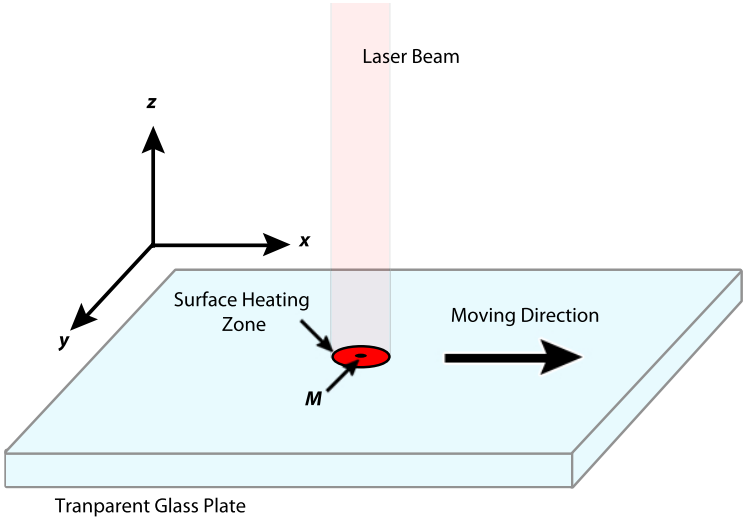

Figure 4.6: Heating model.

laser beam as a surface heating source, so the impulse function $\delta(z)$ is applied in Eq. (4.7).

$$I(x, y, z, t) = \frac{P_0}{\pi r^2} \exp\left(-\frac{(x - vt)^2 + y^2}{r^2}\right) \delta(z) \tag{4.7}$$

where P_0 and r are the power and the radius of the CO_2 laser beam respectively. Figure 4.7 presents the prediction of the model to heat a glass plate with an ambient temperature of 20 °C to 80 °C. The CO_2 laser has a focus of 1.5mm (half width), and the movement speed of the system is set to 10mm/second. The model predicts the laser power as 3W. The experimental results obtained with the same configuration and a 3W laser are also shown in Figure 4.7. The experimental results fit the model reasonably. The surface temperature increases rapidly when the glass enters the

heating region. The temperature reaches its peak at a position at the center of laser irradiation, where the highest laser intensity is imposed. Then it decreases sharply due to a high rate of cooling by radiation, air convection and conduction into the glass.

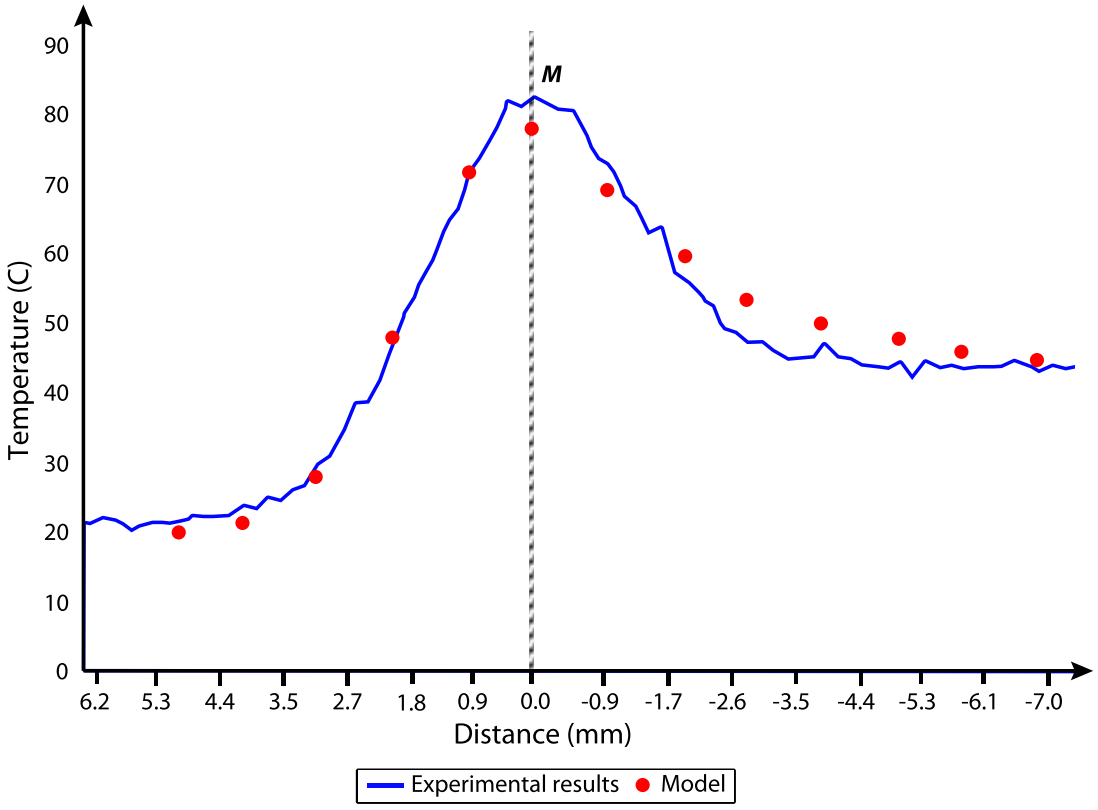

Figure 4.7: Experimental results compared to the heating model.

4.4.5 Detection of the Laser Irradiation

Detection of the laser irradiation is complicated by the fact that the laser beam in reality has a given radius and that the surface is heated at a region and not at a

single point. Additionally thermal cameras have low resolutions (320x240 pixels for the experimental setup) and images may contain some noise. However, we know from the heat model that the temperature reaches its peak at the center of laser irradiation zone. On the thermal image, this corresponds to the point with the highest intensity. To precisely detect this point we first apply a Gaussian filter to eliminate the noise on the image. The two dimensional Gaussian filter is defined by [52]:

$$G(x,y) = \frac{1}{2\pi\sigma^2} e^{-\frac{x^2+y^2}{2\sigma^2}} \tag{4.8}$$

In its discrete form for a 11x11 filter with $\sigma = 2.36$ the Gaussian kernel (x255) is given as:

$$\begin{bmatrix} 0.082 & 0.18 & 0.34 & 0.546 & 0.733 & 0.809 & 0.733 & 0.546 & 0.34 & 0.18 & 0.082 \\ 0.18 & 0.395 & 0.747 & 1.2 & 1.61 & 1.78 & 1.61 & 1.2 & 0.747 & 0.395 & 0.18 \\ 0.34 & 0.747 & 1.41 & 2.27 & 3.04 & 3.36 & 3.04 & 2.27 & 1.41 & 0.747 & 0.34 \\ 0.546 & 1.2 & 2.27 & 3.64 & 4.88 & 5.4 & 4.88 & 3.64 & 2.27 & 1.2 & 0.546 \\ 0.733 & 1.61 & 3.04 & 4.88 & 6.55 & 7.24 & 6.55 & 4.88 & 3.04 & 1.61 & 0.733 \\ 0.809 & 1.78 & 3.36 & 5.4 & 7.24 & 7.99 & 7.24 & 5.4 & 3.36 & 1.78 & 0.809 \\ 0.733 & 1.61 & 3.04 & 4.88 & 6.55 & 7.24 & 6.55 & 4.88 & 3.04 & 1.61 & 0.733 \\ 0.546 & 1.2 & 2.27 & 3.64 & 4.88 & 5.4 & 4.88 & 3.64 & 2.27 & 1.2 & 0.546 \\ 0.34 & 0.747 & 1.41 & 2.27 & 3.04 & 3.36 & 3.04 & 2.27 & 1.41 & 0.747 & 0.34 \\ 0.18 & 0.395 & 0.747 & 1.2 & 1.61 & 1.78 & 1.61 & 1.2 & 0.747 & 0.395 & 0.18 \\ 0.082 & 0.18 & 0.34 & 0.546 & 0.733 & 0.809 & 0.733 & 0.546 & 0.34 & 0.18 & 0.082 \end{bmatrix} \tag{4.9}$$

The graphical representation of the filter is illustrated in Fig.4.8.

The input image is then approximated by a quadratic polynomial in x and y and subsequently, the polynomial is examined for local maxima. This allows de-

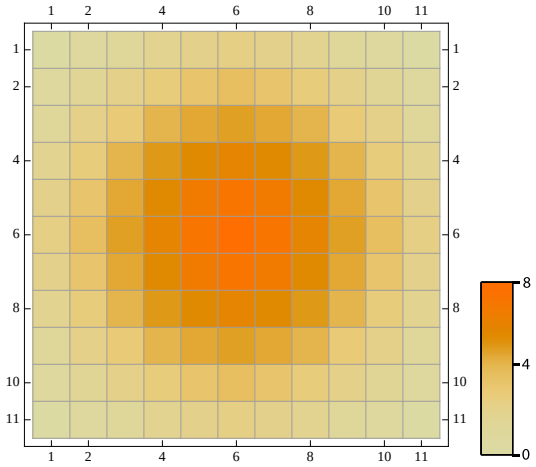

Figure 4.8: Graphical representation of the 11x11 Gaussian kernel with $\sigma = 2.36$ (x255).

termination of the point with sub-pixel precision. Figure 4.9 illustrates the result of the detection process. Once the maxima is determined, the world coordinates of the surface point are recovered using triangulation. The operation is repeated for each thermal image, for different positions of the moving platform, to obtain surface reconstruction of the object.

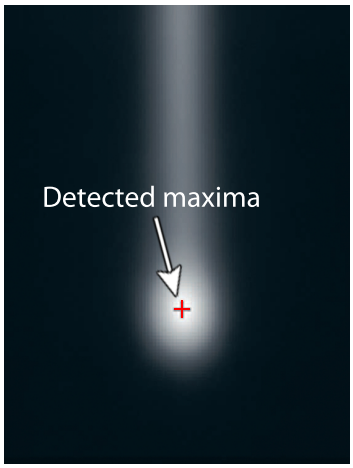

Figure 4.9: Result of the detection process.

4.5 Implementation and Experimental Results

4.5.1 Scanner Prototype

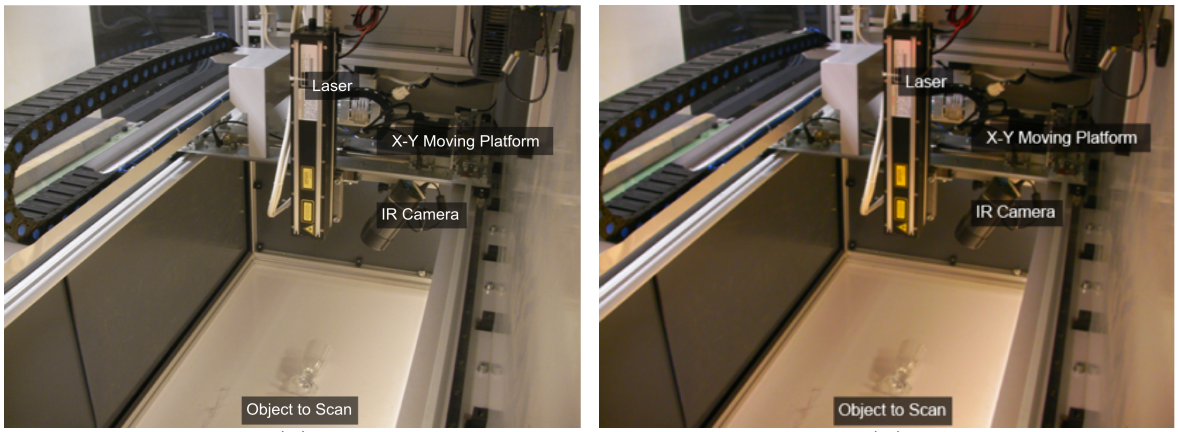

(a) (b)

Figure 4.10: (a) Conception of the scanner prototype (b) Realization of the scanner prototype (inside view).

A scanner which is able to reconstruct models of large objects up to 80x150x30cm in size, has been designed and implemented. The scanner uses a Synrad 48 Series 10W CO_2 Laser at 10.6μm as heating source. Thermal images are acquired with a Flir A320G LWIR Camera sensitive to 8 - 14 μm. The power of the laser is controlled by a Synrad UC2000 Laser Power Controller. The laser and thermal camera are placed on an x-y positioning system, which is programmable to scan a given area in predefined steps of x and y with a precision of 50μm (Fig.4.10). Additionally, the laser is set to fire continuously as it moves over the object during the scan, permitting acquisition of thermal images without stopping and the recovery of 3D points at the maximum speed of the camera (50fps).

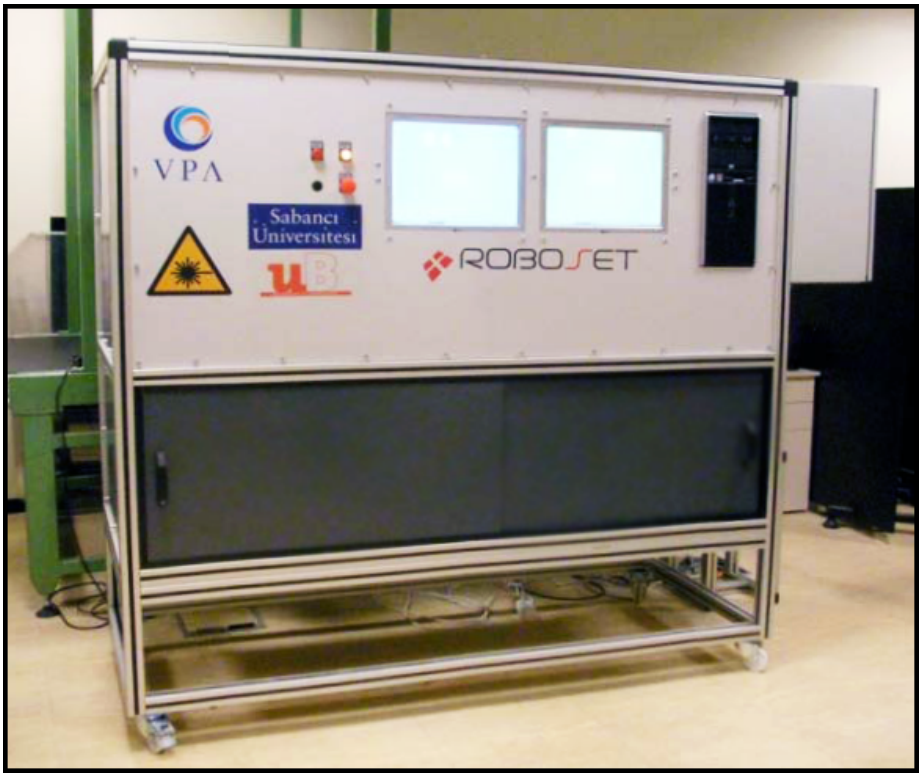

Figure 4.11: 3D scanner prototype based on *Scanning from Heating* (front view).

4.5.2 Results

To validate the *Scanning from Heating* method and to show its effectiveness, we present 3D scanning results of several objects, from a glass plate to complex surfaces. Furthermore the result obtained on a transparent plastic bottle is shown.

Transparent glass plate Figure 4.12 illustrates the results obtained by *Scanning from Heating* on a 10x5cm glass plate from 65 points. The distance between the camera and the plane is set to 50cm. The histogram of the deviation between the results and a perfect plane is presented. The average deviation is calculated as 150μm. This deviation is quite significant and permits us to validate the efficiency of the method.

Automotive Window Glass Figure 4.13 illustrates a glass window used in the automotive industry. Figure 4.14 illustrates its reconstruction by a probe scanner in comparison to the reconstruction by the *Scanning from Heating* method. The density of reconstruction obtained by the probe scanner (200 points) is much smaller than the reconstruction obtained by *Scanning from Heating* measurement (6000 points). Therefore the interpolation of the point cloud obtained with the probe scanner increases the estimated error. The average deviation between the two reconstructions is 360μm.

Glass Cup Figure 4.16 illustrates the 3D reconstruction of the transparent glass cup presented in Figure 4.15 by *Scanning from Heating* method. After being scanned the object is powdered with white dust and then re-scanned by Minolta VI-910 Non

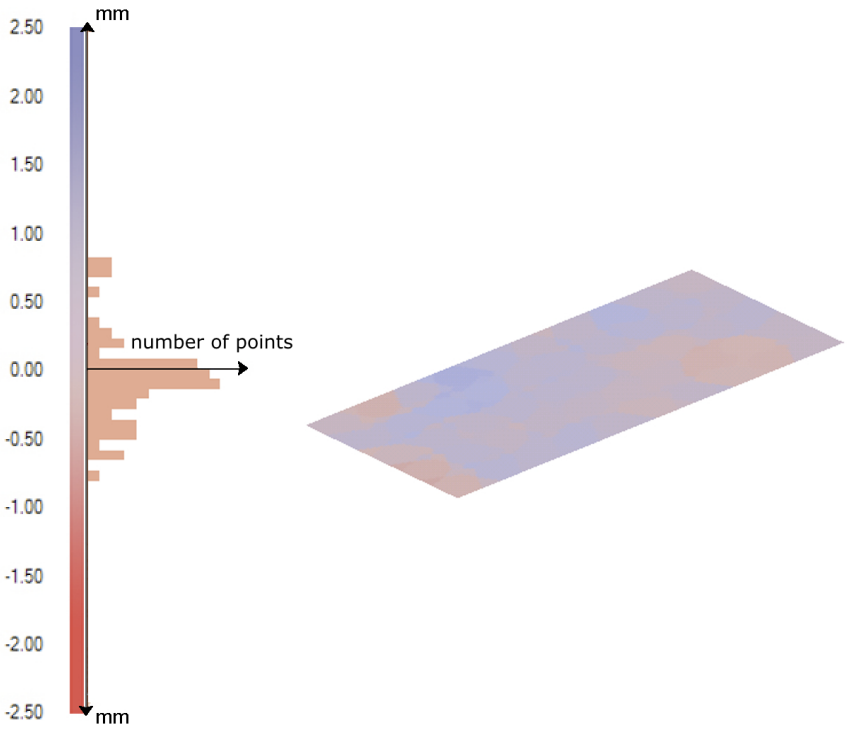

Figure 4.12: 3D reconstruction of the transparent glass plate, compared to a perfect plane.

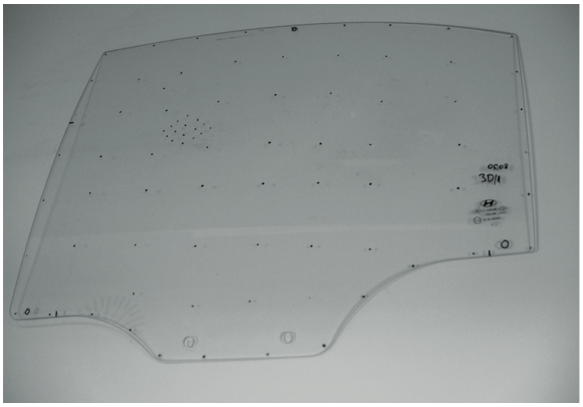

Figure 4.13: Car window.

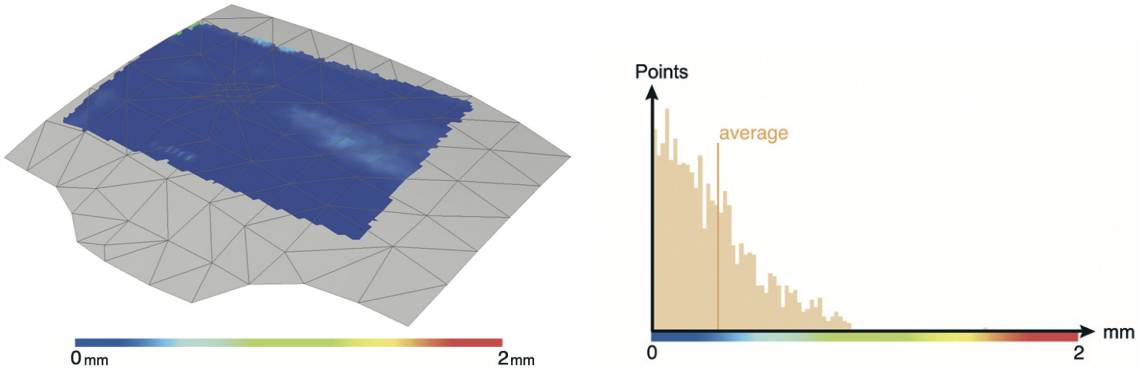

(a) (b)

Figure 4.14: (a) Reconstruction by a probe scanner in comparison to the reconstruction by the *Scanning from Heating* method. (b) Histogram of the difference between two reconstructions.

Figure 4.15: Glass cup.

Contact 3D Digitizer. To obtain a surface from the 3D points acquired from the *Scanning from Heating* scanner and from the Minolta scanner, the Rapidform software [53] is used. For the comparison, the software first aligns the two coordinates systems and then calculates the average deviation between polygon surfaces. Figure 4.16 presents 3D comparison of the reconstructions and the histogram of the deviation. The results fit reasonably well, and the average deviation is $210\mu m$. Differences between the two models are mostly located on the borders of the scanning region and are probably due to calibration errors in both reconstruction systems.

Complex Glass Objects Figure 4.17 illustrates the results obtained from the scanning of a complex transparent glass object 7x7x15cm in size from 2100 points and Figure 4.18 illustrates the results obtained from another complex transparent glass object 9x9x14cm in size from 1300 points. Hence, the system is applicable to wide range of objects ranging from flat surfaces in the automotive industry to more complex objects in the packaging industry.

Application to Plastic It is also possible to apply the *Scanning from Heating* method to different transparent materials. Figure 4.19 illustrates 3D reconstruction of a plastic bottle by *Scanning from Heating* method and compares the result to the 3D reconstruction obtained by Minolta 3D Laser Scanner . The average deviation is determined as $200\mu m$.

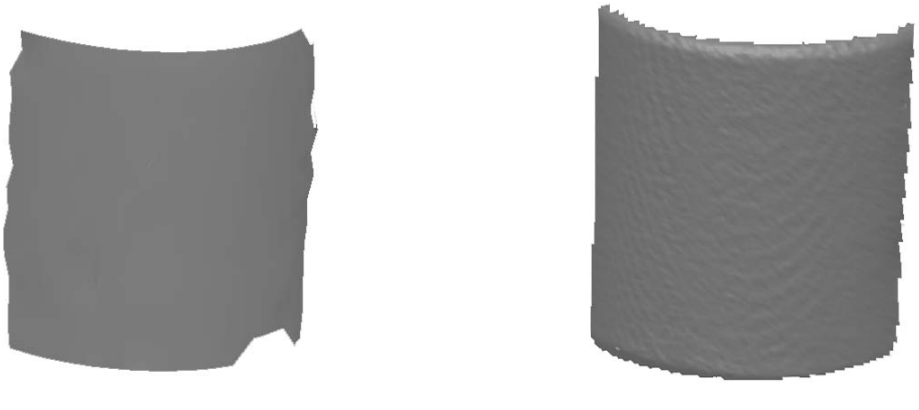

(a) (b)

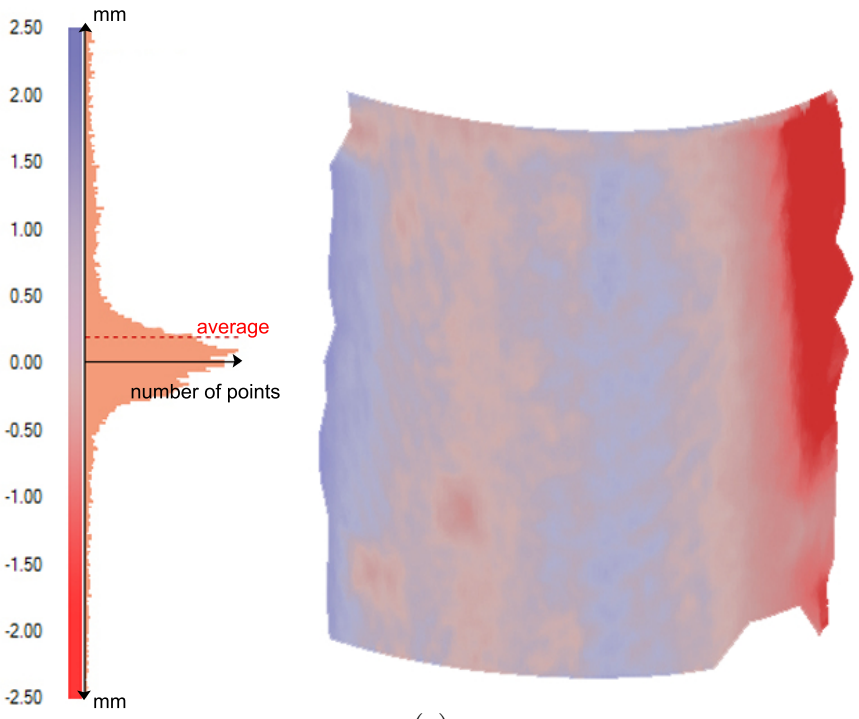

(c)

Figure 4.16: (a) 3D reconstruction of the transparent glass cup presented in Fig.4.15 by the *Scanning from Heating* method, (b) 3D reconstruction of the transparent glass cup, after being powdered, by the Minolta 3D Laser Scanner, (c) 3D comparison of the reconstructions and the histogram of the deviation.

(a) (b)

Figure 4.17: (a) Transparent glass object, (b) 3D reconstruction by *Scanning from Heating* method

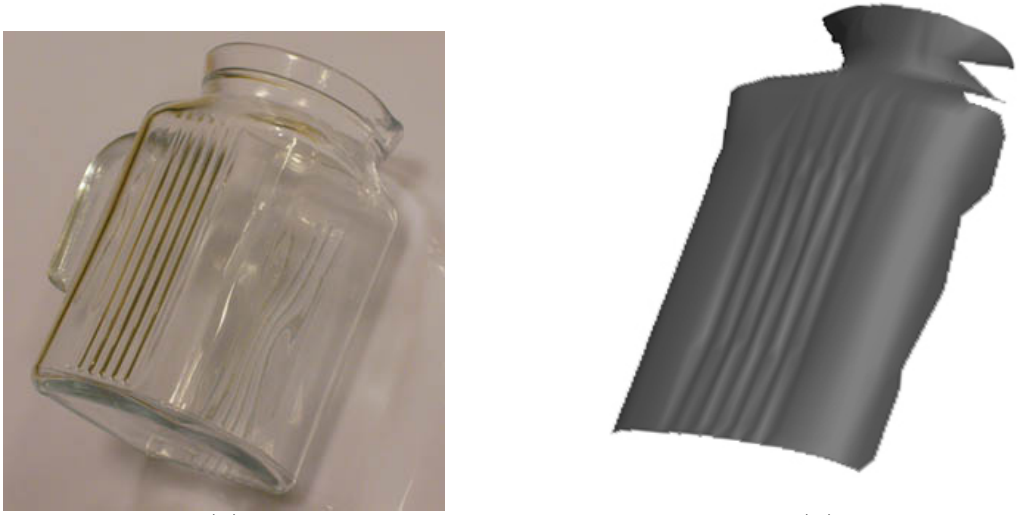

(a) (b)

Figure 4.18: (a) Transparent glass object, (b) 3D reconstruction *Scanning from Heating* method

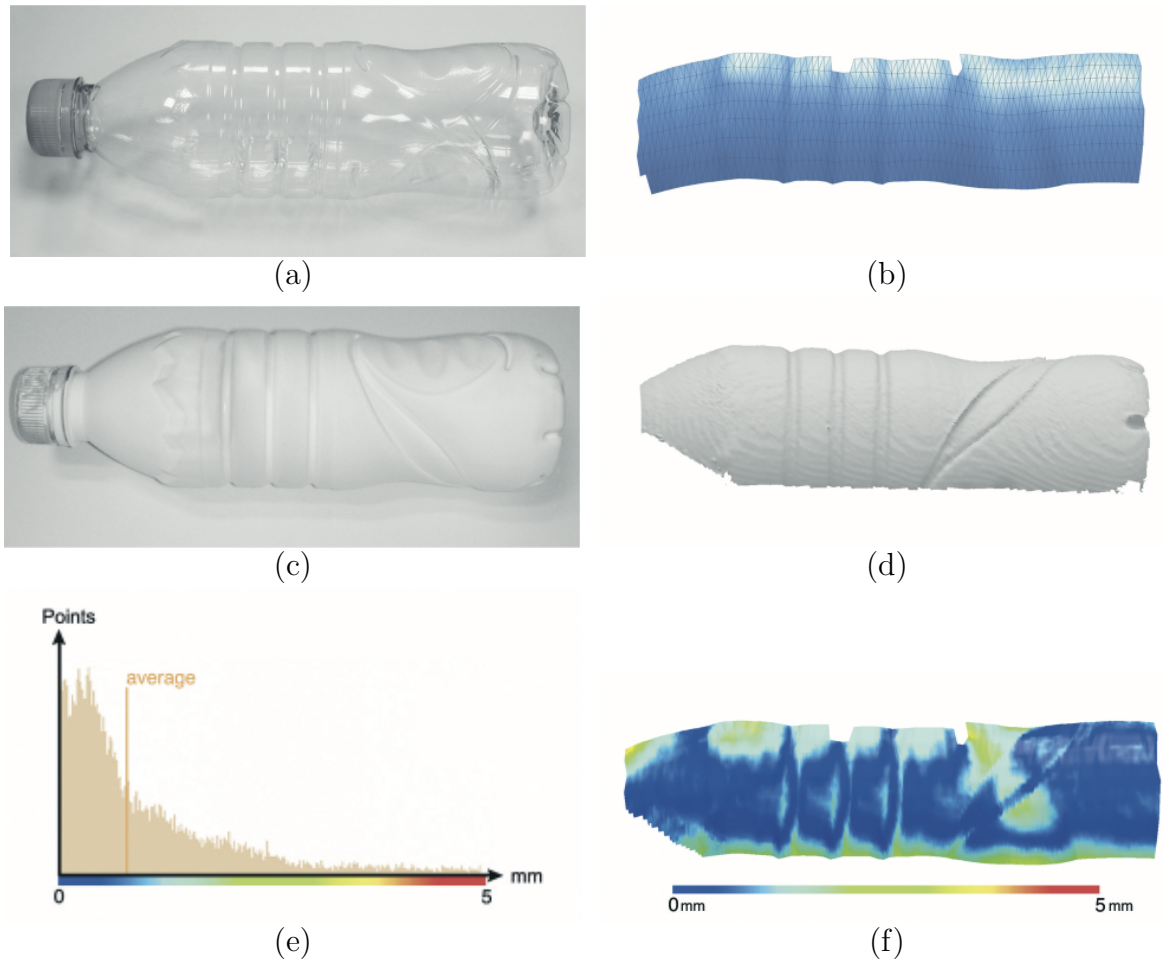

Figure 4.19: (a) Transparent plastic bottle. (b) Reconstruction obtained by the SFH method. (c) Powdered plastic bottle. (d) Reconstruction of powdered bottle obtained by a Minolta VI-910 Non Contact 3D Digitizer. (e) Histogram of the difference between the two reconstruction. (f) 3D representation of the difference between the two reconstructions.

4.5.3 Line Projection

An application of *Scanning from Heating* method using a laser line projection system has been realized in collaboration with Prof. F. Mériaudeau, Prof. D. Fofi and L. Alonso Sánchez Secades from LE2I Laboratory [54]. Figure 4.20 illustrates the experimental setup. A $400mW$ CO_2 laser is used as heating source. A line generator lens is placed in front of the laser. A FLIR S40 LWIR Camera is used to acquire thermal images. On each thermal image, the line corresponding to the laser heating zone, is extracted and the 3D profile is calculated.

Figure 4.21 presents the experimental results obtained on a wine glass. The glass was translated in front of the experimental system by using steps of 1mm along the x direction. The object is then coated with white powder to be able to be scanned by an conventional laser scanner. Figure 4.22 illustrates the comparison of the reconstruction to the one obtained on Minolta VI-910 Non Contact 3D Digitizer. The average deviation is calculated as $210\mu m$.

4.6 Conclusion

We have presented in this chapter our new method, called *Scanning from Heating*, to determine the surface shape of transparent objects using laser heating and thermal imaging. When the object is opaque to the laser source, the surface is heated at the impact zone. The laser irradiation is observed with an infrared camera, and 3D coordinates of the surface at that point are computed using triangulation and the initial calibration of the system.

We have discussed the application of the method on transparent glass objects and

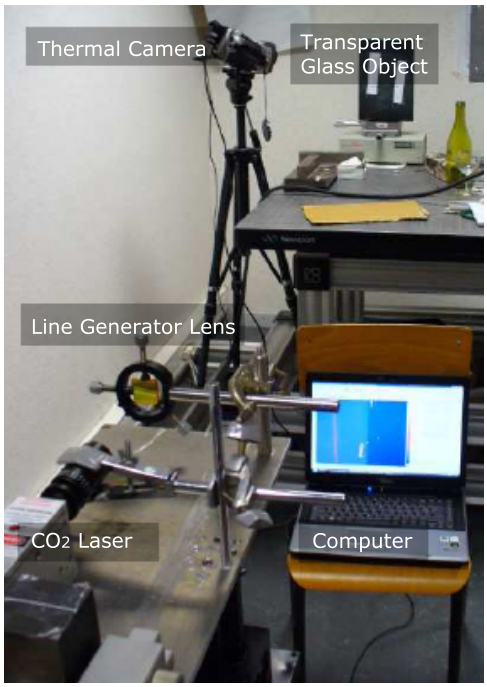

Figure 4.20: Experimental setup for the laser line projection system based on *Scanning from Heating*.

(a) (b) (c)

Figure 4.21: (a) Transparent wine glass, (b) reconstruction by *Scanning from Heating*, (c) the object is coated with white powder to be able to be scanned by an conventional laser scanner.

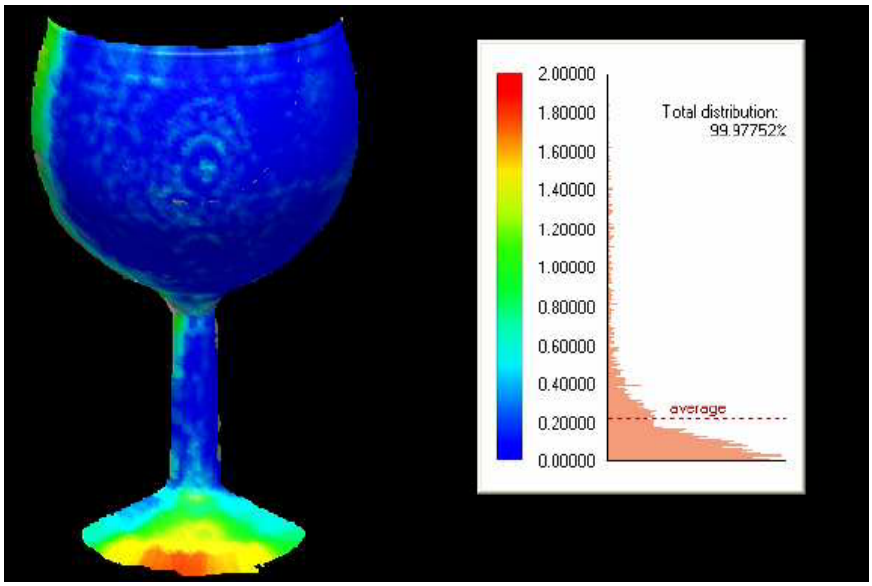

Figure 4.22: 3D reconstruction and error map of the scanned wine glass, scale from 0 to 2 mm. The results are compared to Minolta VI-910 Non Contact 3D Digitizer.

presented a scanner prototype based on *Scanning from Heating* method. The scanner was implemented and tested on diverse glass objects. Experiments show that the quality of the reconstructed models is accurate as conventional laser scanners in the visible domain when the object is coated by white powder. While we have studied only the application to transparent glass, the results show that extension to other transparent materials, such as plastic, is possible.

Finally the line projection application demonstrates that it is feasible to develop, based on *Scanning from Heating* method, several systems similar to commercial scanners working in the visible domain, to acquire surface profiles of transparent objects. Thus, the method holds promise for a wide range of industrial applications.

In the next chapter we present the extension to *Scanning from Heating* which allows us to determine the surface normal at the laser impact zone.

5 RECOVERY OF SURFACE NORMALS BASED ON SCANNING FROM HEATING

5.1 Introduction

As a result of a scanning process, a 3D scanner provides a set of 3D points $P(x, y, z)$, where x, y and z represents the coordinates of the point in the world coordinate system. To obtain a continuous smooth surface, new data points within the range of the discrete set are constructed. This process is called interpolation. There exist a variety of techniques for interpolation depending on the application and the properties of acquired 3D data points [55]. In this chapter, we first present some principal interpolation methods. We discuss how the recovery of surface normals can be used for a better surface reconstruction. Furthermore, we demonstrate the extension to *Scanning from Heating* method to recover the surface normals, in addition to the 3D coordinates. The surface normals are calculated using the isotherms formed during the heating process. We suppose that the surface of the object is locally flat at the laser impact zone, and the isotherms have a circular propagation. Using a calibrated acquisition system, we determine the 3D pose of these isotherms on the surface of the object and deduce the surface normals. Experimental setup and results are presented at the end of the chapter.

5.2 Interpolation and Surface Normals

The following paragraphs discuss some key interpolation methods, such as linear interpolation, bi-linear interpolation and bezier curves. Moreover, we introduce a technique to construct bezier surfaces from 3D points and their normal vectors.

5.2.1 Linear Interpolation

A basic approach for interpolation is the linear one where a straight line between two neighbor points is determined. Given two arbitrary points P_0 and P_1, the parametric representation of the line segment from P_0 to P_1 is given by

$$P(t) = (1-t)P_0 + tP_1 = P_0 + (P_1 - P_0)t = P_0 + td, 0 \leq t \leq 1 \qquad (5.1)$$

Figure 5.1 shows a 2D example of linear interpolation. In 3D the linear interpolation can be used to obtain a polygonal surface, constructed of triangles, which is the simplest type of surface (Fig.5.2).

5.2.2 Bilinear Interpolation

The bilinear surface is the simplest nonflat (curved) surface which it is fully defined by means of its four corner points P_{00}, P_{01}, P_{10}, and P_{11}. The top and bottom boundary curves are straight lines and are given by $P(u,0) = P_{10} - P_{00}u + P_{00}$ and $P(u,1) = P_{11} - P_{01}u + P_{01}$. To linearly interpolate between these boundary curves, we first calculate two corresponding points on each curve $P(u_0,0) = (P_{10} - P_{00})u_0 + P_{00}$ and $P(u_0,1) = (P_{11} - P_{01})u_0 + P_{01}$, then connect them with a straight line $P(u_0,w) = (P(u_0,1) - P(u_0,0))w + P(u_0,0)$. The expression for the entire surface is given by:

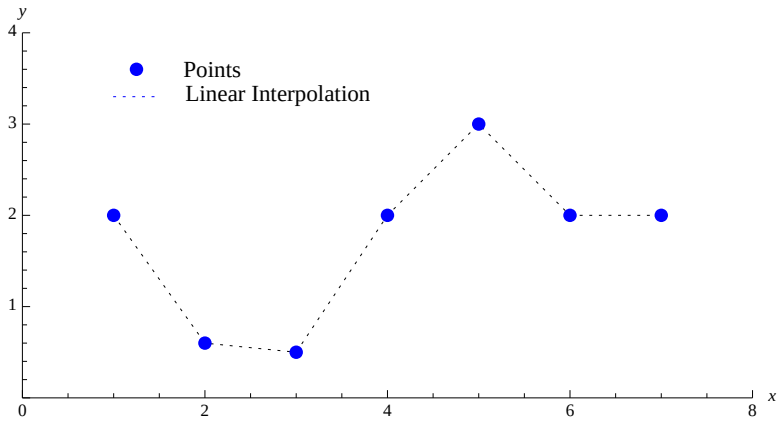

Figure 5.1: Linear interpolation.

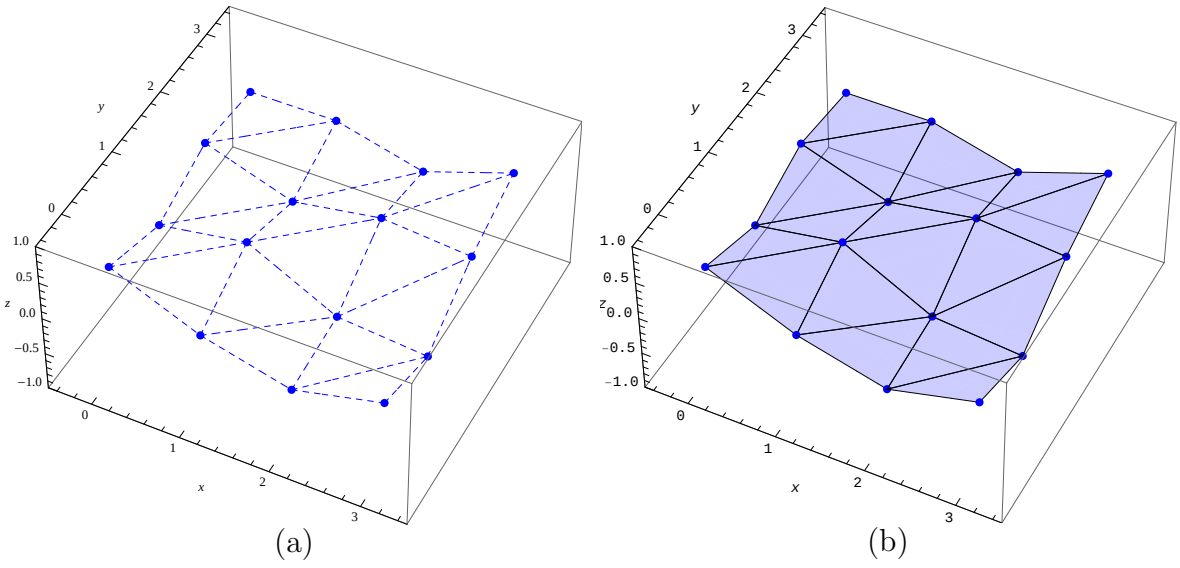

Figure 5.2: (a) 3D points and linear interpolants, (b) 3D polygon surface.

$$
\begin{aligned}
P(u,w) &= P_{00}(1-u)(1-w) + P_{01}(1-u)w + P_{10}u(1-w) + P_{11}uw \\
&= \sum_{i=0}^{1}\sum_{j=0}^{1} B_{1i}(u)P_{ij}B_{1j}(w) \\
&= [B_{10}(u), B_{11}(u)] \begin{bmatrix} P_{00} & P_{01} \\ P_{10} & P_{11} \end{bmatrix} \begin{bmatrix} B_{10}(w) \\ B_{11}(w) \end{bmatrix} \qquad (5.2)
\end{aligned}
$$

where the functions $B_{1i}(t)$ are the Bernstein polynomials of degree 1. Figure(5.4) illustrates the bilinear surface obtained from the same points presented in Fig.(5.2.a).

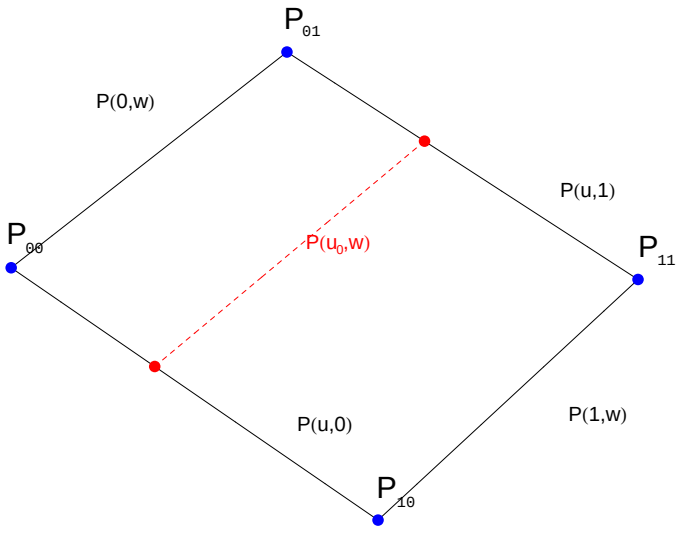

Figure 5.3: Bilinear interpolation.

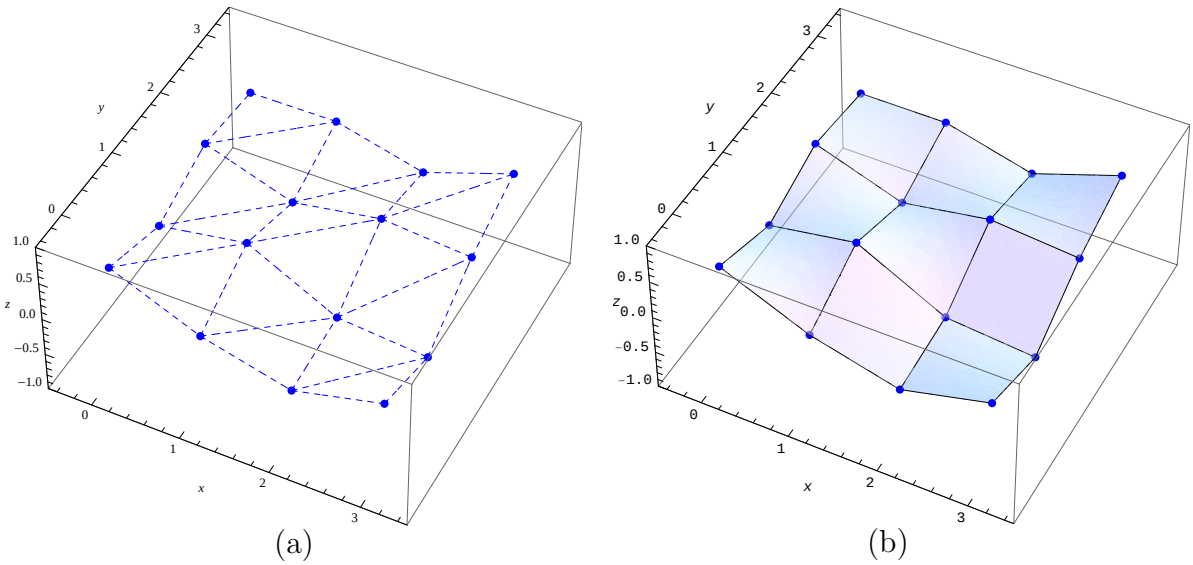

Figure 5.4: (a) 3D points and linear interpolants, (b) Bilinear surface.

5.2.3 Bezier Interpolation

The Bezier curve is a parametric curve $P(t)$ that is a polynomial function of the parameter t. The degree of the polynomial depends on the number of points used to define the curve. The method employs control points and produces an approximating curve. The curve does not pass through the interior points but is attracted by them. Each point influences the direction of the curve by pulling it toward itself, and that influence is strongest when the curve gets nearest the point. Figure 5.5 shows an example of cubic Bezier curve. Such a curve is defined by four points and is a cubic polynomial.

Given a set of $n+1$ control points $P_0, P_0, ..., P_n$ the corresponding Bezier curve (or Bernstein-Bezier curve) is given by

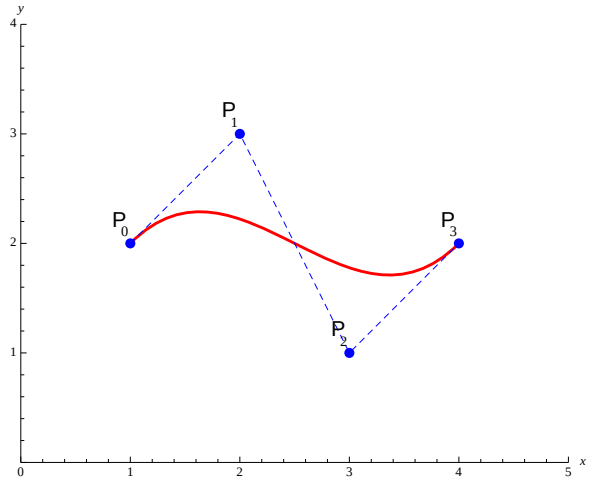

Figure 5.5: A Bezier curve and its control points.

$$C(t) = \sum_{i=0}^{n} P_i B_{i,n}(t) \tag{5.3}$$

where $t \in [0, 1]$ and $P_i B_{i,n}(t)$ is a Bernstein polynomial which is defined by

$$B_{i,n}(t) = \binom{n}{i} t^i (1-t)^{n-i}, \text{where } \binom{n}{i} = \frac{n!}{i!(n-i)!} \tag{5.4}$$

Figure 5.6 illustrates Bernstein basis functions of degree 3.

The Bezier curve always passes through the first and last control points and lies within the convex hull of the control points. The curve is tangent to $P_1 - P_0$ and $P_n - P_{n-1}$ at the endpoints.

Connection of Two Bezier Curves The Bezier curve is a polynomial of degree n, which makes it slow to compute for large values of n. It is therefore preferable

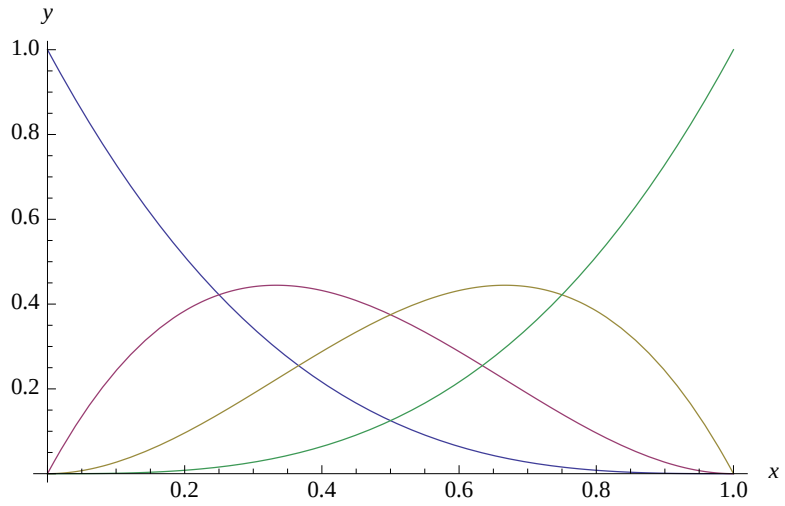

Figure 5.6: Bernstein basis functions of degree 3.

to connect several Bezier segments, each defined by a few points, typically four, into one smooth curve. Lets assume P and Q, two Bezier curves defined respectively by the control points $P_0, P_1, ..., P_n$ and $Q_0, Q_1, ..., Q_n$. The extreme tangent vectors of the Bezier curve satisfy:

$$\begin{aligned} Q^t(0) &= m(Q_1 - Q_0), \\ P^t(1) &= n(P_n - P_{n-1}) \end{aligned} \tag{5.5}$$

The condition for smooth connection of two such segments is given by:

$$\begin{aligned} Q_t(0) &= P_t(1) \\ mQ_1 - mQ_0 &= nP_n - nP_{n-1} \end{aligned} \tag{5.6}$$

Substituting $Q_0 = P_n$ yields:

$$P_n = \frac{m}{m+n}Q_1 + \frac{n}{m+n}P_{n-1} \tag{5.7}$$

The three points P_{n-1}, P_n, and Q_1 must therefore be dependent. Hence, the condition for smooth linking is that the three points P_{n-1}, P_n, and Q_1 be collinear (Fig 5.7).

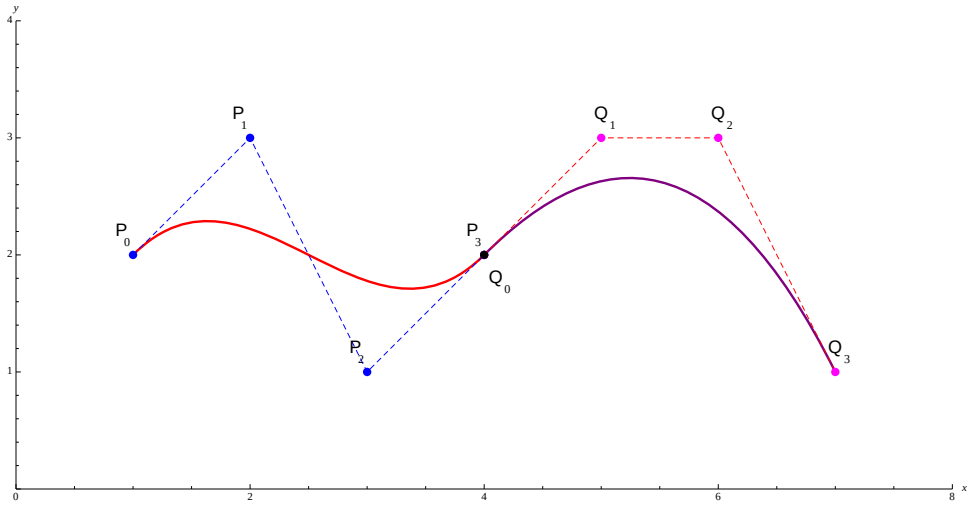

Figure 5.7: Smooth connection of two Bezier curves.

5.2.4 Bezier Curve and Normal Vectors

It is possible to construct a Bezier curve from two points and their normal vectors. We propose the following procedure to calculate the control points and to trace the curve.

Let's assume two points $P_1(x_1, y_1)$,$P_2(x_2, y_2)$ and their respective normal vectors

$N_1(x_{N_1}, y_{N_1})$,$N_2(x_{N_2}, y_{N_2})$ (Fig.5.8). We want to determine two control points using normal vectors to trace a Bezier curve between P_1 and P_2

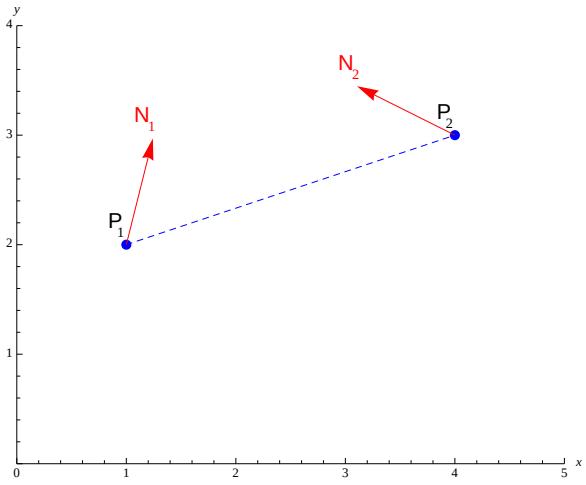

Figure 5.8: Two points and their respective normal vectors.

We first define two points $D_1(x_{D_1}, y_{D_1})$ and $D_2(x_{D_2}, y_{D_2})$ on the line passing by P_1 and P_2 as:

$$D_1 = P_1 + \frac{1}{3}(P_2 - P_1) = (\frac{2}{3}x_1 + \frac{1}{3}x_2, \frac{2}{3}y_1 + \frac{1}{3}y_2)$$
$$D_2 = P_1 + \frac{2}{3}(P_2 - P_1) = (\frac{1}{3}x_1 + \frac{2}{3}x_2, \frac{1}{3}y_1 + \frac{2}{3}y_2) \quad (5.8)$$

The selection of these points can be modified depending on the application. Selection of a different D_1 and D_2 will result in different control points for the reconstruction of the bezier curve.

We define K_1 and K_2 the lines perpendicular to the line P_1P_2 passing respectively through the points D_1 and D_2:

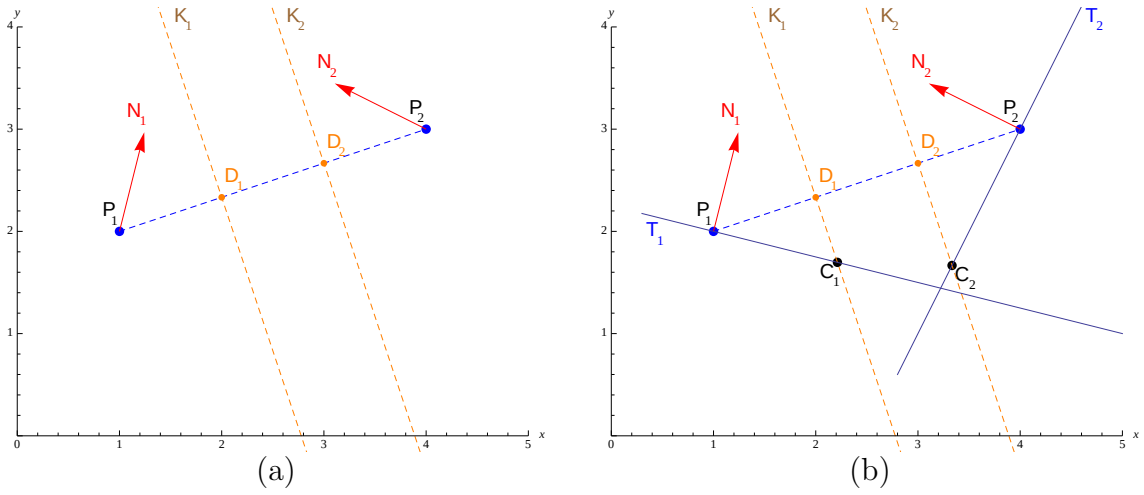

Figure 5.9: Construction of a Bezier curve from two points and their normal vectors.

$$
\begin{aligned}
K_1 : y &= -\frac{x_2 - x_1}{y_2 - y_1}(x - x_{D_1}) + y_{D_1} \\
&= -\frac{x_2 - x_1}{y_2 - y_1}(x - (\frac{2}{3}x_1 + \frac{1}{3}x_2)) + \frac{2}{3}y_1 + \frac{1}{3}y_2 \\
K_2 : y &= -\frac{x_2 - x_1}{y_2 - y_1}(x - x_{D_2}) + y_{D_2} \\
&= -\frac{x_2 - x_1}{y_2 - y_1}(x - (\frac{1}{3}x_1 + \frac{2}{3}x_2)) + \frac{1}{3}y_1 + \frac{2}{3}y_2 \qquad (5.9)
\end{aligned}
$$

The equations of the tangent lines T_1 and T_2 passing respectively through the points P_1 and P_2 are (Fig.5.9):

$$
T_1 : y = -\frac{x_{N_1}}{y_{N_1}}(x - x_1) + y_1
$$

$$T_2 : y = -\frac{x_{N_2}}{y_{N_2}}(x - x_2) + y_2 \tag{5.10}$$

We call C_1 the intersection of the lines K_1 and T_1; and C_2 the intersection of the lines K_2 and T_2 which are given by:

$$\begin{aligned} C_1(x_{C_1}, y_{C_1}) &= (\frac{m_2 x_1 - m_1 x_{D_1} - y_1 + y_{D_1}}{m_2 - m_1}, \\ &\quad \frac{m_2^2 x_1 - m_1 m_2 x_{D_1} - m_2 y_1 + m_2 y_{D_1}}{m_2 - m_1} - m_2 x_1 + y_1) \end{aligned} \tag{5.11}$$

$$\begin{aligned} C_2(x_{C_2}, y_{C_2}) &= (\frac{m_3 x_2 - m_1 x_{D_2} - y_2 + y_{D_2}}{m_3 - m_1}, \\ &\quad \frac{m_3^2 x_2 - m_1 m_3 x_{D_2} - m_3 y_2 + m_3 y_{D_2}}{m_2 - m_1} - m_3 x_2 + y_2) \end{aligned} \tag{5.12}$$

with

$$\begin{aligned} m_1 &= -\frac{(x_2 - x_1)}{(y_2 - y_1)} \\ m_2 &= -\frac{x_{N_1}}{y_{N_1}} \\ m_3 &= -\frac{x_{N_2}}{y_{N_2}} \end{aligned} \tag{5.13}$$

Using P_1, P_2, and the calculated control points C_1 and C_2 the Bezier curve is traced. The procedure places the control points on the tangent lines at the end-points of the curve. This verifies the continuity condition between two Bezier curves, discussed in the previous paragraphs.

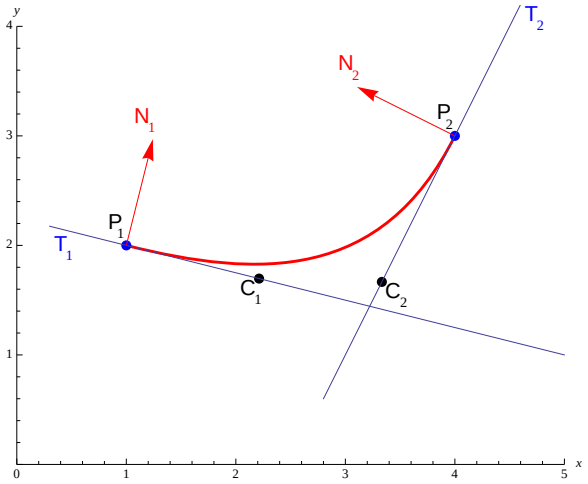

Figure 5.10: Result of the applied technique to reconstruct a Bezier curve from two points and normal vectors.

5.2.5 Bezier Surfaces

The Bezier surface patch, like the Bezier curve, is popular and is commonly used in practice. A rectangular Bezier surface patch is defined by a grid of $(m+1)(n+1)$ control points and is given by:

$$\begin{aligned} P(u,w) &= \sum_{i=0}^{m}\sum_{j=0}^{n} B_{m,i}(u)P_{i,j}B_{n,j}(w) \\ &= (B_{m,0}(u), B_{m,1}(u), ..., B_{mm}(u))\mathbf{P}\begin{pmatrix} B_{n,0}(w) \\ B_{n,1}(w) \\ \vdots \\ B_{n,n}(w) \end{pmatrix} \\ &= B_m(u)\mathbf{P}B_n(w) \end{aligned} \tag{5.14}$$

where,

$$\mathbf{P} = \begin{bmatrix} P_{0,0} & P_{0,1} & \cdots & P_{0,n} \\ P_{1,0} & P_{1,1} & \cdots & P_{1,n} \\ \vdots & \vdots & \ddots & \vdots \\ P_{m,0} & P_{m,1} & \cdots & P_{m,n} \end{bmatrix} \tag{5.15}$$

The surface patch is anchored at the four corner points and employs the other grid points to determine its shape. Figure 5.11 illustrates the bezier surface obtained from the same points presented in Fig.5.2.

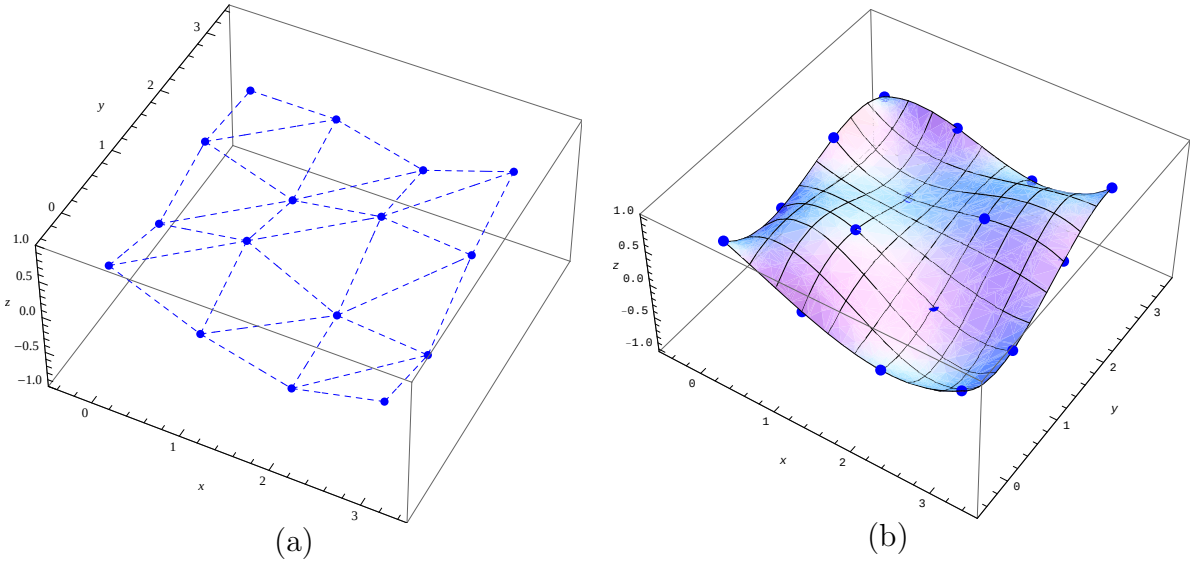

Figure 5.11: (a) 3D points and linear interpolants, (b) Bezier surface from the same points.

5.2.6 Bezier Surfaces and Normal Vectors

To obtain a 3D surface from the determined 3D point coordinates and the normal vectors at these points, we propose to construct rectangular bezier surface patches. To achieve this, we propose the following technique:

From four points $P_1(x_1, y_1, z_1)$, $P_2(x_2, y_2, z_2)$, $P_3(x_3, y_3, z_3)$, $P_4(x_4, y_4, z_4)$ and from their respective normal vectors $N_1(x_{n1}, y_{n1}, z_{n1})$, $N_2(x_{n2}, y_{n2}, z_{n2})$, $N_3(x_{n3}, y_{n3}, z_{n3})$, $N_4(x_{n4}, y_{n4}, z_{n4})$, the additional twelve control points, which are necessary to define the bezier surface patch are determined. To do so, for each point, three planes parallel to z axis and passing respectively by the three other points are defined. A plane passing by two points P_i and P_j parallel to z axis is given by:

$$K_{ij} : \begin{vmatrix} x - x_j & y - y_j & z - z_j \\ x_i - x_j & y_i - y_j & z_i - z_j \\ 0 & 0 & 1 \end{vmatrix} = 0 \tag{5.16}$$

For example for P_2, the three planes are defined as:

$$K_{21} : \begin{vmatrix} x - x_1 & y - y_1 & z - z_1 \\ x_2 - x_1 & y_2 - y_1 & z_2 - z_1 \\ 0 & 0 & 1 \end{vmatrix} = 0$$

$$K_{23} : \begin{vmatrix} x - x_3 & y - y_3 & z - z_3 \\ x_2 - x_3 & y_2 - y_3 & z_2 - z_3 \\ 0 & 0 & 1 \end{vmatrix} = 0$$

$$K_{24} : \begin{vmatrix} x - x_4 & y - y_4 & z - z_4 \\ x_2 - x_4 & y_2 - y_4 & z_2 - z_4 \\ 0 & 0 & 1 \end{vmatrix} = 0 \tag{5.17}$$

Then the projection of the normal vectors on these planes are determined. The projection of a normal vector N_i on the plane K_{ij} is given by:

$$(N_i.u)u + (N_i.\frac{v_{ij}}{|v_{ij}|})v_{ij} \tag{5.18}$$

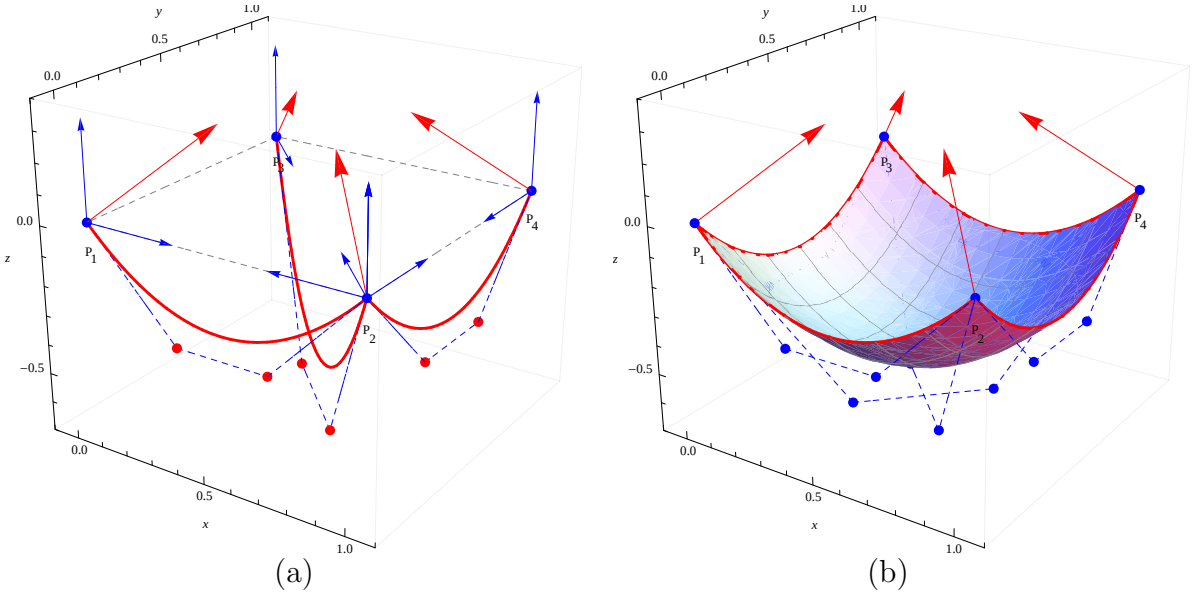

Figure 5.12: (a) Construction of Bezier surface control points from normal vectors, (b) Bezier surface patch from the same points.

where,

$$\begin{aligned} u &= \{0, 0, 1\} \\ v &= \{x_j - x_i, y_j - y_i, 0\} \end{aligned} \tag{5.19}$$

On each plane K_{ij}, the problem is then reduced to 2D determination of the control points from two points P_i and P_j and the projection of their respective normal vectors N_i and N_j on K_{ij}. The aforementioned technique in Section 5.2.4 is applied to obtain the control points. Figure 5.12 illustrates the process and presents the results obtained from four points and their normal vectors.

The condition for smooth joining of the two surface patches is that the two tangent vectors at the common boundary are in the same direction, although they may have

different magnitudes [55]. The process, by definition, uses normal vectors to obtain the control points and naturally validates the conditions necessary for smooth joining of bezier surface patches.

Figure 5.13 illustrates the 3D data points presented in Fig.5.2, the 3D Bezier surface passing through these points, and the surface obtained with the normal vectors. The interpolation obtained only from the points does not have any information about the curvature of the surface in between the acquired points. As a consequence, we obtain a smooth surface. On the other hand, when the normal vectors are used, the reconstruction takes into account the curvature, and a surface which fits better the real data is obtained.

5.3 Recovery of Surface Normals from Isotherms

The *Scanning from Heating* method, to recover the 3D positions of the points on the surface of a transparent object, makes use of a laser heating source and creates a temperature difference at a point on the surface. If we suppose the surface locally flat at the impact point, and the object isotropic and homogeneous, the heat propagation by conduction is given by Fourier's law as:

$$\frac{\delta u}{\delta t} = \alpha \left(\frac{\delta^2 u}{\delta x^2} + \frac{\delta^2 u}{\delta y^2} + \frac{\delta^2 u}{\delta z^2} \right) \tag{5.20}$$

where $u = u(x, y, z, t)$ is the temperature as a function of space and time and $\alpha = \frac{k}{c_p \varrho}$ is the thermal diffusivity with k, the thermal conductivity, ϱ, the mass density, and c_p, the heat capacity. This presumes, on the surface of the object, where $z = 0$, that the propagation in x and y directions are equal. As a consequence,

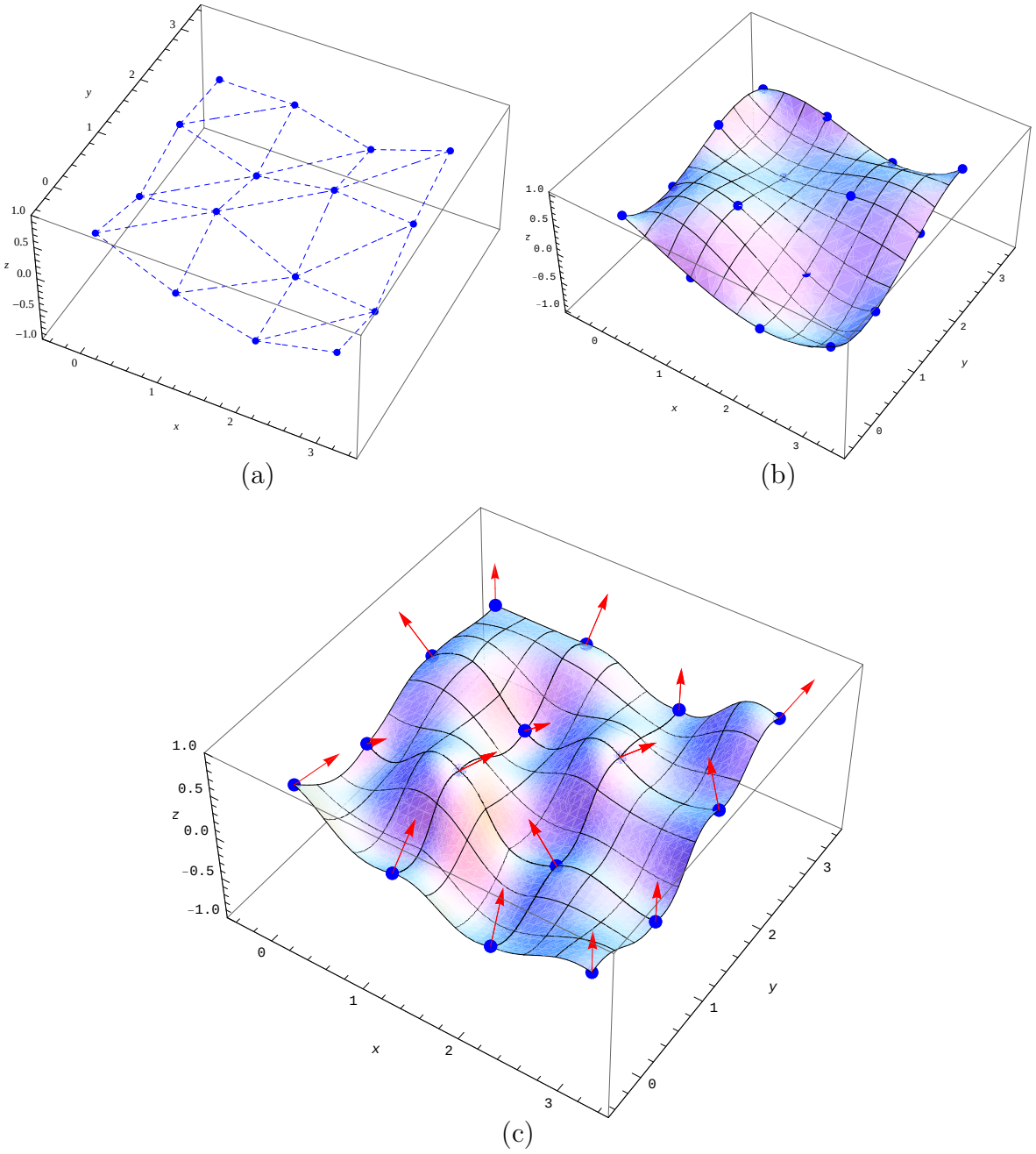

Figure 5.13: Comparison of the interpolation using normal vectors (a) 3D points and linear interpolation, (b) Bezier surface passing from the same points, (c) The Bezier surface obtained using normal vectors.

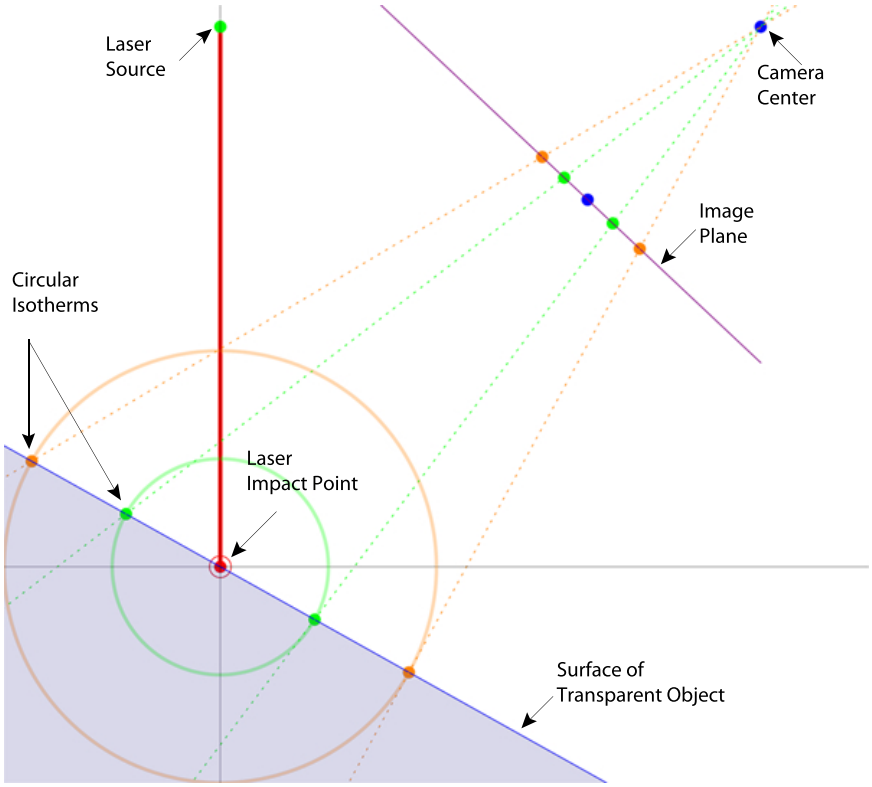

Figure 5.14: 2D representation of the technique to recover surface normals based on *Scanning from Heating* method.

circular isotherms, points of equal temperature, are formed on the surface around the impact point. When observed with a thermal camera, these isotherms corresponds on the image to the pixels with the same intensities. In the perspective camera model, a projected circle appears as an ellipse in the image plane, and the 3D pose of the circle can be extracted from a single image using the inverse projection model of a calibrated camera [56]. Therefore, it is possible to recover from a isotherm and a calibrated acquisition system, the surface normal at the laser impact point. Figure 5.14 illustrates the 2D representation of the technique.

5.3.1 Assumptions

For the extension of the *Scannning From Heating* method to recover the surface normals, the following assumptions are made:

1. The transparent object is supposed to be homogenous, i.e. uniform in structure and composition, and isotropic, i.e. the physical properties of the material are independent of direction.

2. The surface of the object is locally supposed to be flat and consequently the propagation of the heat on the surface from the laser impact point is considered to be circular.

3. To be able to recover the 3D pose of the circle from the detected ellipse on the image plane, the interior camera parameters are supposed to be known. These parameter are recovered from an initial calibration of the acquisition system.

5.3.2 Calibration of the Acquisition System

Camera calibration is defined as the determination of the parameters that model the optical projection of a 3D world point $P_w = (x_w, y_w, z_w)$ into pixel coordinates (r, c) in the image. The process has previously been described in Chapter 3. To recover the internal and external camera parameters, known 3D points are projected in the image and the sum of the squared distance between these projections and the corresponding image points is minimized. If the minimization converges, the interior and exterior camera parameters are determined. The minimization process

of the calibration depends on the initial values of the interior and exterior camera parameters. These initial parameters are usually provided by the manufacturer.

5.3.3 Determination of the Ellipse Equation

The circular isotherms formed due to the heating of the surface appears as ellipses on the thermal image. The equation of these ellipses is necessary for the determination of the 3D circle pose. There exist several methods to determine the equation of an ellipse on an image [57]. Depending on the input data, required accuracy and computational time, different methods can be applied. For example, one of the most commonly used methods is selecting a set of points on the contour of the ellipse on the image and using a least square approach to find out the equation of the ellipse passing through these points minimizing the algebraic distance $ax_i^2+bx_iy_i+cy_i^2+dx_i+ey_i+f$ between the contour points (x_i, y_i) and the resulting ellipse [57]. However, to obtain accurate results with this technique many points have to be used, complicating the calculations and increasing the computational time.

We propose first to extract an isotherm using thresholding and to calculate the moments of the resultant image. Using the first and second order moments, we can easily determine the parameters of the ellipse, and find out its equation on the image plane. The moments M_{00}, M_{10} and M_{01} on an image f of size m x n are defined as:

$$M_{00} = \sum_{i=1}^{n}\sum_{j=1}^{m} f(i,j) \tag{5.21}$$

$$M_{10} = y_0 = \frac{1}{M_{00}}\sum_{x=1}^{n}\sum_{y=1}^{m} xf(x,y) \tag{5.22}$$

$$M_{01} = x_0 = \frac{1}{M_{00}} \sum_{x=1}^{n} \sum_{y=1}^{m} y f(x,y) \tag{5.23}$$

The point (x_0, y_0) is called the center of gravity of the ellipse. The moments M_{11}, M_{20} and M_{02} are given by:

$$M_{11} = \frac{1}{M_{00}} \sum_{x=1}^{n} \sum_{y=1}^{m} (x - x_0)(y - y_0) f(x,y) \tag{5.24}$$

$$M_{20} = \frac{1}{M_{00}} \sum_{x=1}^{n} \sum_{y=1}^{m} (x - x_0)^2 f(x,y) \tag{5.25}$$

$$M_{02} = \frac{1}{M_{00}} \sum_{x=1}^{n} \sum_{y=1}^{m} (y - y_0)^2 f(x,y) \tag{5.26}$$

From these moments we can determine r_1, r_2 the minor and major radii of the ellipse and θ the rotation angle as follows:

$$r_1 = \sqrt{2(M_{20} + M_{02} + \sqrt{(M_{20} + M_{02})^2 + 4M_{11}^2})} \tag{5.27}$$

$$r_2 = \sqrt{2(M_{20} + M_{02} - \sqrt{(M_{20} + M_{02})^2 + 4M_{11}^2})} \tag{5.28}$$

$$\theta = -\frac{1}{2} ArcTan(\frac{2M_{11}}{M_{02} - M_{20}}) \tag{5.29}$$

We define P, P_0 and N as:

$$P = \begin{pmatrix} x \\ y \end{pmatrix}, P_0 = \begin{pmatrix} x_0 \\ y_0 \end{pmatrix}, N = \begin{pmatrix} \frac{1}{r_1^2} & 0 \\ 0 & \frac{1}{r_2^2} \end{pmatrix} \tag{5.30}$$

and the rotation matrix R by:

$$R = \begin{pmatrix} Cos(\theta) & -Sin(\theta) \\ Sin(\theta) & Cos(\theta) \end{pmatrix} \tag{5.31}$$

The equation of the ellipse is the given by:

$$(P - P_0)^{\mathsf{T}}.R.N.R^{\mathsf{T}}.(P - P_0) - 1 = 0 \tag{5.32}$$

It can be also written in the form:

$$c_1x^2 + c_2xy + c_3y^2 + c_4x + c_5y + c_6 = 0 \tag{5.33}$$

where $c_1, c_2, ..., c_6$ as the coefficients of the Eq.5.32.

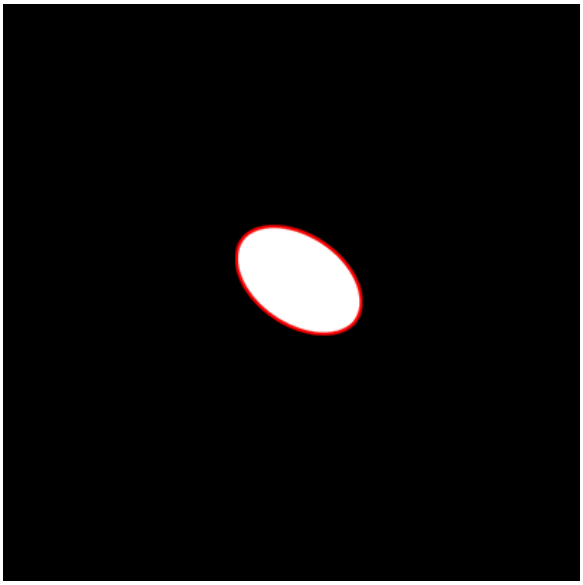

Figure 5.15: Example of ellipse detection using moments.

5.3.4 3D Circle Pose Recovery

The 3D pose of an isotherm on the thermal image, is recovered as follows: [56]. The origin of the world reference frame is set to be located at the center of the 3D circle. The z-axis is then perpendicular to the 3D circle plane. The coordinates of a circle point can be represented as $P_w = [\ x_w \quad y_w \quad 0 \quad 1\ ]^T$. For the pixel coordinates of the corresponding image point $P_i = [\ sr \quad sc \quad s\ ]^T$, we have:

$$P_i = C[\ R \quad t\ ]P_w \tag{5.34}$$

where s is a scale factor, R and t represents the relative rotation and translation between the world coordinate system and the camera coordinate system, are denoted as:

$$R = \begin{bmatrix} r_{11} & r_{21} & r_{31} \\ r_{12} & r_{22} & r_{32} \\ r_{13} & r_{23} & r_{33} \end{bmatrix}, t = \begin{bmatrix} t_x \\ t_y \\ t_z \end{bmatrix} \tag{5.35}$$

C represents the camera intrinsic matrix and is denoted as:

$$C = \begin{bmatrix} S_x f & \gamma & c_x \\ 0 & S_y f & c_y \\ 0 & 0 & 1 \end{bmatrix} = \begin{bmatrix} \alpha_x & \gamma & c_x \\ 0 & \alpha_y & c_y \\ 0 & 0 & 1 \end{bmatrix} \tag{5.36}$$

where S_x and S_y are scale factors to convert from metric to pixel units, f represents the focal length, c_x and c_y are the coordinates of the principal point in pixels, and γ denotes the skewness of the CCD plane.

Equation 5.34 can be simplified as:

$$P_i = C\begin{bmatrix} r_1 & r_2 & t \end{bmatrix} P_w \tag{5.37}$$

where r_1 and r_2 represent the first two columns of rotation matrix R, P_w represents $\begin{bmatrix} x_w & y_w & 1 \end{bmatrix}^T$. We define M as:

$$\begin{aligned} M &= C \begin{bmatrix} r_1 & r_2 & t \end{bmatrix} \\ &= \begin{bmatrix} \alpha_x & \gamma & c_x \\ 0 & \alpha_y & c_y \\ 0 & 0 & 1 \end{bmatrix} \begin{bmatrix} r_{11} & r_{21} & t_x \\ r_{12} & r_{22} & t_y \\ r_{13} & r_{23} & t_z \end{bmatrix} \\ &= \begin{bmatrix} \alpha_x r_{11} + \gamma r_{12} + c_x r_{13} & \alpha_x r_{21} + \gamma r_{22} + c_x t_x & \alpha_x t_y + \gamma r_{22} + c_x t_z \\ \alpha_y r_{12} + c_y r_{13} & \alpha_y r_{22} + c_y r_{23} & \alpha_y t_y + c_y t_z \\ r_{13} & r_{23} & t_z \end{bmatrix} \end{aligned} \tag{5.38}$$

Equation 5.34 can then be written as:

$$P_i = M P_w \tag{5.39}$$

A 3-D circle centered at (x_0, y_0) with the radius r is:

$$(x - x_0)^2 + (y - y_0)^2 = r^2 \tag{5.40}$$

and in a matrix form it becomes:

$$\begin{bmatrix} x \\ y \\ 1 \end{bmatrix}^T \begin{bmatrix} 1 & 0 & -x_0 \\ 0 & 1 & -y_0 \\ -x_0 & -y_0 & x_0^2 + y_0^2 - r^2 \end{bmatrix} \begin{bmatrix} x \\ y \\ 1 \end{bmatrix} = P_w^T Q P_w = 0 \tag{5.41}$$

The corresponding image ellipse can be written as:

$$ax^2 + bxy + cy^2 + dx + ey + f = 0 \tag{5.42}$$

and in matrix form it becomes:

$$\begin{bmatrix} x \\ y \\ 1 \end{bmatrix}^T \begin{bmatrix} a & \frac{b}{2} & \frac{d}{2} \\ \frac{b}{2} & c & \frac{e}{2} \\ \frac{d}{2} & \frac{e}{2} & f \end{bmatrix} \begin{bmatrix} x \\ y \\ 1 \end{bmatrix} = P_i^T A P_i = 0 \tag{5.43}$$

From Eq (5.41) and Eq (5.43) , we obtain:

$$\lambda A = M^{-T} Q M^{-1} \tag{5.44}$$

In our case where the exact diameter of the circle, i.e the isotherm on the surface of the transparent object, is unknown, it is not possible to estimate the distance between the camera plane, the circles center, and the scale factor λ. On the other hand we are only interested in the 3D pose of the circle, so r can be set to an arbitrary value, such as 1. Finally Eq. (5.44) is resolved using singular value decomposition (SVD) in order to determine the 3D pose of the circle relative to the camera plane.

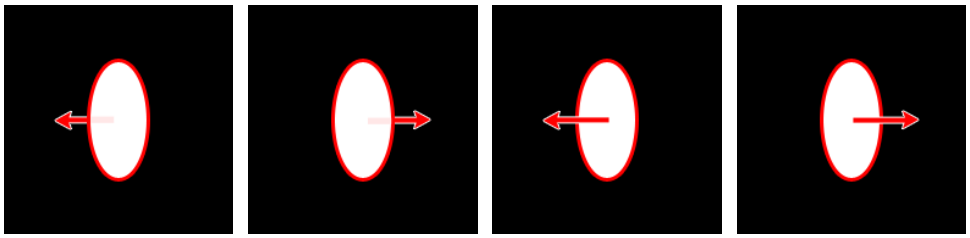

(a) (b) (c) (d)

Figure 5.16: Possible 3D poses for a given ellipse.

The solution to the 3D pose detection is not unique. There is four possible 3D poses for a given ellipse. Figure 5.16 illustrates the possible 3D poses. The first two poses (a) and (b) are eliminated using the sign of the vector in the camera plane coordinate system. However we can not separate between the poses (c) and (d). For

the real world application we need prior knowledge of the surface orientation to be able to select the correct 3D pose. For instance by manually selecting some correct normals it is possible to define angle constraints on a smooth surface. Another possible solution is to use a second camera to resolve the ambiguity.

5.4 Implementation and Experimental Results

Two different implementations of the method to recover the surface normals have been realized. The first one makes use of a rotating mechanical system and is used for the validation of the method. The second implementation is identical to *Scanning from Heating* experimental setup, and uses a $X - Y$ moving platform to scan the surface of the transparent object.

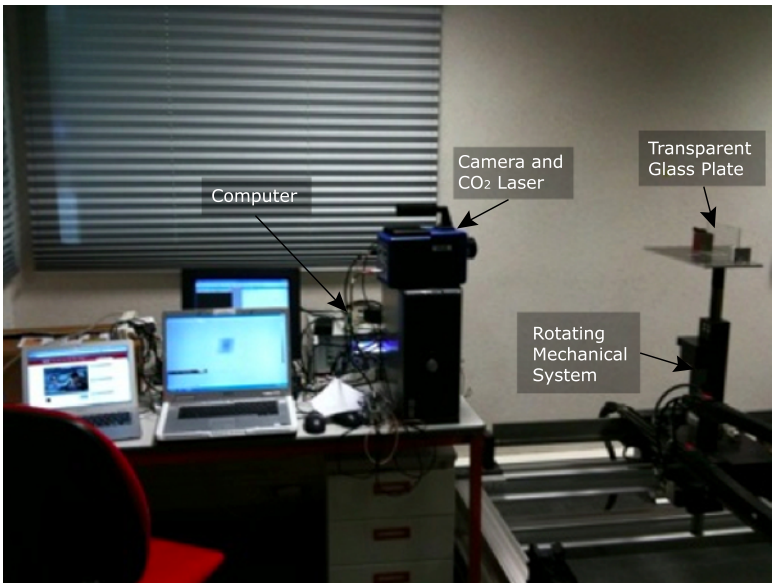

Figure 5.17: Experimental setup to validate the method.

The first experimental setup for the validation of the method is presented in

Fig.5.17. A Flir SC 7000 infrared camera is used to acquire thermal images. The resolution of the camera is 640x512 (twice of the resolution of the camera used in *Scanning from Heating* prototype). A glass plate is placed on a remotely controlled rotating platform which has a precision of 0.01 degrees. For different positions of the platform the surface of the glass plate is heated at a point with a $400mW$ CO_2 laser and a thermal image is acquired.

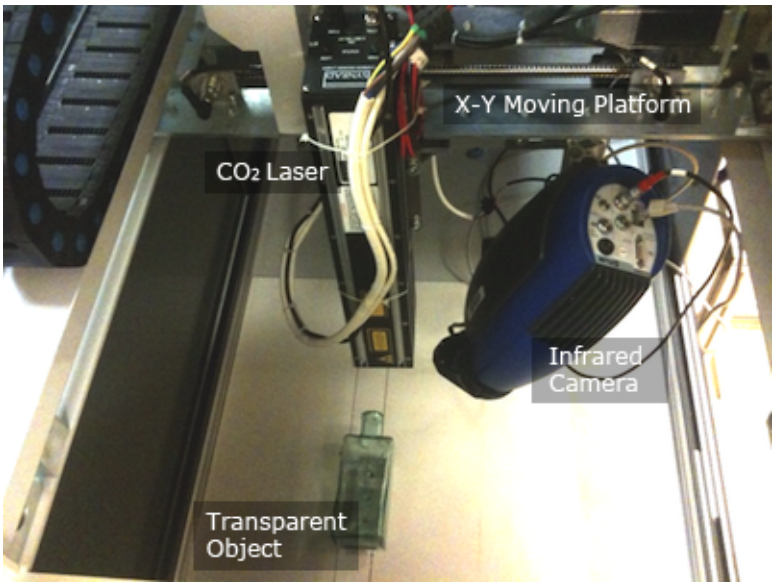

Figure 5.18: Experimental setup for the acquisition of 3D points and their normals on the surface of a transparent object.

The second experimental setup (Fig.5.18) is used to obtain 3D points and their corresponding normals on the surface of transparent objects. A Flir SC 5500 infrared camera, sensible to $3 - 12\mu m$, is used to acquire thermal images. The resolution of the camera is 320x256 pixels. A Synrad $10W$ CO_2 laser is used as heating source. The output power of the laser is controlled by the computer via Synrad UC2000 Laser Power Controller, over serial port. The camera and the laser are attached to a

$X-Y$ moving platform. The position of the platform is controlled by the computer over the ethernet interface via Siemens S200 PLC Controller. The moving platform has a precision of $50\mu m$.

5.4.1 Calibration

For the recovery of the surface normals both systems needs to be calibrated. For this purpose a custom calibration plate has been designed. A known pattern has been imprinted on an electrical circuit board. Once heated, the pattern on the plate is visible to thermal cameras. The calibration procedure for the cameras has been described in Chapter 3.

As a result of the calibration process, f, the focal length of the camera, κ, the radial distortion coefficient, S_x, the horizontal distance between two neighboring cells on the sensor, S_y, the vertical distance between two neighboring cells on the sensor, C_x, column coordinate of the image center point and, C_y, row coordinate of the image center point are determined. The following results, using MVTec Halcon Calibration Libraries, have been obtained for the interior camera parameters (Table 5.1, Table 5.2).

Table 5.1: Calculated interior camera parameters for the first experimental setup:

Focal length of the lens:	0.02503245135
Radial distortion coefficient:	-262.3453465754
Width of a cell on the sensor:	0.000001530012
Height of a cell on the sensor:	0.000001500345
X-coordinate of the image center:	321.678356245
Y-coordinate of the image center:	258.45613245234
Width of the images:	640
Height of the images:	512

Table 5.2: Calculated interior camera parameters for the second experimental setup:

Focal length of the lens:	0.0330831798312779
Radial distortion coefficient:	-235.408590483261
Width of a cell on the sensor:	0.0000030005938013238
Height of a cell on the sensor:	0.000003
X-coordinate of the image center:	184.1761694627
Y-coordinate of the image center:	128.343509507569
Width of the images:	320
Height of the images:	256

5.4.2 Validation of the Method

The first experimental setup is used for the validation of the method. Figure 5.19 illustrates the process.

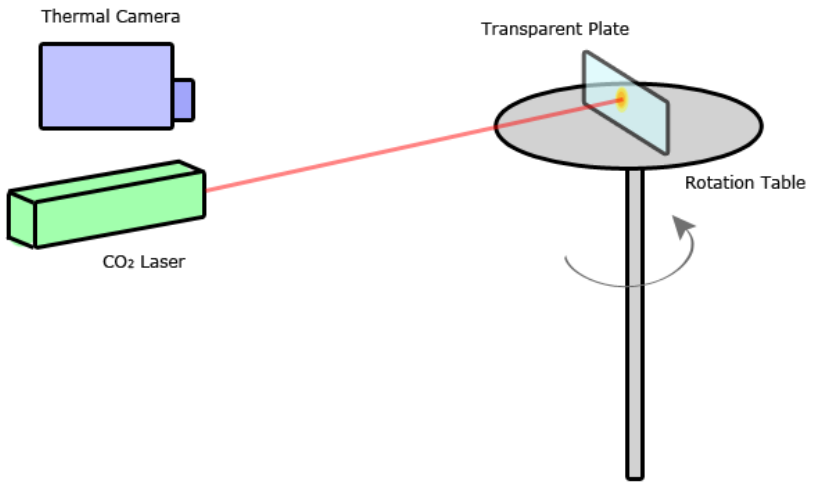

Figure 5.19: Procedure for the validation of the method.

The mechanical rotation table is turned by steps of 3 degrees. For each step a

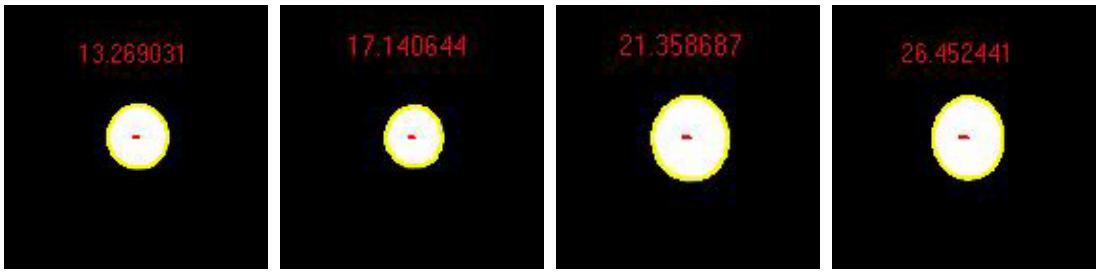

(a) (b) (c) (d)

Figure 5.20: Thermal images and the result of the ellipse detection process using moments (in yellow) and the angle of the calculated normal vector in x-axis, compared to the initial position (in red)

thermal image is acquired. To obtain accurate results several isotherms, corresponding respectively to the gray values 8500, 8550, 8600, 8650, 8700, 8750, 8800, 8850 and 8900, are extracted from the image. For each isotherm the equation of the ellipse on the image is determined using moments. From these equations, using the process described in Section 4.3.4, the normals on the surface of the transparent glass plate are calculated. Finally the mean normal is obtained summing all the normals obtained from the isotherms and normalizing it.

Figure 5.20 illustrates thermal images and the result of the ellipse detection process using moments (in yellow) on one of the isotherms. Additionally the angle of the calculated normal vector in x-axis, compared to the initial position, is given (in red). Figure 5.21 shows for each isotherm the result of the procedure to detect the normals giving the angle of the calculated normal vector in x-axis, compared to the initial position. The reference line (in blue) shows the angle of the mechanical rotation table. For each step of three degrees, the calculated angles are represented. The mean angle of the mean normal vector (in red) is also given. The average devi-

ation between the reference angle and the angle of the mean vector is determined as 1.58029 degrees. This results demonstrate that, it is possible using the isotherms to detect the normal vectors on a planar surface. Assuming the surface locally flat this method can be applied in addition to *Scanning from Heating* to recover the normal vectors at the determined 3D points.

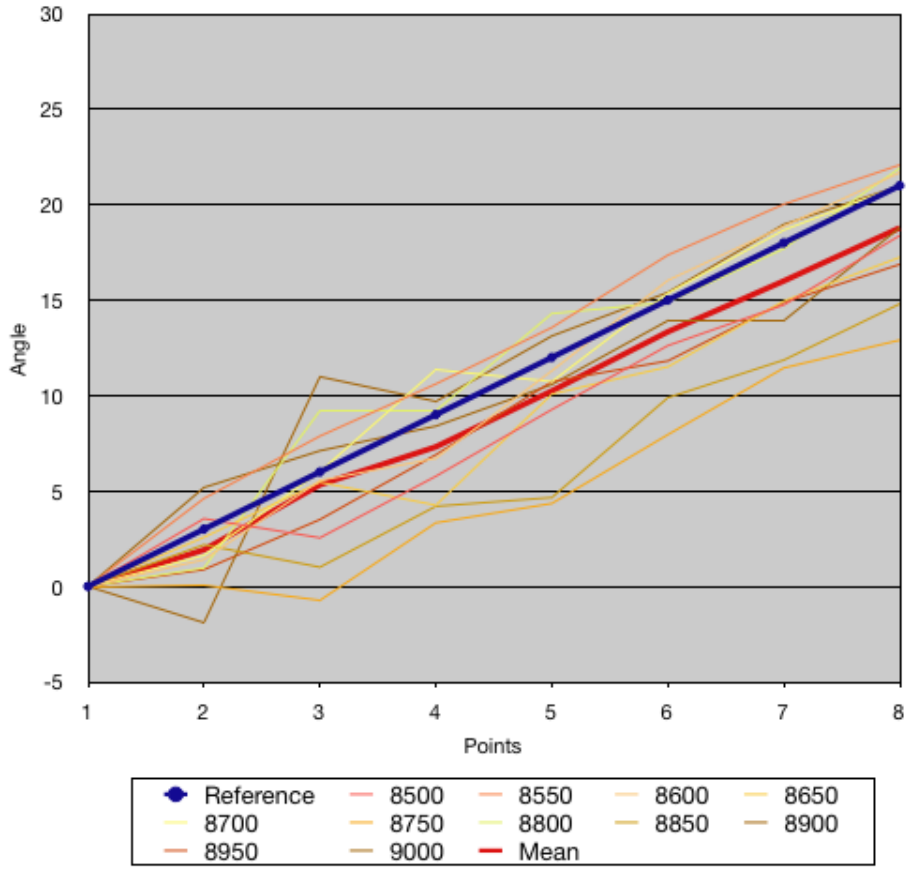

Figure 5.21: Result of the procedure to detect the normals giving the angle of the calculated normal vector in x-axis, compared to the initial position. The reference line (in blue) shows the angle of the mechanical rotation table. For each step the calculated angles are represented. The mean angle of the mean normal vector is given in red.

5.4.3 Results

Once the method has been validated, the second experimental setup has been used to acquire 3D points and normals on the surface of transparent objects. Figure 5.22 illustrates a false color image acquired by the scanner and shows the result of the normal detection process.

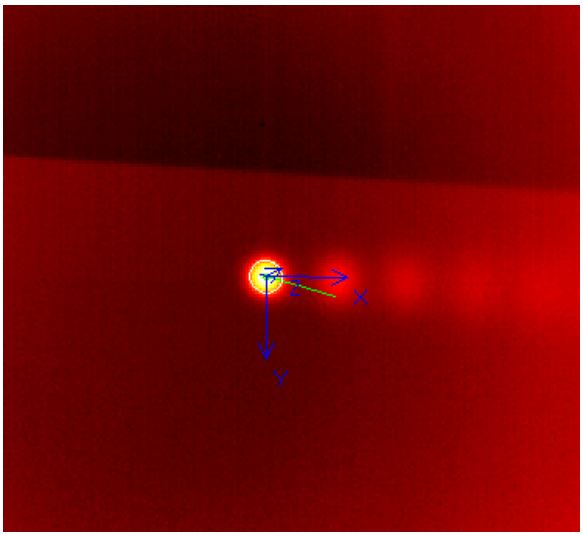

Figure 5.22: False color image acquired by the scanner showing the result of the normal detection process.

At the end of each scanning operation, two different interpolation of the surface, one using only the 3D points and the other using the 3D points and the normals, is calculated. These results are compared to a surface obtained from 3D points acquired by a touch probe scanner. The touch probe scanner has a precision of $5\mu m$ and is considered in these experiments as the ground truth. To obtain a surface from the 3D points acquired from the *Scanning from Heating* scanner and from the touch probe scanner, the Rapidform software [53] is used. On the other hand, when using the

3D points and the normals, as a result of the procedure described in Section 4.2.6, bezier surface patches are obtained. To be able to compare this surface to the other ones, first a set of points between the four 3D points used for the calculation of the patch are determined. This calculation is repeated for all the patches which forms the surface. Finally, the point cloud is imported in Rapidform to generate a polygon surface. To obtain a comparison between the surfaces from *Scanning from Heating* scanner and from the touch probe scanner the two coordinates systems have to be aligned. To achieve this, three identical points are selected on each surface and the transformation between the two coordinate systems is calculated.

Glass Plate: Figure 5.23.a illustrates the result obtained from *Scanning from Heating* scanner on a 10x20cm glass plate from 625 points. Figure 5.23.b shows in addition the calculated normal vectors at these 3D points. From these 3D points and normal vectors the bezier surface is calculated. Figure 5.24 shows an enlarged portion of the bezier surface. At each bezier patch, additional points are determined for the comparison of the surface to the one obtained by the touch probe scanner. Figure 5.25 illustrates four 3D points and their respective normal vectors. Additionally 625 points, between the scanned ones, have been interpolated according to the bezier surface patch. This operation is repeated for each patch and a point cloud is obtained. To compare the results the glass plate is also scanned by Wenzel LH 54 touch probe scanner from 625 points. Figure 5.26.a illustrates the comparison of the surface obtained from the 3D points acquired by the *Scanning from Heating* scanner to the surface obtained by the touch probe scanner. The average deviation is 145μm. Figure 5.26.b illustrates the comparison of the surface obtained from the 3D points

and the normals to the surface obtained by the touch probe scanner. The average deviation is $135\mu m$.

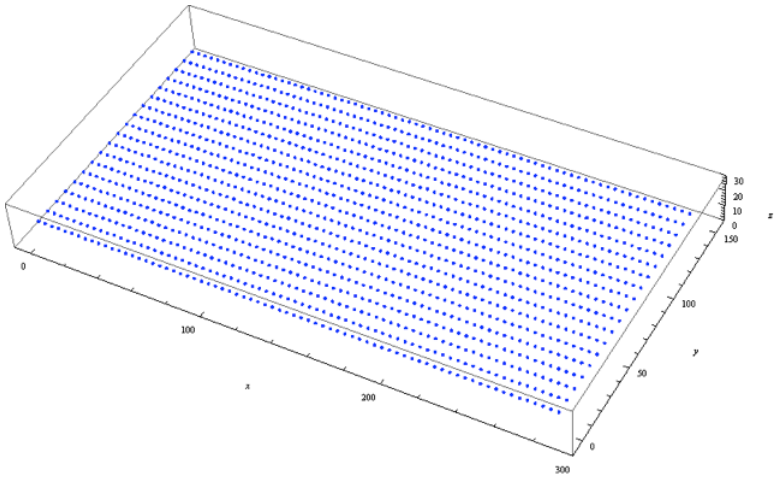

(a)

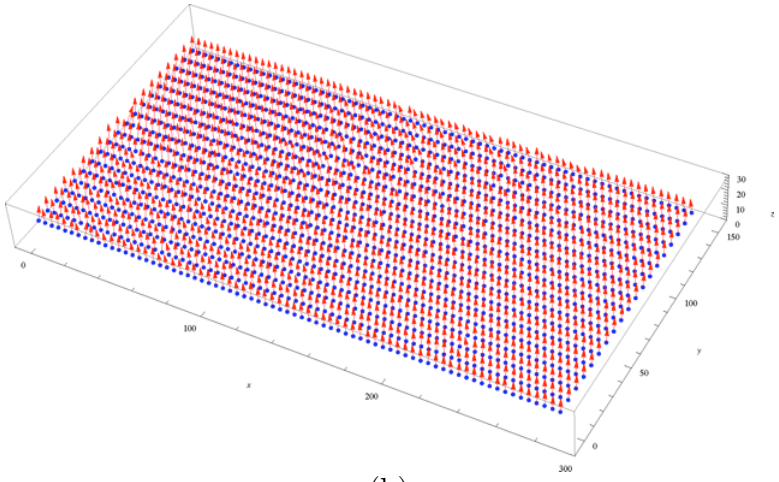

(b)

Figure 5.23: (a) Result obtained from *Scanning from Heating* scanner on a 10x20cm glass plate from 625 points, (b) calculated normal vectors at these 3D points.

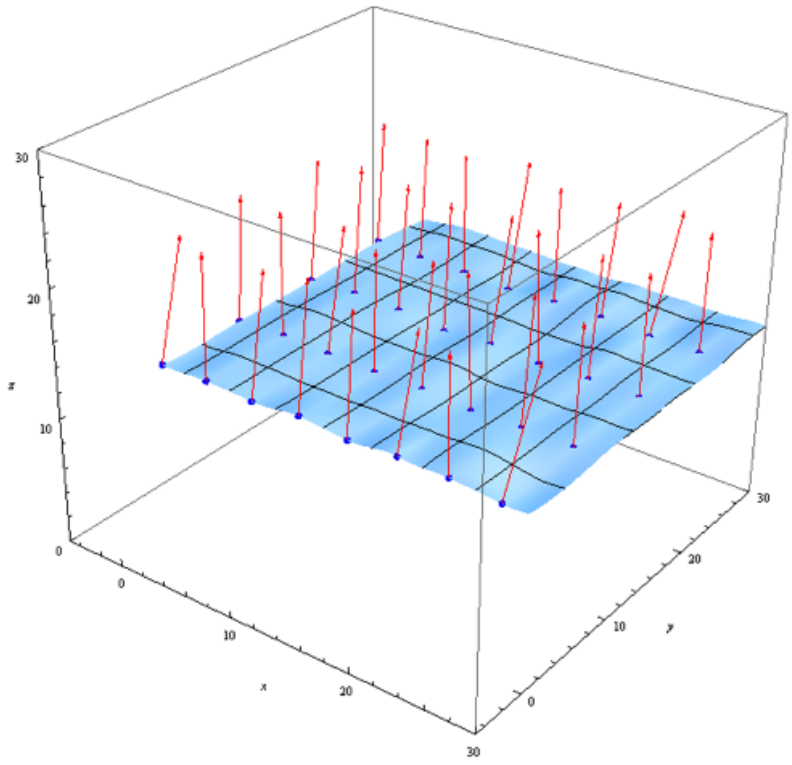

Figure 5.24: An enlarged portion of the constructed bezier surface.

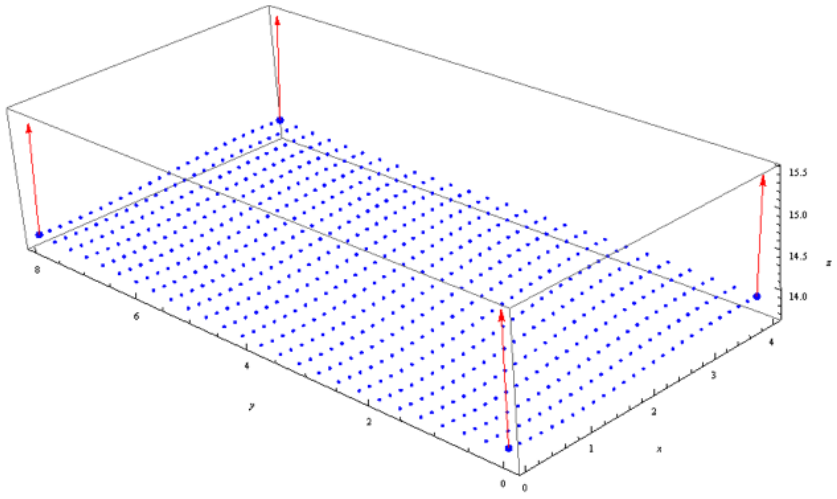

Figure 5.25: Four 3D points and their respective normal vectors. 625 points between the scanned ones have been interpolated according to the bezier surface patch.

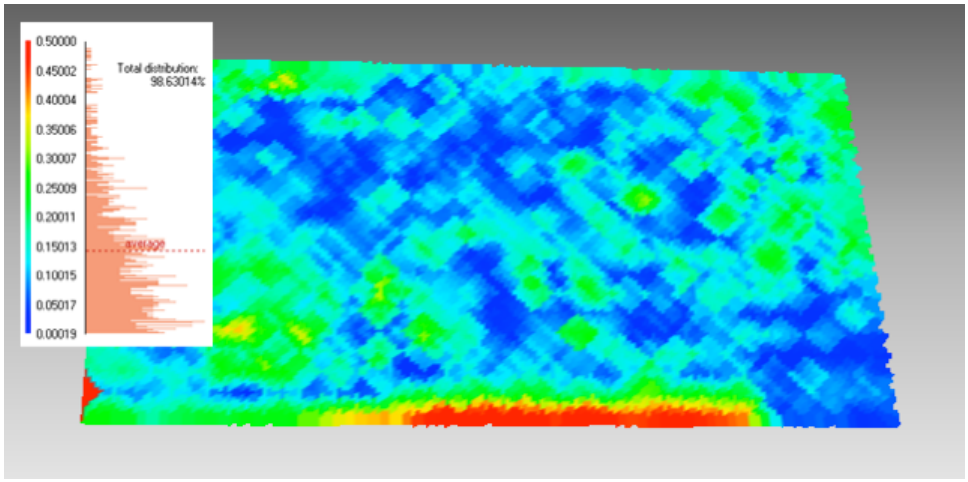

(a)

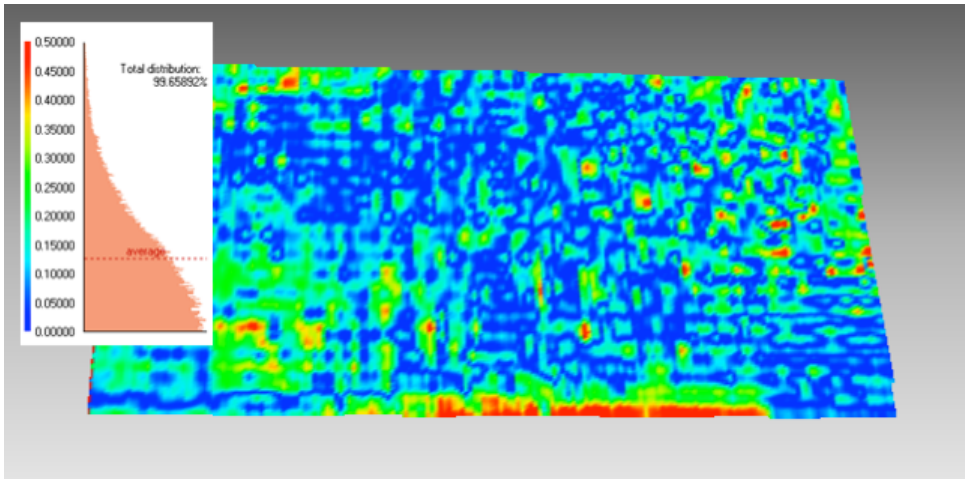

(b)

Figure 5.26: (a) Comparison of the surface obtained from the 3D points acquired by the *Scanning from Heating* scanner to the surface obtained by the touch probe scanner. The average deviation is $145\mu m$, (b) Comparison of the surface obtained from the 3D points and the surface normals to the surface obtained by the touch probe scanner. The average deviation is $135\mu m$.

Figure 5.27: Glass bottle.

Glass Bottle Figure 5.29.a illustrates the 3D points obtained from *Scanning from Heating* on the glass bottle presented in Fig.5.27. Figure 5.29.b shows in addition the calculated normal vectors at each 3D point. Figure 5.29.c illustrates the bezier surface, obtained using the points and the vectors, applying the procedure described in Section 4.2.6. Figure 5.30 demonstrates an enlarged portion of the bezier surface. At each bezier patch, additional points are determined for the comparison of the surface to the one obtained by the touch probe scanner. Figure 5.25 illustrates four 3D points and their respective normal vectors. Additionally 625 points, between the scanned ones, have been interpolated according to the bezier surface patch. This operation is repeated for each patch and a point cloud is obtained. To compare the results the glass plate is also scanned by Wenzel LH 54 touch probe scanner from 900 points. Figure 5.28 shows the scanning of the glass bottle by the touch probe

scanner. Figure 5.32.a illustrates the comparison of the surface obtained from the 3D points acquired by the *Scanning from Heating* scanner to the surface obtained by the touch probe scanner. The average deviation is $120\mu m$. Figure 5.32.b illustrates the comparison of the surface obtained from the 3D points and the normals to the surface obtained by the touch probe scanner. The average deviation is $110\mu m$.

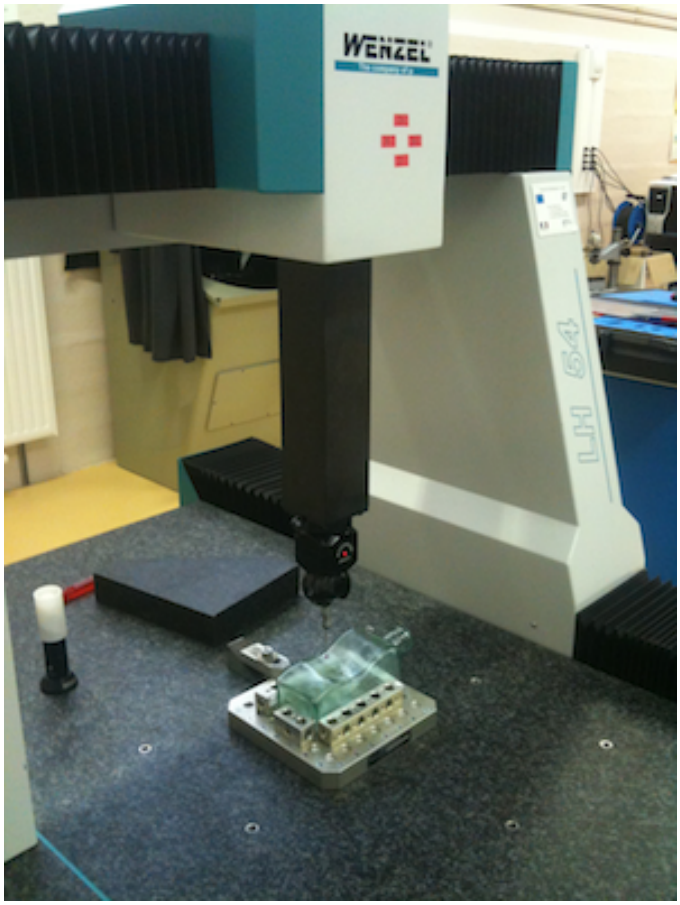

Figure 5.28: Scanning of the glass bottle by Wenzel LH 54 touch probe scanner.

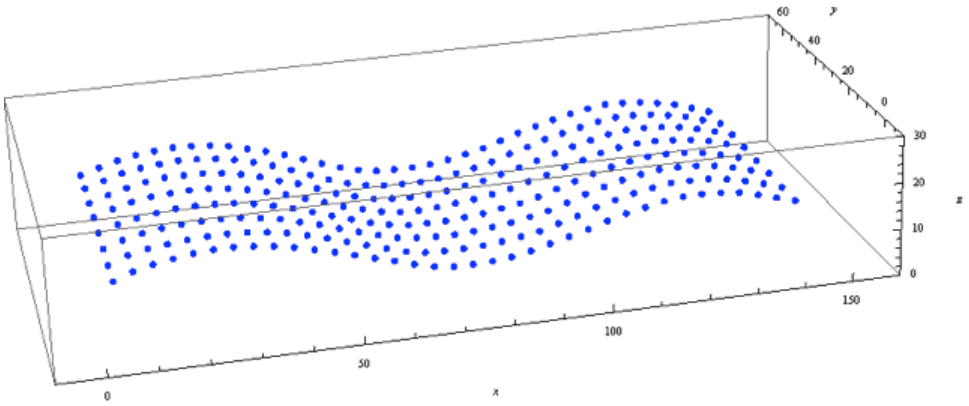

(a)

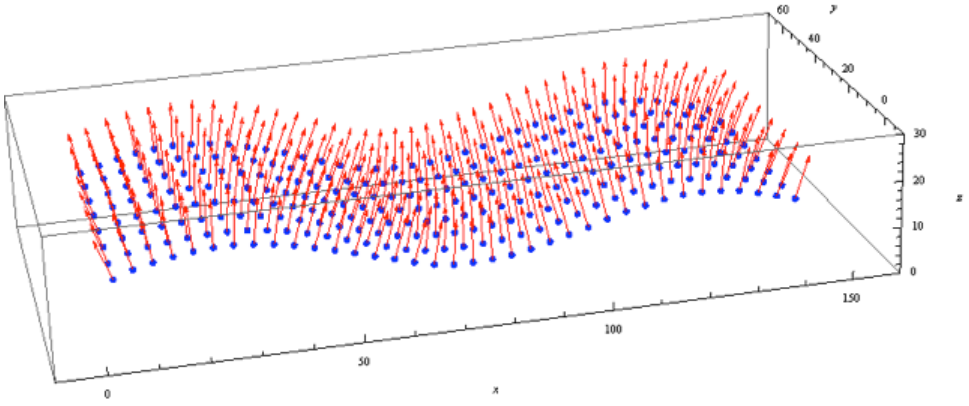

(b)

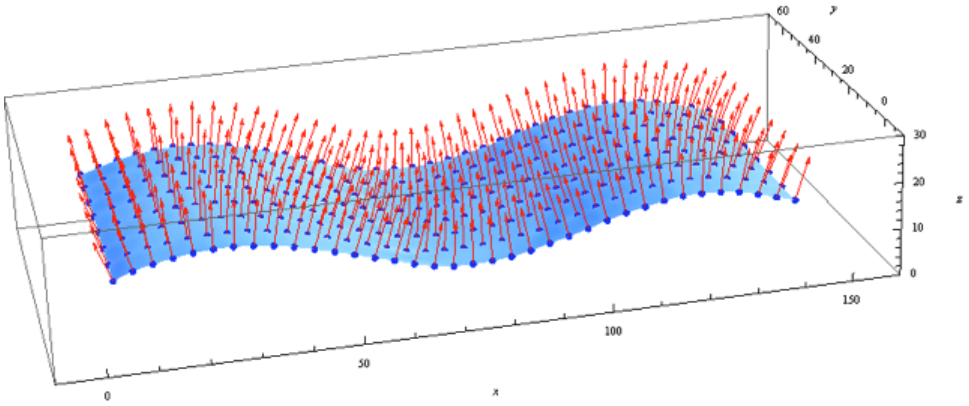

(c)

Figure 5.29: 3D points obtained from *Scanning from Heating*, (b) calculated normal vectors at each 3D point, (c) the bezier surface, obtained using the points and the vectors, applying the procedure described in Section 4.2.6.

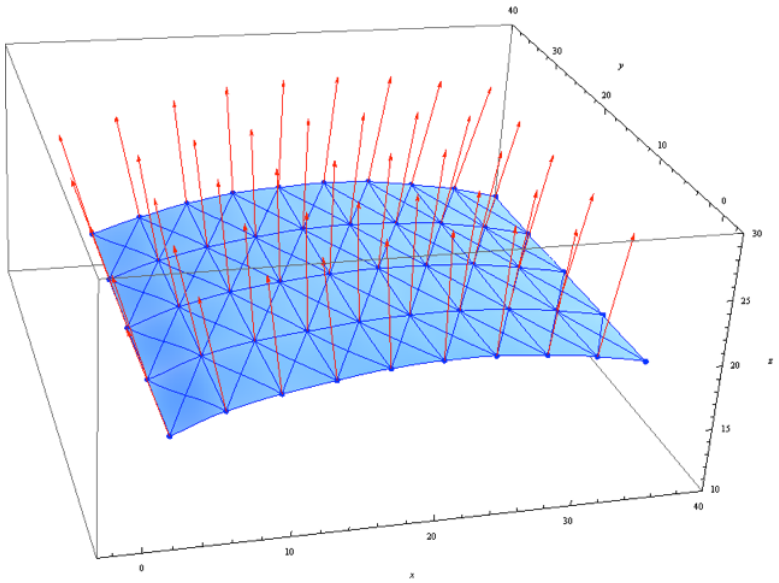

Figure 5.30: An enlarged portion of the constructed bezier surface.

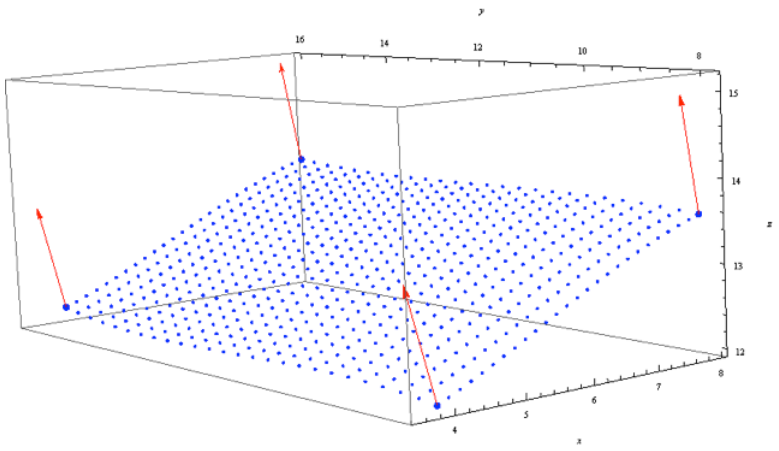

Figure 5.31: Four 3D points and their respective normal vectors. 625 points between the scanned ones have been interpolated according to the bezier surface patch.

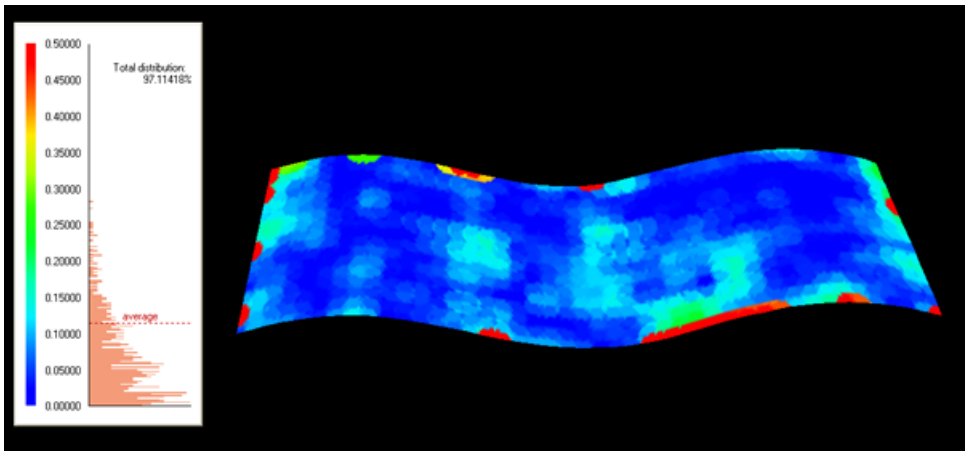

(a)

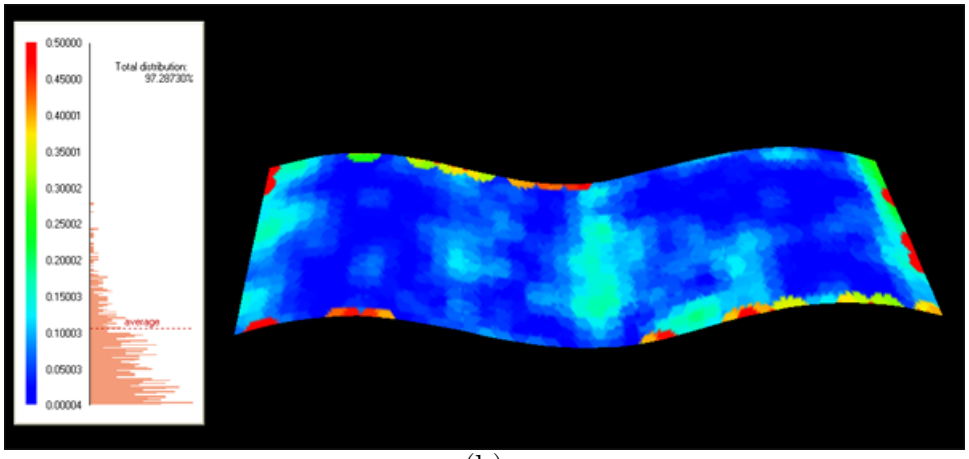

(b)

Figure 5.32: (a) Comparison of the surface obtained from the 3D points acquired by the *Scanning from Heating* scanner to the surface obtained by the touch probe scanner. The average deviation is $120\mu m$, (b) Comparison of the surface obtained from the 3D points and the surface normals to the surface obtained by the touch probe scanner. The average deviation is $110\mu m$.

Looking at the results obtained on the previously presented glass plate and on the glass bottle, the effect of the surface normals on the reconstruction is not directly visible. The average deviation between the ground truth surface obtained using the touch probe scanner and the reconstruction using the scanned points and the normals is just slightly better then the one obtained using only the 3D points. This is mainly due to the low curvatures on the surface of the scanned objects. On the other hand we observe that we have a better localization of the erroneous zones on the surface obtained using the normals. Figure 5.33 illustrates this fact:

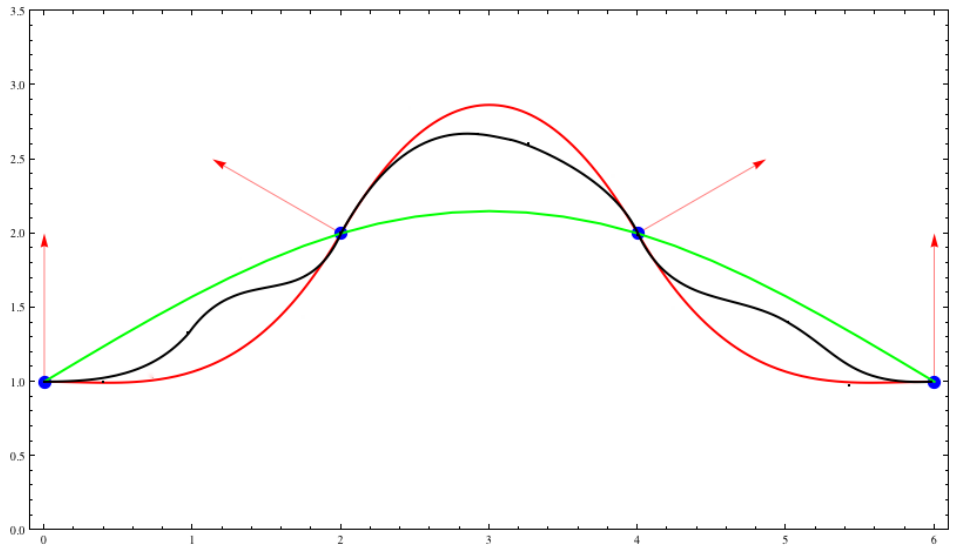

Figure 5.33: Example showing that the reconstruction using the surface normals provides better localization of the erroneous zones.

Figure 5.33 shows a surface profile (in black), four points on this profile (in blue) and the corresponding surface normals (in red). The green line shows the bezier curve obtained using the 3D points. The red line shows the bezier curve obtained using the points and the normals. The average deviation between the black and red

curve, and the deviation between the black and green curve may be equal but the curve constructed using normals fits better the real data. This effect can be seen on the experimental results, especially on the glass plate. Another important aspect is the density of the scanned points. Figure 5.34.a illustrates a 2D profile obtained on the glass bottle by Scanning From Heating, and the calculated normals. The interpolation using the points (in red), and the interpolation using the points and the normals (in blue) is illustrated in Fig.5.34.b. If the number of scanned points is reduced, as shown in Fig.5.34.c, the interpolations differ from each other.

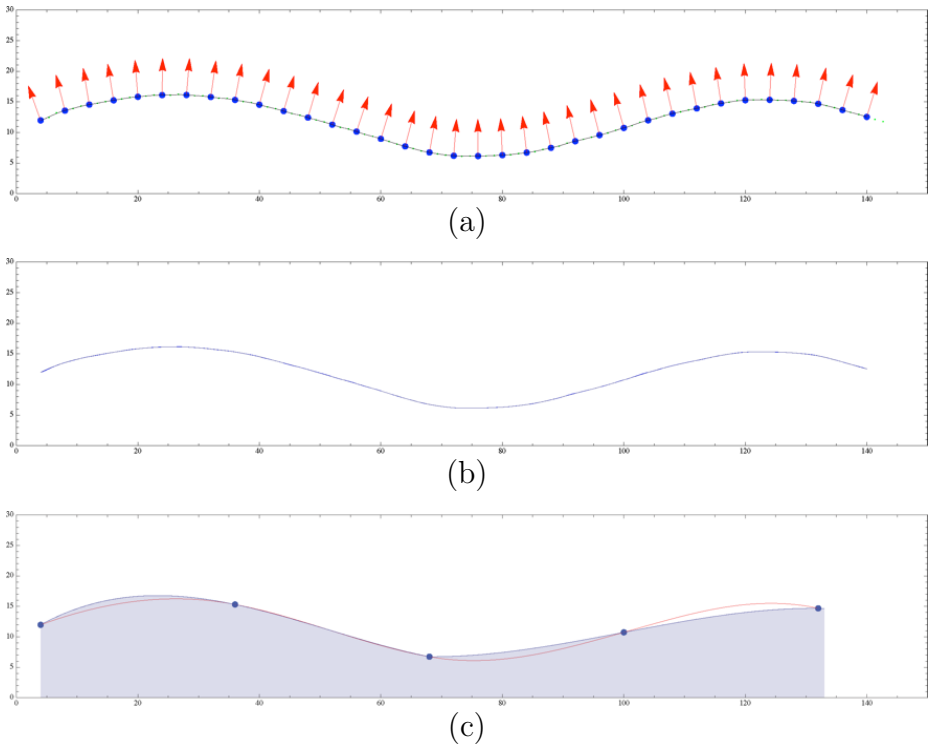

Figure 5.34: (a) 2D profile obtained on the glass bottle by Scanning From Heating, and the respective calculated normals, (b) interpolation using the points (in red), and the interpolation using the points and the normals (in blue), (c) the interpolations differ from each other when the number of scanned points is reduced.

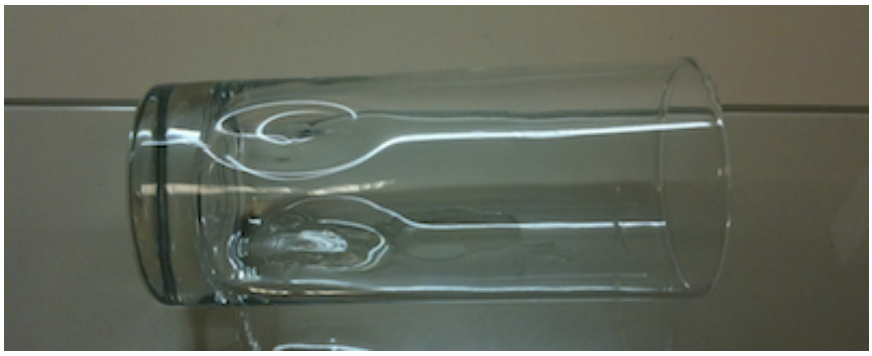

Figure 5.35: Glass object containing accentuated curvatures on its surface.

Glass object with accentuated curvatures: To demonstrate the effect of the surface normals on real data, a glass object, shown in Fig.5.35, which contains accentuated curvatures has been scanned. 108 3D points have been acquired using the *Scanning from Heating* scanner. Normals at these points have been calculated and the procedure for the interpolation of the points has been applied. Figure 5.36.a shows the results obtained from *Scanning from Heating* scanner and Fig.5.36.b shows the results of the interpolation using the normals. The two surfaces are compared and the result is presented in Fig.5.36.c. The average deviation between the two surfaces is determined as $250\mu m$. Differences are mainly located on zones with high curvatures. Figure 5.37.a and Fig.5.37.b compares a profile taken from these surfaces, obtained from the *Scanning from Heating* scanner, to the one acquired from touch probe scanner. The average deviation between the surface from the touch probe scanner and the surface obtained from the 3D points from *Scanning from Heating* is $380\mu m$. On the other hand, when normals are used for the interpolation in addition to the 3D points, the average deviation drops down to $125\mu m$. This result demonstrates the importance of the surface normals and the efficiency of the method.

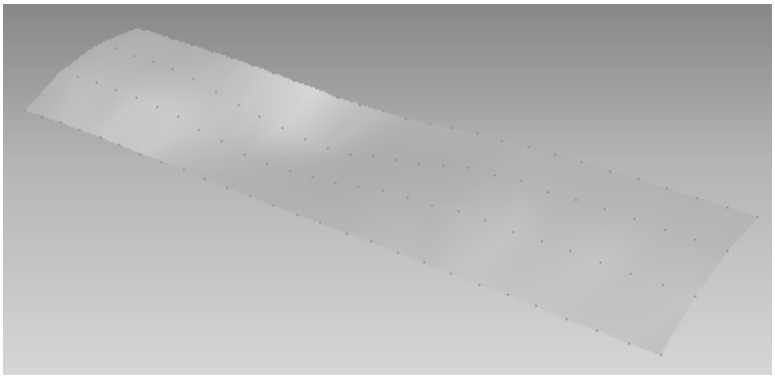

(a)

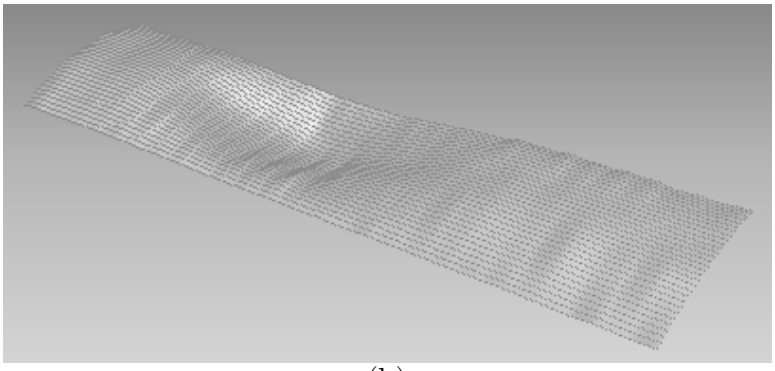

(b)

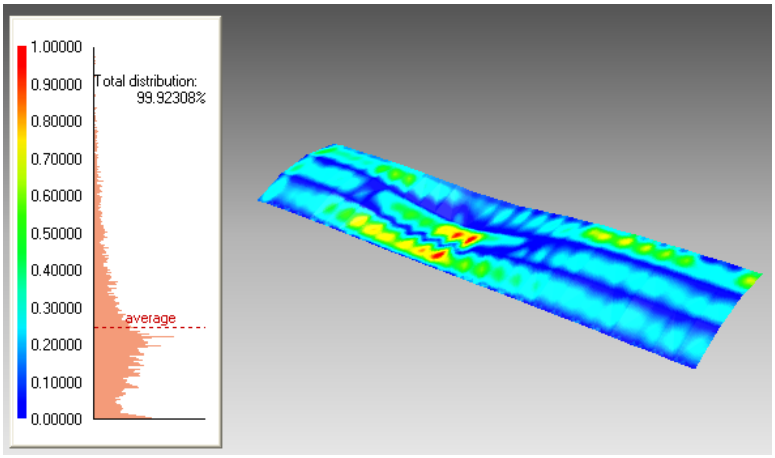

(c)

Figure 5.36: (a) Results obtained from *Scanning from Heating* scanner on the object presented in Fig.5.35 (b) results of the interpolation using the normals.

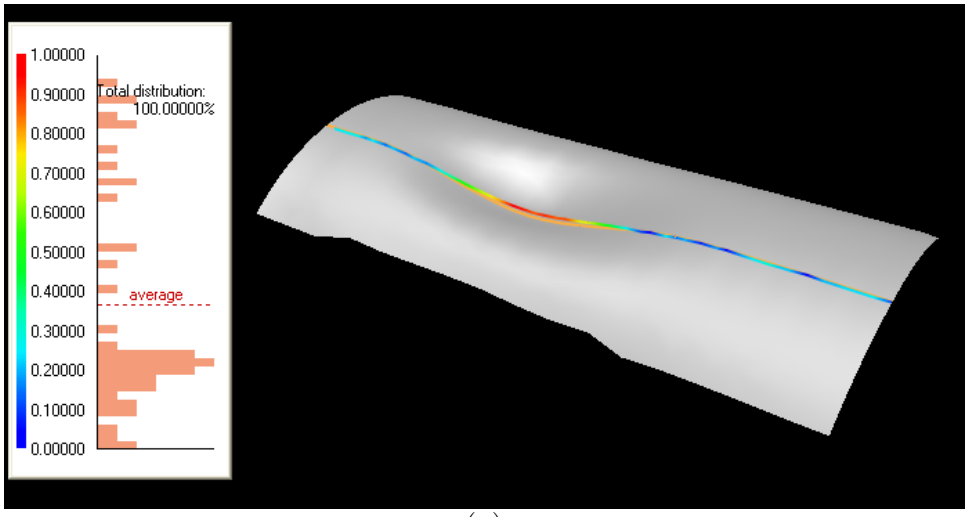

(a)

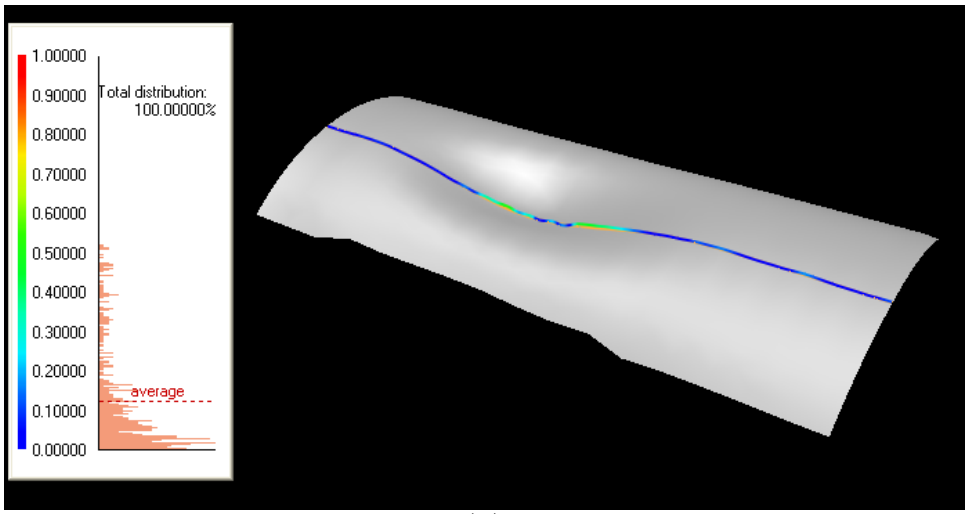

(b)

Figure 5.37: Comparison of a profile taken from the surface, obtained from the 3D points from *Scanning from Heating*, to the one acquired from touch probe scanner. The average deviation is $380\mu m$, (b) comparison of the same profile taken from the surface, obtained from the 3D points and the normals, to the one acquired from touch probe scanner. The average deviation is $125\mu m$.

5.5 Conclusion

We have shown in this chapter the extension to Scanning from Heating method to recover the surface normals, in addition to the 3D coordinates. Experimental results show that it is possible to obtain, from the isotherms, the normal vectors at the laser impact zones. These normal vectors helps improving the reconstruction of the surface and give a better localization of the erroneous zones. This extension can have several real world application such as the quality control of automotive glasses. The accuracy of the method can be improved using a laser with a smaller diameter and a thermal camera with a higher resolution.

6 CONCLUSION

6.1 Summary

In this thesis we have proposed a new method of determining the surface shape of transparent objects. The method makes use of selective light absorption properties of the transparent material to create a heat spot on the surface. To achieve this, a laser heating source, working in the absorption frequencies of the material, is used. Once the heat spot is created on the surface, the method makes use of radiative properties of the material. The spot is observed by a thermal camera and the coordinates on the image plane are determined. Knowing the internal and external camera parameters, by an initial calibration of the system, we determine the 3D world coordinates of the heated spot. The process is repeated moving the object to recover the whole surface shape. We named this method "Scanning From Heating". We have studied the application of the method in detail on transparent glass objects and demonstrated that it is possible, by Scanning From Heating, to obtain surface profiles of various transparent specimens, including glass planes, curved automotive glass windows, complex glass objects and even plastic bottles. Furthermore, considering the laser beam as a point heating source and the surface of the object locally flat at the impact zone, we have extended the method to obtain the surface normals of the object, in addition to the 3D world coordinates. Additionally we have shown different applications of the method using a laser line projection instead of a spot, to accelerate

the acquisition process. A scanner prototype have been realized during the thesis and a patent on the method has been deposited.

6.2 Contribution

Papers in peer-reviewed academic journals: Optics Express and IEEE Transactions on Instrumentation and Measurement, a paper in proceedings of international conference: ICIAP 2009 and a SPIE Newsroom article have been published:

(1) Gonen Eren, Olivier Aubreton, Fabrice Meriaudeau, L.A. Sanchez Secades, David Fofi, A. Teoman Naskali, Frederic Truchetet, and Aytul Ercil, Scanning from heating: 3D shape estimation of transparent objects from local surface heating, Opt. Express 17, 11457-11468 (2009).

(2) Fabrice Meriaudeau, Luis Alonzo Sanchez Secades, Gonen Eren, Aytul Ercil, Frdric Truchetet, Olivier Aubreton, David Fofi, "3D Scanning of Non-Opaque Objects by means of Imaging Emitted Structured Infrared Patterns ", IEEE Transactions on Instrumentation and Measurement (accepted), 2010

(3) Eren G., Aubreton O. , Meriaudeau F., Secades L.A.S., Fofi D., Naskali T., Truchetet F., Ercil A., A 3D Scanner for Transparent Objects, Proceedings of 15th International Conference on Image Analysis and Processing (ICIAP 2009).

(4) Eren G., Aubreton O. , Meriaudeau F., Secades L.A.S., Fofi D., Truchetet F., Ercil A., Using heat to scan transparent surfaces, Industrial Sensing and Measurement, SPIE Newsroom (2009).

We can also remark that the article published in Optics Express has been cited in Nature Photonics:

- David Pile, A Clear Picture, Nature and Photonics, Vol3, August 2009, pp 434.

and in the state of the art in transparent and specular object reconstruction:

- I.Ihrke, K.N. Kutulakos, H.P.A. Lensch, M.Magnor, and W.Heidrich,"Transparent and specular object reconstruction," *Computer Graphics Forum*, p. to appear, 2010.

A patent on a scanner prototype using Scanning From Heating method has been deposited. Details on the patent application can be found in appendix section.

- PCT/IB08/055328: "A 3D Scanner"

A 3D scanner prototype based on *Scanning From Heating* method has been realized.

6.3 Discussion

Current reconstruction methods for transparent objects are mainly working in the visible domain of the spectrum and are trying to resolve difficulties caused by transparency using algorithms and systems based on reflection, refraction or polarization of the visible light. Scanning From Heating differs mainly in this aspect where it makes use of the selective light absorption property of materials and employs a laser heating source which works in this domain of the spectrum. In these zones the object is opaque to the laser heating source and the and laser energy is absorbed by

the surface without penetrating into the object. This creates a detectable point by the thermal camera. The problem of scanning the transparent material is then reduced to 3D triangulation, which is the among the most proven and widely used 3D reconstruction methods.

Scanning From Heating has many advantages over actual methods. Techniques for estimating the 3D surface shape of transparent objects based on structured lighting do not yield good results for protruding objects, whereas Scanning From Heating method, as 3D scanners in the visible domain, can acquire different types of surfaces. Shape-from-focus based methods change the focus of the camera and can only estimate the depth of the edge of the object and cannot estimate the shape of a curved surface whereas Scanning From Heating can also acquire surface profiles. Refraction based methods, like shape from motion, require complex calculations and estimate basic shapes represented by a small number of parameters such as a sphere or rounded cube. It is possible to scan complex surfaces with Scanning From Heating method. Polarization based methods have difficulties to acquire realtime measurements and necessitate delicate calibration procedures which may be difficult to implement on an industrial production line. Scanning From Heating can acquire realtime surface profiles and uses 3D triangulation which is easy to calibrate. Furthermore the extension of the method to obtain the surface normals in addition to the 3D world coordinates gives precise information about the surface curvatures. Moreover the method is capable of scanning different types of materials like glass and plastic. The method can also be applied to opaque objects and is beneficial when the object is composed of different types of materials, transparent and non-transparent.

On the other hand, the method and its implementation have some drawbacks.

The use of a laser heating source requires important precaution measures. The laser can damage the surface of the object if the laser power is not properly adjusted according to the heating model. Reflection of the laser heating source can harm humans or cause damage to other equipment, especially to the thermal cameras. The cameras should be protected by mechanical shutters or filters. A controlled environment is necessary for the industrial application of the method. Additionally, the method uses sophisticated equipment that is costly at the present and the accuracy of the method is limited by the resolution of the thermal cameras. Fortunately, with the rapid growth of the need for thermal cameras in different industries such as, military, construction and medicine, prices of thermal cameras are dropping rapidly, where their resolutions getting higher. This will allow the method to be cost effective and to be applied to high demanding applications in the future.

In conclusion, we have developed a novel technique which is capable of acquiring the 3D surface shape of transparent objects. Scanner prototypes were implemented and tested on diverse transparent glass objects. Experiments show that the quality of the reconstructed models is as accurate as conventional laser scanners in the visible domain. Additionally, the obtained results demonstrated that it is possible to scan different types of surfaces. The method holds promise for a wide range of applications in automotive and packaging industries.

6.4 Future Work

Future work includes the extension of the method on specular surfaces such as metals and polished materials. Burgundy University LE2I Laboratory and Sabanci Univer-

sity VPA Laboratory have started together an EUREKA project for this purpose. Industrial applications of Scanning From Heating method is also envisaged.

A PATENT: A 3D SCANNER (PCT/IB08/055328)

The following patent application has been made for the Scanning From Heating method, which has been developed during this thesis.

Receipt of Electronic Submission

It is hereby acknowledged that a PCT International Application has been received via the Secure Electronic Submission Software of the IB. Upon receipt, Application Number and a Date of Receipt (Administrative Instructions, Part 7) has been automatically assigned.

Submission Number:	23873		
Application Number:	PCT/IB2008/055328		
Date of Receipt:	16 December 2008		
Receiving Office:	International Bureau of the World Intellectual Property Organization		
Your Reference:	24318.06		
Applicant:	SABANCI UNIVERSITESI		
Number of Applicants:	8		
Title:	A 3D SCANNER		
Documents Submitted:	PCT101.GML	4088	16 December 2008 10:30:16
	2431806-requ.xml	6063	16 December 2008 11:28:38
	2431806-appb.xml	8990	16 December 2008 11:15:22
	2431806-vlog.xml	4069	16 December 2008 11:15:22
	2431806-fees.xml	1897	16 December 2008 11:15:22
Signed by:	ekin dericioglu kurt		
Timestamp of Receipt:	16 December 2008 10:30		
Official Digest of Submission:	F5:3D:67:9E:6C:FB:96:F7:FD:3F:72:3B:2D:82:58:1A:EB:21:C7:D6		

/Geneva, RO/IB/

PCT REQUEST

Print Out (Original in Electronic Form)

0	For receiving Office use only	
0-1	International Application No.	
0-2	International Filing Date	
0-3	Name of receiving Office and "PCT International Application"	
0-4	Form PCT/RO/101 PCT Request	
0-4-1	Prepared Using	PCT-SAFE Version 3.51.029.204 MT/FOP 20080701/0.20.5.12
0-5	Petition The undersigned requests that the present international application be processed according to the Patent Cooperation Treaty	
0-6	Receiving Office (specified by the applicant)	International Bureau of the World Intellectual Property Organization (RO/IB)
0-7	Applicant's or agent's file reference	24318.06
I	Title of Invention	A 3D SCANNER
II	Applicant	
II-1	This person is	applicant only
II-2	Applicant for	all designated States except US
II-4	Name	SABANCI UNIVERSITESI
II-5	Address	Sabanci Universitesi Orhanlı Tuzla 34956 ISTANBUL Turkey
II-6	State of nationality	TR
II-7	State of residence	TR

PCT REQUEST

Print Out (Original in Electronic Form)

III-1	Applicant and/or Inventor	
III-1-1	This person is	applicant and inventor
III-1-2	Applicant for	US only
III-1-4	Name (LAST, First)	EREN, Gönen
III-1-5	Address	Sabancı Universitesi Orhanlı Tuzla 34956 ISTANBUL Turkey
III-1-6	State of nationality	TR
III-1-7	State of residence	TR
III-2	Applicant and/or Inventor	
III-2-1	This person is	applicant and inventor
III-2-2	Applicant for	US only
III-2-4	Name (LAST, First)	ERCIL, Aytul
III-2-5	Address	Sabancı Universitesi Orhanlı Tuzla 34956 ISTANBUL Turkey
III-2-6	State of nationality	TR
III-2-7	State of residence	TR
III-3	Applicant and/or Inventor	
III-3-1	This person is	applicant and inventor
III-3-2	Applicant for	US only
III-3-4	Name (LAST, First)	SANCHEZ, Luis Alonso
III-3-5	Address	Bourgogne University France
III-3-6	State of nationality	FR
III-3-7	State of residence	FR
III-4	Applicant and/or Inventor	
III-4-1	This person is	applicant and inventor
III-4-2	Applicant for	US only
III-4-4	Name (LAST, First)	AUBRETON, Olivier
III-4-5	Address	Bourgogne University France
III-4-6	State of nationality	FR
III-4-7	State of residence	FR

PCT REQUEST

Print Out (Original in Electronic Form)

III-5	**Applicant and/or inventor**	
III-5-1	This person is	applicant and inventor
III-5-2	Applicant for	US only
III-5-4	Name (LAST, First)	FOFI, David
III-5-5	Address	Bourgogne University France
III-5-6	State of nationality	FR
III-5-7	State of residence	FR
III-6	**Applicant and/or inventor**	
III-6-1	This person is	applicant and inventor
III-6-2	Applicant for	US only
III-6-4	Name (LAST, First)	MERIAUDEAU, Fabrice
III-6-5	Address	Bourgogne University France
III-6-6	State of nationality	FR
III-6-7	State of residence	FR
III-7	**Applicant and/or inventor**	
III-7-1	This person is	applicant and inventor
III-7-2	Applicant for	US only
III-7-4	Name (LAST, First)	TRUCHETET, Frederic
III-7-5	Address	Bourgogne University France
III-7-6	State of nationality	FR
III-7-7	State of residence	FR
IV-1	**Agent or common representative; or address for correspondence** The person identified below is hereby/ has been appointed to act on behalf of the applicant(s) before the competent International Authorities as.	agent
IV-1-1	Name	ANKARA PATENT BUREAU LIMITED
IV-1-2	Address	Bestekar Sokak No.10 Kavaklidere 06680 ANKARA Turkey
IV-1-3	Telephone No.	3124172323
IV-1-4	Facsimile No.	3124255804
IV-1-5	e-mail	apatent@apb.com.tr

PCT REQUEST

Print Out (Original in Electronic Form)

V	DESIGNATIONS		
V-1	The filing of this request constitutes under Rule 4.9(a), the designation of all Contracting States bound by the PCT on the international filing date, for the grant of every kind of protection available and, where applicable, for the grant of both regional and national patents.		
VI-1	Priority Claim	NONE	
VII-1	International Searching Authority Chosen	European Patent Office (EPO) (ISA/EP)	
VIII	Declarations	Number of declarations	
VIII-1	Declaration as to the identity of the inventor	-	
VIII-2	Declaration as to the applicant's entitlement, as at the international filing date, to apply for and be granted a patent	-	
VIII-3	Declaration as to the applicant's entitlement, as at the international filing date, to claim the priority of the earlier application	-	
VIII-4	Declaration of inventorship (only for the purposes of the designation of the United States of America)	-	
VIII-5	Declaration as to non-prejudicial disclosures or exceptions to lack of novelty	-	
IX	Check list	number of sheets	electronic file(s) attached
IX-1	Request (including declaration sheets)	5	✓
IX-2	Description	3	✓
IX-3	Claims	1	✓
IX-4	Abstract	1	✓
IX-5	Drawings	1	✓
IX-7	TOTAL	11	
	Accompanying Items	paper document(s) attached	electronic file(s) attached
IX-8	Fee calculation sheet	-	✓
IX-18	PCT-SAFE physical media	-	-
IX-20	Figure of the drawings which should accompany the abstract	1	
IX-21	Language of filing of the international application	English	
X-1	Signature of applicant, agent or common representative	(PKCS7 Digital Signature)	
X-1-1	Name	ANKARA PATENT BUREAU LIMITED	
X-1-2	Name of signatory	ekin dericioglu kurt	
X-1-3	Capacity		

FOR RECEIVING OFFICE USE ONLY

10-1	Date of actual receipt of the purported international application	
10-2	Drawings:	
10-2-1	Received	
10-2-2	Not received	
10-3	Corrected date of actual receipt due to later but timely received papers or drawings completing the purported international application	
10-4	Date of timely receipt of the required corrections under PCT Article 11(2)	
10-5	International Searching Authority	ISA/EP
10-6	Transmittal of search copy delayed until search fee is paid	

FOR INTERNATIONAL BUREAU USE ONLY

11-1	Date of receipt of the record copy by the International Bureau	

Description

A 3D SCANNER

[1] Field of the Invention

[2] The present invention relates to a 3D scanner which builds up 3D models of transparent objects without having their problem of multi-reflection, by means of realizing analysis of temperature differences on surfaces of said objects.

[3] Background of the Invention

[4] As the light not only reflects from transparent objects but also passes through them, making the 3D measurements of transparent materials like glass and acrylic leads to the problem of multi-reflection. For this reason, making the 3D measurements of transparent objects gets difficult. Therefore in measurement of the objects' surfaces with imaging systems, the opaque objects are being focused on in general, not the transparent objects. The surface measurements of the objects which reflect the light can be carried out by the methods of photometric stereo or coloured photometric stereo which can make shaping by means of shading. Whereas a new method reflects the light band to the transparent object and calculates the surface shape of the transparent object by using a generic algorithm. Polarization is another useful method in calculating the shape of the transparent objects. However the said methods can operate under special conditions and they are quite slow to be able to make real-time 3D modeling on production line and to be used in quality control.

[5] In United States patent document No. US6367968 within the state of the art, a system which is used to make measurement and controls on the surfaces of the objects by utilizing infrared thermography is mentioned. In said method, focal-plane array cameras are used as well. The apparatus which is mentioned in United States patent document No. US6367968 determines changes taken place in the thickness of the object which has become thin. In said document by using a lamp, a particular region is heated in an equal distribution. Then the temperature distribution in the course of time is examined by the method of FFT (Fast Fourier Transform) and as the temperature distribution is different in regions which are thinner or thicker than normal, these regions are determined. As is seen, any 3D modeling is not made in said document, only errors are measured from surface roughnesses by using thermography method.

[6] Summary of the Invention

[7] The objective of the present invention is to realize a 3D scanner which can make 3D modeling of the transparent objects in real-time to make quality control in the industry.

[8] Another object of the present invention is to realize a 3D scanner which is able to make 3D modeling of the transparent objects without being effected by the internal reflections arising from the structure of the transparent objects, by utilizing the ther-

mography technique.

[9] Another object of the present invention is to realize a 3D scanner having not only the structures of the transparent objects but also the different materials' and being able to make the 3D modeling of the opaque objects as well.

[10] Detailed Description of the Invention

[11] A 3D scanner realized to fulfill the objective of the present invention is illustrated in the accompanying figure, in which:

[12] Figure 1 is schematic view of a 3D scanner.

[13] The parts shown in the figures are individually numbered, where the numbers refer to the following:

[14] 1. 3D scanner

[15] 2. Slider

[16] 3. Heater

[17] 4. Optical object

[18] 5. Thermal camera

[19] 6. Control unit

[20] The 3D scanner (1) comprises at least one slider (2) on which the object (A) whose surface shape is desired to be determined is placed, and which has a moving structure; at least one heater (3) which provides to territorially heat the object (A) placed on the slider (2); at least one optical object (4) which disperses said beams in order to enable the beams coming from the heater (3) to reach the different points on the slider (2); at least one thermal camera (5) which senses temperature differences on the surface of the object (A) heated territorially and at least one control unit (6) which carries out the 3D modeling of the object (A) with the values sensed by the thermal camera (5).

[21] The slider (2) which is present on the inventive 3D scanner (1) and carries the object (A) whose surface shape is desired to be determined, is controlled by the control unit (6) with the purpose of heating all the regions by the heater (3) to get clear information. The object (A) which is present on the slider (2) while it is moving, is heated territorially by the heater (3). Said heater (3) heats the surface of the object (A) preferably by using CO2 laser as a specific shape such as dot, dash or grid. According to height changes on the surface, deformations or transpositions may occur on these shapes. By determining these changes via the thermal camera (5), the 3D surface shape is calculated by the control unit (6).

[22] In the inventive 3D scanner (1) the power of the heater (3) is determined by the control unit (6) in order to obtain the minimum temperature which can be determined by the thermal camera (5) according to the type and thickness of the material.

[23] The thermal camera (5) used in the inventive 3D scanner (1) preferably has a spectral range between 7,5-13 micrometer and a 320*240 pixel resolution. The light

transmission coefficient of the glass is 1 % in mentioned spectral range and the light reflection coefficient is in maximum value. In the present case, the glass can be thought as an opaque and reflective object.

[24] In a preferred embodiment of the invention the object (A) is present on a fixed base and the system of camera (5) and heater (3) present on the scanner (1) is moving.

[25] Within the framework of this basic concept, it is possible to develop a wide variety of embodiments of the inventive 3D scanner (1) and the invention can not be limited to the examples described herein, it is essentially according to the claims.

Claims

[1] A 3D scanner (1) characterized by at least one slider (2) on which the object (A) whose surface shape is desired to be determined is placed, and which has a moving structure; at least one heater (3) which provides to territorially heat the object (A) placed on the slider (2); at least one optical object (4) which disperses said beams in order to enable the beams coming from the heater (3) to reach the different points on the slider (2); at least one thermal camera (5) which senses temperature differences on the surface of the object (A) heated territorially and at least one control unit (6) which carries out the 3D modeling of the object (A) with the values sensed by the thermal camera (5).

[2] A 3D scanner (1) according to Claim 1 characterized by a thermal camera (5) which has a spectral range between 7.5-13 micrometer and a 320*240 pixel resolution.

[3] A 3D scanner (1) according to Claim 1 characterized in that the heater (3) which territorially heats the surface of the object (A), is a CO2 laser.

Abstract

The present invention relates to a 3D scanner (1) which is able to make 3D modeling of the transparent objects in real-time by utilizing the thermography technique in order to make quality control in the industry; comprising a slider (2), a heater (3), a thermal camera (5) and a control unit (6).

Figure 1

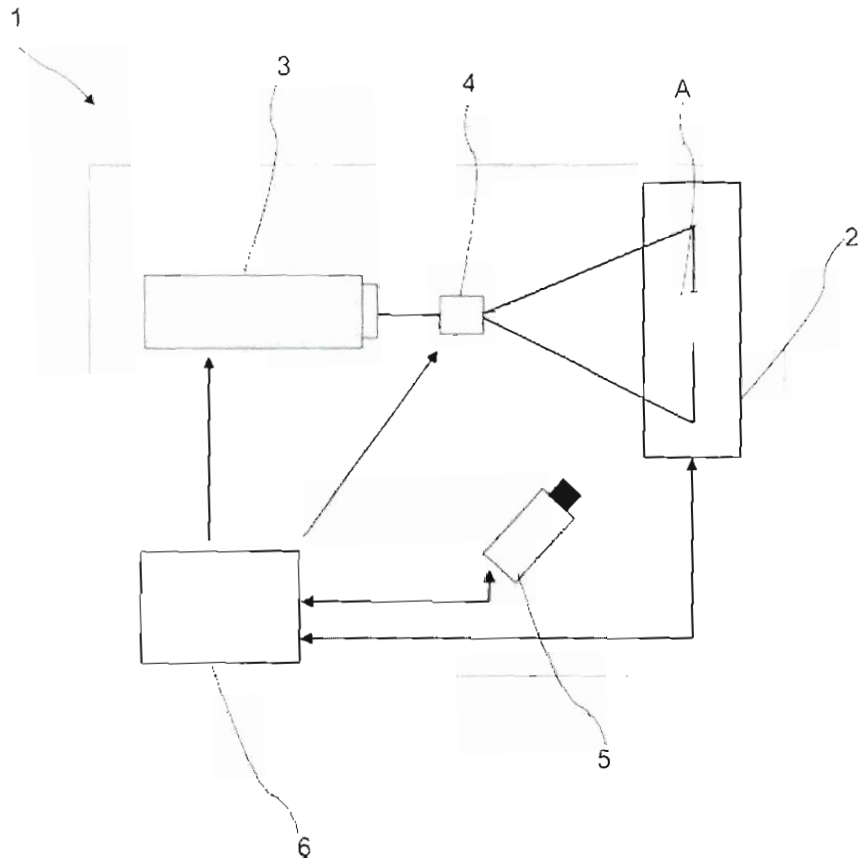

B OPTICAL PROPERTIES OF MATERIALS

Light interacts with matter in many different ways. The wide-ranging optical properties observed in solid state materials can be classified into a small number of general phenomena. The simplest group, namely reflection, propagation and transmission, is illustrated in Fig.B.1. This shows a light beam incident on an optical medium. Some of the light is reflected from the front surface, while the rest enters the medium and propagates through it. If any of this light reaches the back surface, it can be reflected again, or it can be transmitted through to the other side. The amount of light transmitted is therefore related to the reflectivity at the front and back surfaces and also to the way the light propagates through the medium.

Refraction causes the light waves to propagate with a smaller velocity than in free space. This reduction of the velocity leads to the bending of light rays at interfaces described by Snell's law of refraction. Refraction, in itself, does not affect the intensity of the light wave as it propagates. Snells law of refraction states that:

$$n_1 \sin\theta_1 = n_2 \sin\theta_2 \tag{B.1}$$

where n_1 and n_2 are the indices of refraction in the two media. The incident ray, the reflected ray, the refracted ray, and the normal to the surface all lie in the same plane. The index of refraction n of a medium is defined by the ratio:

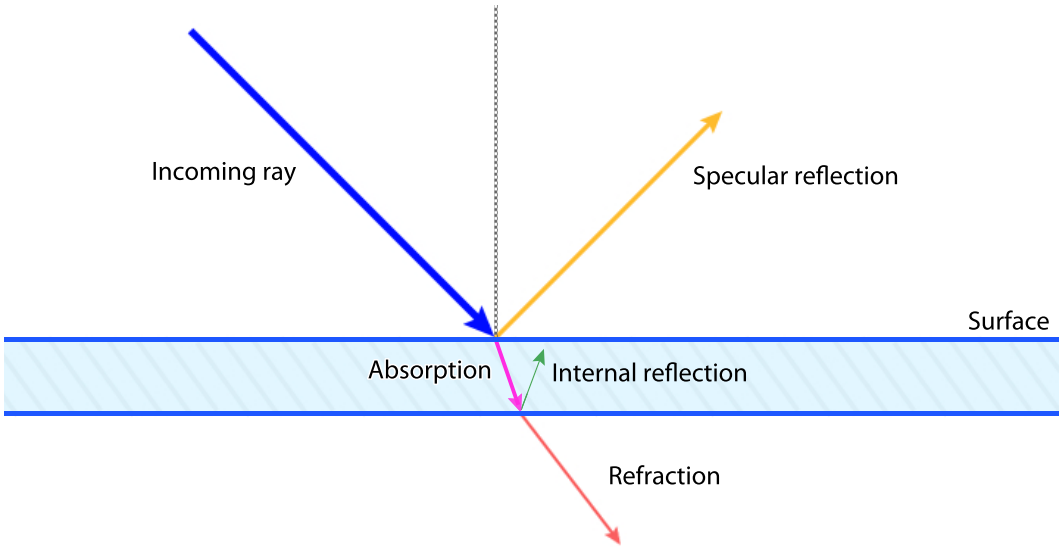

Figure B.1: Reflection, propagation and transmission of a light beam incident on an optical medium.

$$n \equiv \frac{c}{v} \tag{B.2}$$

where c is the speed of light in a vacuum and v is the speed of light in the medium. In general, n varies with wavelength and is given by:

$$n = \frac{\lambda}{\lambda_n} \tag{B.3}$$

where λ is the vacuum wavelength and λ_n is the wavelength in the medium. As light travels from one medium to another, its frequency remains the same.

In the case of reflection, the interaction depends on the physical and chemical properties of the material. If the materials surface is perfectly smooth (e.g. a mirror), rays of light collectively undergo total reflection (or specular reflection), leaving the

surface of the object at a particular angle and all in a parallel line with each other. The law of reflection states that for a light ray traveling in air and incident on a smooth surface, the angle of reflection $\theta_1^{'}$ equals the angle of incidence θ_1:

$$\theta_1^{'} = \theta_1 \tag{B.4}$$

Internal reflection occurs when light travels from a medium of high index of refraction to one of lower index of refraction. The critical angle θ_c for which total internal reflection occurs at an interface is given by:

$$\sin\theta_c = \frac{n_2}{n_1} \tag{B.5}$$

Bibliography

[1] I. Ihrke, K. Kutulakos, H. Lensch, M. Magnor, and W. Heidrich, "State of the art in transparent and specular object reconstruction," *STAR Proc. of Eurographics*, 2008.

[2] B. Curless, "Overview of active vision techniques," *SIGGRAPH 99 Course on 3D Photography*, 1999.

[3] "Intelligent glass production," August 2010. [Online]. Available: http://www.israglassvision.com/

[4] H. Takasaki, "Moiré topography," *Applied optics*, vol. 9, no. 6, pp. 1467–1472, 1970.

[5] A. Haasteren and H. Frankena, "Real-time displacement measurement using a multicamera phase-stepping speckle interferometer," *Applied optics*, vol. 33, no. 19, pp. 4137–4142, 1994.

[6] P. Vuylsteke and A. Oosterlinck, "3d perception with a single binary coded illumination pattern," *Proc. SPIE 728*, pp. 195–202, 1986.

[7] F. Blais, "Review of 20 years of range sensor development," *Journal of Electronic Imaging*, vol. 13, no. 1, pp. 231–243, 2004.

[8] B. Curless and M. Levoy, "Better optical triangulation through spacetime analysis," in *Proceedings of IEEE International Conference on Computer Vision*, vol. 95, 1995, pp. 987–994.

[9] S. Nayar and Y. Nakagawa, "Shape from focus," *IEEE Transactions on Pattern Analysis and Machine Intelligence*, pp. 824–831, 1994.

[10] F. Remondino and S. El-Hakim, "Image-based 3d modelling: A review," *The Photogrammetric Record*, vol. 21, no. 115, pp. 269–291, 2006.

[11] D. Bhat and S. K. Nayar, "Stereo in the presence of specular reflection," in *In ICCV*, 1995, pp. 1086–1092.

[12] S. Nayar, X. Fang, and T. Boult, "Removal of specularities using color and polarization," in *1993 IEEE Computer Society Conference on Computer Vision and Pattern Recognition, 1993. Proceedings CVPR'93.*, 1993, pp. 583–590.

[13] S. Hata, Y. Saitoh, S. Kumamura, and K. Kaida, "Shape extraction of transparent object using genetic algorithm," in *Pattern Recognition, Proceedings of the 13th International Conference on*, vol. 4, 1996.

[14] N. Morris and K. Kutulakos, "Reconstructing the surface of inhomogeneous transparent scenes by scatter-trace photography," in *Proc. of 11th Int. Conf. Computer Vision*, 2007.

[15] M. Ben-Ezra and S. Nayar, "What does motion reveal about transparency?" in *Proc. IEEE Int'l Conf. Computer Vision*, 2003, pp. 1025–1032.

[16] S. Agarwal, S. Mallick, D. Kriegman, and S. Belongie, "On refractive optical flow," in *Proc. ECCV'04*, 2004, pp. 483–494.

[17] M. B. Hullin, M. Fuchs, I. Ihrke, H.-P. Seidel, and H. P. A. Lensch, "Fluorescent immersion range scanning," *ACM Trans. Graph.*, vol. 27, no. 3, pp. 1–10, 2008.

[18] R. Rantoson, C. Stolz, D. Fofi, and F. Meriaudeau, "3d reconstruction of transparent objects exploiting surface fluorescence caused by uv irradiation," in *IEEE International Conference on Image Processing (ICIP)*, 2010.

[19] K. Kutulakos and E. Steger, "A theory of refractive and specular 3D shape by light-path triangulation," *International Journal of Computer Vision*, vol. 76, no. 1, pp. 13–29, 2008.

[20] M. Tarini, H. Lensch, M. Goesele, and H. Seidel, "3d acquisition of mirroring objects using striped patterns," *Graphical Models*, vol. 67, no. 4, pp. 233–259, 2005.

[21] S. Savarese and P. Perona, "Local analysis for 3d reconstruction of specular surfaces," in *IEEE Computer Society Conference on Computer Vision and Pattern Recognition*, vol. 2, 2001.

[22] S. Savarese, M. Chen, and P. Perona, "Local shape from mirror reflections," *International Journal of Computer Vision*, vol. 64, no. 1, pp. 31–67, 2005.

[23] K. Ikeuchi, "Determining surface orientations of specular surfaces by using the photometric stereo method," *IEEE Transactions on Pattern Analysis and Machine Intelligence*, vol. 3, no. 6, pp. 661–669, 1981.

[24] J. Zheng and A. Murata, "Acquiring 3D object models from specular motion using circularlights illumination," in *Computer Vision, 1998. Sixth International Conference on*, 1998, pp. 1101–1108.

[25] D. Miyazaki and K. Ikeuchi, "Inverse polarization raytracing: estimating surface shapes of transparent objects," in *IEEE Computer Society Conference on Computer Vision and Pattern Recognition*, vol. 2, 2005, p. 910.

[26] D. Miyazaki, M. Saito, Y. Sato, and K. Ikeuchi, "Determining surface orientations of transparent objects based on polarization degrees in visible and infrared wavelengths," *Journal of the Optical Society of America A*, vol. 19, no. 4, pp. 687–694, 2002.

[27] M. Ferraton, C. Stolz, and F. Mériaudeau, "Optimization of a polarization imaging system for 3D measurements of transparent objects." *Optics Express*, vol. 17, no. 23, pp. 21 077–21 082, 2009.

[28] A. Kanitsar, T. Theußl, L. Mroz, M. Srámek, A. Bartrolí, B. Csébfalvi, J. Hladuvka, D. Fleischmann, M. Knapp, R. Wegenkittl *et al.*, "Christmas tree case study: computed tomography as a tool for mastering complex real world objects with applications in computer graphics," in *Proceedings of the conference on Visualization'02*. IEEE Computer Society Washington, DC, USA, 2002, pp. 489–492.

[29] P. Allen and P. Michelman, "Acquisition and interpretation of 3-D sensor data from touch," *IEEE Transactions on Robotics and Automation*, vol. 6, no. 4, pp. 397–404, 1990.

[30] R. Ibrayev and Y. Jia, "Tactile recognition of algebraic shapes using differential invariants," in *IEEE International Conference on Robotics and Automation*, vol. 2, 2004, pp. 1548–1553.

[31] I. Ihrke, K. N. Kutulakos, H. P. A. Lensch, M. Magnor, and W. Heidrich, "Transparent and specular object reconstruction," *Computer Graphics Forum*, p. to appear, 2010.

[32] R. A. Serway and J. W. Jewett, *Physics for Scientists and Engineers.* Thomson Brooks/Cole, 2004.

[33] M. Fox, *Optical Properties of Solids.* Oxford University Press, 2002.

[34] J. Phalippou, "Verres propriétés et applications," *Techniques de l'ingénieur. Matériaux fonctionnels*, vol. 1, no. AF3601, 2001.

[35] J. E. Shelby, *Introduction to Glass Science and Technology.* Royal Society of Chemistry, 2005.

[36] K. Cheung, S. Baker, and T. Kanade, "Shape-from-silhouette across time part i: Theory and algorithms," *International Journal of Computer Vision*, vol. 62, no. 3, pp. 221–247, 2005.

[37] S. Prakash, P. Y. Lee, and T. Caelli, "3d mapping of surface temperature using thermal stereo," *Proceedings of ICARCV 2006*, 2006.

[38] S. Roth and M. Black, "Specular flow and the recovery of surface structure," in *Proc. CVPR*, 2006, pp. 1869–1876.

[39] K. Nakano, Y. Watanabe, and S. Kanno, "Extraction and recognition of 3-dimensional information byprojecting a pair of slit-ray beams," in *Pattern Recognition, 9th International Conference on*, 1988, pp. 736–743.

[40] M. Oren and S. Nayar, "A theory of specular surface geometry," *International Journal of Computer Vision*, vol. 24, no. 2, pp. 105–124, 1997.

[41] D. Bhat and S. Nayar, "Stereo and specular reflection," *International Journal of Computer Vision*, vol. 26, no. 2, pp. 91–106, 1998.

[42] M. Osadchy, D. Jacobs, R. Ramamoorthi, and N. Princeton, "Using specularities for recognition," in *International Conference on Computer Vision*, 2003, pp. 1512–1519.

[43] R. Siegel and J. Howell, *Thermal radiation heat transfer*. Taylor & Francis, 2002.

[44] M. Bertozzi, E. Binelli, A. Broggi, and M. Rose, "Stereo vision-based approaches for pedestrian detection," in *2005 IEEE Computer Society Conference on Computer Vision and Pattern Recognition*, 2005, pp. 16–16.

[45] X. Maldague and X. Maldague, *Nondestructive evaluation of materials by infrared thermography*. Springer, 1993.

[46] J. Pelletier and X. Maldague, "Shape from heating: a two-dimensional approach for shape extraction in infrared images," *Optical Engineering*, vol. 36, p. 370, 1997.

[47] G. Gaussorgues and S. Chomet, *Infrared thermography*. Kluwer Academic Publishers, 1994.

[48] D. Forsyth and J. Ponce, *Computer vision: a modern approach*. Prentice Hall Professional Technical Reference, 2002.

[49] A. W. Fitzgibbon, "Simultaneous linear estimation of multiple view geometry and lens distortion," *Computer Vision and Pattern Recognition, IEEE Computer Society Conference on*, vol. 1, p. 125, 2001.

[50] J. L. Miller, *Principles of Infrared Technology*. Springer, 1994.

[51] J. Jiao and X. Wang, "A numerical simulation of machining glass by dual co2-laser beams," *Optics & Laser Technology*, vol. 40, no. 2, pp. 297–301, 2008.

[52] L. G. Shapiro and G. C. Stockman, *Computer Vision*. Prentice Hall, 2001.

[53] (2010, August). [Online]. Available: http://www.rapidform.com

[54] F. Meriaudeau, L. A. S. Secades, G. Eren, A. Ercil, F. Truchetet, O. Aubreton, and D. Fofi, "3d scanning of non-opaque objects by means of imaging emitted structured infrared patterns," *IEEE Transactions on Instrumentation and Measurement*, (to be published) 2010.

[55] D. Salomon, *Curves and surfaces for computer graphics*. Springer-Verlag New York Inc, 2006.

[56] J. Philip, "An algorithm for determining the position of a circle in 3d from its perspective 2d projection," *NASA*, 1997.

[57] W. Gander, G. Golub, and R. Strebel, "Least-squares fitting of circles and ellipses," *BIT Numerical Mathematics*, vol. 34, no. 4, pp. 558–578, 1994.

Biography

Mr. Eren obtained his Bachelors degree in Computer Engineering in 2004 and his Masters degree in Computer Engineering in 2007 from Galatasaray University in Turkey. His master thesis subject was to conceive a semi-autonomous underwater robot. He obtained sponsorship form Ideal Technology, a private company, and support from TUBITAK, the Scientific and Technological Research Council of Turkey.

In 2007, he received full scholarship from the Government of France and from Sabanci University and started a double PhD in Computer Science at Bourgogne University LE2I Laboratory in France and Sabanci University VPA Laboratory in Turkey. His thesis subject was on 3D scanning of Transparent Objects. He proposed a new method called *Scanning from Heating*. His research gave place to several publications in international journals and conferences and recently the two universities started, with industrial partners, an Eureka Project on the extension of the method on specular metal surfaces.

Since 2004, Mr. Eren has been working as a Research Assistant at Galatasaray University where he also teaches the Object Oriented Programming course. In 2006, Mr. Eren realized projects for Bosch, Sisecam and Ipragaz with his thesis advisor Prof. Aytul Ercil and the support of Sabanci University.

Mr. Eren is fluent in English, French, Turkish and speaks beginner level German and Japanese.